

**EFFECT OF ACUTE ADMINISTRATION OF ANGIOPOIETIN-1 IN
EXPERIMENTAL TRAUMATIC SPINAL CORD INJURY:
MAGNETIC RESONANCE IMAGING AND
NEUROBEHAVIORAL STUDIES**

by

Chirag B. Patel, M.S.E.

APPROVED:

Ponnada A. Narayana, Ph.D.
Supervisory Professor

Hesham Amin, M.D.

Raymond J. Grill, Ph.D.

Claire Hulsebosch, Ph.D.

Jerry S. Wolinsky, M.D.

APPROVED:

Dean, The University of Texas
Graduate School of Biomedical Sciences at Houston

**EFFECT OF ACUTE ADMINISTRATION OF ANGIOPOIETIN-1 IN
EXPERIMENTAL TRAUMATIC SPINAL CORD INJURY:
MAGNETIC RESONANCE IMAGING AND
NEUROBEHAVIORAL STUDIES**

A

DISSERTATION

Presented to the Faculty of
The University of Texas
Health Science Center at Houston
and
The University of Texas
M.D. Anderson Cancer Center
Graduate School of Biomedical Sciences
in Partial Fulfillment
of the Requirements
for the Degree of
DOCTOR OF PHILOSOPHY

by

Chirag B. Patel, M.S.E.
Houston, TX

August, 2010

DEDICATION

To my parents, Bihesh and Daksha, for their sacrifices, love, and support.

ACKNOWLEDGEMENTS

First and foremost, I deeply thank my advisor, Professor Ponnada A. Narayana, Ph.D., for his support and guidance. He has been a mentor in the truest sense of the word, and his generous sharing of his expertise and time has been invaluable in my ongoing development as an independent scientist. I am inspired by his unwavering dedication to and pursuit of excellence in research.

I would not have been able to accomplish this work without the additional support from the faculty members who took the time to serve on my Advisory, Examination, and Supervisory committees: Hesham Amin, M.D., Russell Broaddus, M.D., Ph.D., Raymond J. Grill, Ph.D., Khader M. Hasan, Ph.D., Ruth Heidelberger, M.D., Ph.D., Claire Hulsebosch, Ph.D., and Jerry S. Wolinsky, M.D. I am grateful to these faculty members for valuable suggestions and conversations that have resulted in my more robust appreciation for the various aspects of this project.

Many thanks to former members of Dr. Narayana's laboratory, including Shi-Jie Liu, M.D (who performed the rodent surgeries), David M. Cohen, Ph.D. (who trained me in DCE-MRI analysis and scan acquisition), Pallavi Jaivijay, Venkata Mogatadakala, Ph.D., Junchao Qian, M.D., and Jaivijay Ramu. Laura M. Sundberg, Ph.D. has been a great resource, providing suggestions on various aspects of the project. I am also thankful to Kurt Bockhorst, Ph.D. (for assistance with DTI data processing and questions during scan acquisition and post-processing), Juan Herrera, Ph.D. (for assistance with questions about the molecular and biological aspects of the project), and Tessy Chacko (for assistance with neurobehavioral assessment and animal care).

Additional lab and non-lab members have provided input and assistance on related aspects of the project and I am also thankful to them: Rene Colorado, Jennifer Dulin, Emilio Esparza-Coss, Ph.D., Sushmita Datta, Ph.D., Cheukkai Hui, Vaibhav Juneja, Rui Liu, Ph.D., and Bindu Nair.

**EFFECT OF ACUTE ADMINISTRATION OF ANGIOPOIETIN-1 IN
EXPERIMENTAL TRAUMATIC SPINAL CORD INJURY:
MAGNETIC RESONANCE IMAGING AND
NEUROBEHAVIORAL STUDIES**

Publication No. _____

Chirag B. Patel, M.S.E.

Supervisory Professor: Ponnada A. Narayana, Ph.D.

Spinal cord injury (SCI) is a devastating condition that affects people in the prime of their lives. A myriad of vascular events occur after SCI, each of which contributes to the evolving pathology. The primary trauma causes mechanical damage to blood vessels, resulting in hemorrhage. The blood-spinal cord barrier (BSCB), a neurovascular unit that limits passage of most agents from systemic circulation to the central nervous system, breaks down, resulting in inflammation, scar formation, and other sequelae. Protracted BSCB disruption may exacerbate cellular injury and hinder neurobehavioral recovery in SCI.

In these studies, angiopoietin-1 (Ang1), an agent known to reduce vascular permeability, was hypothesized to attenuate the severity of secondary injuries of SCI. Using longitudinal magnetic resonance imaging (MRI) studies (dynamic contrast-enhanced [DCE]-MRI for quantification of BSCB permeability, high-resolution anatomical MRI for calculation of lesion size, and diffusion tensor imaging for assessment of axonal integrity), the acute, subacute, and chronic effects of Ang1 administration after SCI were evaluated. Neurobehavioral assessments were also

performed. These non-invasive techniques have applicability to the monitoring of therapies in patients with SCI.

In the acute phase of injury, Ang1 was found to reduce BSCB permeability and improve neuromotor recovery. Dynamic contrast-enhanced MRI revealed a persistent compromise of the BSCB up to two months post-injury. In the subacute phase of injury, Ang1's effect on reducing BSCB permeability was maintained and it was found to transiently reduce axonal integrity. The SCI lesion burden was assessed with an objective method that compared favorably with segmentations from human raters. In the chronic phase of injury, Ang1 resulted in maintained reduction in BSCB permeability, a decrease in lesion size, and improved axonal integrity.

Finally, longitudinal correlations among data from the MRI modalities and neurobehavioral assays were evaluated. Locomotor recovery was negatively correlated with lesion size in the Ang1 cohort and positively correlated with diffusion measures in the vehicle cohort. In summary, the results demonstrate a possible role for Ang1 in mitigating the secondary pathologies of SCI during the acute and chronic phases of injury.

TABLE OF CONTENTS

DEDICATION.....	iii
ACKNOWLEDGEMENTS.....	iv
ABSTRACT.....	vi
LIST OF FIGURES.....	x
LIST OF TABLES.....	xiv
ABBREVIATIONS.....	xvi
CHAPTER 1 – Introduction.....	1
CHAPTER 2 – Materials and Methods.....	10
CHAPTER 3 – Effect of Single Acute Ang1 Dose on Blood-Spinal Cord Barrier Compromise and Permeability.....	33
<i>INTRODUCTION.....</i>	<i>34</i>
<i>RESULTS.....</i>	<i>37</i>
<i>DISCUSSION.....</i>	<i>59</i>
CHAPTER 4 – Effect of Single Acute Ang1 Dose on Spinal Cord Atrophy and SCI Lesion Size.....	65
<i>INTRODUCTION.....</i>	<i>66</i>
<i>RESULTS.....</i>	<i>68</i>
<i>DISCUSSION.....</i>	<i>82</i>
CHAPTER 5 – Effect of Single Acute Ang1 Dose on Axonal Integrity and Neurobehavioral Recovery and Longitudinal Correlation with Lesion Size.....	87
<i>INTRODUCTION.....</i>	<i>88</i>
<i>RESULTS.....</i>	<i>90</i>

<i>DISCUSSION</i>	102
CHAPTER 6 – Conclusions and Future Studies	106
BIBLIOGRAPHY	111
VITA	134

LIST OF FIGURES

Figure 2.1 – Stabilization of vertebral column at T6 and T8 prior to spinal cord injury.....	13
Figure 2.2 – Implantation of radiofrequency coil after spinal cord injury.....	15
Figure 2.3 – Vascular port implantation for access to systemic vasculature during dynamic contrast-enhanced magnetic resonance imaging scans.....	16
Figure 2.4 - Definition of spatial three spatial regions for MR image-based analyses.....	23
Figure 2.5 – Identification of enhancing and non-enhancing tissue areas on dynamic contrast-enhanced magnetic resonance imaging scans using a histogram-based threshold.....	24
Figure 2.6 – Two-compartment pharmacokinetic model of blood-spinal cord barrier (BSCB) permeability.....	26
Figure 2.7 – Example of hyperintense (#) and hypointense (*) tissue areas on anatomical magnetic resonance imaging scans.....	27
Figure 2.8 - Pictorial of white matter regions of interest (ROIs) defined for diffusion tensor imaging analysis.....	30
Figure 3.1 - Frank enhancement (absolute area, mm ²) by day and spatial region.....	38
Figure 3.2 - Frank enhancement (absolute area, mm ²) by day and spatial region (temporal view).....	39
Figure 3.3 - Frank enhancement (absolute area, mm ²) by phase of injury and spatial region (including temporal view).....	40

Figure 3.4 - Frank enhancement (relative area, percent) by day and spatial region.....	43
Figure 3.5 - Frank enhancement (relative area, percent) by day and spatial region (temporal view).....	44
Figure 3.6 - Frank enhancement (relative area, percent) by phase of injury and spatial region (including temporal view).....	45
Figure 3.7 - Blood-spinal cord barrier (BSCB) permeability in spinal cord tissue areas exhibiting contrast enhancement, by day and spatial region.....	49
Figure 3.8 - Blood-spinal cord barrier (BSCB) permeability in spinal cord tissue areas exhibiting contrast enhancement, by day and spatial region (temporal view).....	50
Figure 3.9 - Blood-spinal cord barrier (BSCB) permeability in spinal cord tissue areas exhibiting contrast enhancement, by phase of injury and spatial region (including temporal view).....	51
Figure 3.10 - Blood-spinal cord barrier (BSCB) permeability in non-enhancing spinal cord tissue areas, by day and spatial region.....	55
Figure 3.11 - Blood-spinal cord barrier (BSCB) permeability in non-enhancing spinal cord tissue areas, by day and spatial region (temporal view).....	56
Figure 3.12 - Blood-spinal cord barrier (BSCB) permeability in non-enhancing spinal cord tissue areas, by phase of injury and spatial region (including temporal view).....	57
Figure 4.1 – Representative sample of anatomical images segmented by human raters.....	68

Figure 4.2 Rater segmentation (four raters) in a slice containing both hyperintense and hypointense lesion.....	69
Figure 4.3 – Sensitivity analysis of raters (four human-based segmentations and five histogram-based segmentations) for hyperintense and hypointense lesion.....	72
Figure 4.4 – Specificity analysis of raters (four human-based segmentations and five histogram-based segmentations) for hyperintense and hypointense lesion.....	73
Figure 4.5 – Positive predictive value (PPV) analysis of raters (four human-based segmentations and five histogram-based segmentations) for hyperintense and hypointense lesion.....	74
Figure 4.6 – Negative predictive value (NPV) analysis of raters (four human-based segmentations and five histogram-based segmentations) for hyperintense and hypointense lesion.....	75
Figure 4.7 – Dice similarity coefficient (DSC) analysis of raters (four human-based segmentations and five histogram-based segmentations) for hyperintense and hypointense lesion.....	76
Figure 4.8 – Spinal cord atrophy between day 7 and day 14 post-SCI, and between day 7 and day 28 post-SCI.....	77
Figure 4.9 – Hyperintense lesion determined by objective histogram-based approach (1.0*standard deviation cut-off).....	79
Figure 4.10 – Hypointense lesion determined by objective histogram-based approach (1.0*standard deviation cut-off).....	80
Figure 4.11 – Total lesion determined by objective histogram-based approach (1.0*standard deviation cut-off).....	81

Figure 5.1 – Basso-Beattie-Bresnahan (BBB) score.....	94
Figure 5.2 – Inclined plane assessment.....	95
Figure 5.3 – Grid walk assessment.....	96
Figure 5.4 – Computerized activity box assessment.....	97
Figure 5.5 – Assessment of chronic neuropathic pain.....	98
Figure 6.1 Summary of findings.....	108

LIST OF TABLES

Table 2.1 - Experimental design.....	12
Table 3.1 - Spatial and temporal differences in frank enhancement (absolute area) after spinal cord injury (SCI).	41
Table 3.2 - Spatial and temporal differences in frank enhancement (relative area) after spinal cord injury (SCI).....	46
Table 3.3 - Spatial and temporal differences in blood-spinal cord barrier (BSCB) permeability in enhancing tissue areas after spinal cord injury (SCI).....	52
Table 3.4 - Spatial and temporal differences in blood-spinal cord barrier (BSCB) permeability in non-enhancing tissue areas after spinal cord injury (SCI).	58
Table 3.5 - Evaluating persistently increased blood-spinal cord barrier (BSCB) permeability in normal-appearing tissue after spinal cord injury (SCI).....	58
Table 5.1 – Summary of significant inter-group differences in mean diffusivity (units: mm^2s^{-1}).....	90
Table 5.2 – Summary of significant inter-group differences in fractional anisotropy (unitless).	91
Table 5.3 – Summary of significant inter-group differences in longitudinal diffusivity (units: mm^2s^{-1}).	92
Table 5.4 – Summary of significant inter-group differences in transverse diffusivity (units: mm^2s^{-1}).	93
Table 5.5 – Significant longitudinal correlations between Basso-Beattie-Bresnahan (BBB) score and measures from high-resolution anatomical and diffusion tensor imaging scans.....	99

Table 5.6 – Significant longitudinal correlations between lesion measures and diffusion tensor imaging measures.	100
Table 6.1 – Summary of study findings.	107

ABBREVIATIONS

λ_1 = first eigenvalue	K_{ps} = DCE-MRI parameter indicating BSCB permeability
λ_2 = second eigenvalue	MD = mean diffusivity
λ_3 = third eigenvalue	MRI = magnetic resonance imaging
λ_L = longitudinal diffusivity	MW = molecular weight
λ_T = transverse diffusivity	NF-κB = nuclear factor-kappa B
μ = mean	NPV = negative predictive value
σ = standard deviation of the mean	PDF = probability density function
ABIN-2 = A-20 binding inhibitor of NF- κ B activation	PI3K = phosphoinositide 3-kinase
Ang1 = angiopoietin-1	PPV = positive predictive value
BBB = Basso-Beattie-Bresnahan locomotor score	RARE = rapid acquisition relaxation enhancement
BSCB = blood-spinal cord barrier	RF = radiofrequency
CNS = central nervous system	ROI = region of interest
CSF = cerebrospinal fluid	SCI = spinal cord injury
CST = corticospinal tract	SNR = signal-to-noise ratio
DCE = dynamic contrast-enhanced	TE = echo time
DTI = diffusion tensor imaging	Tn = thoracic level n (e.g., T7 = thoracic level 7)
EES = extravascular extracellular space	TN = true negative
EPI = echo-planar imaging	TP = true positive
FA = fractional anisotropy	TR = repetition time
FDA = Food and Drug Administration	SD = standard deviation of the mean
FOV = field of view	SEM = standard error of the mean
FN = false negative	SID = signal intensity distribution
FP = false positive	STAPLE = simultaneous truth and performance level estimation
Gd = gadodiamide	Uninj = uninjured
GEE = generalized estimating equation	VEGF = vascular endothelial growth factor
ICAM-1 = intercellular adhesion molecule 1	

CHAPTER 1:

INTRODUCTION

Spinal Cord Injury

Spinal Cord Injury (SCI) is a devastating condition that affects people in the prime of their lives. 256,000 Americans currently live with SCI and 12,000 more are injured each year. The estimated lifetime medical care expenses of SCI patients range from \$500,000 to \$3,000,000 depending on the level of SCI and patient's age at the time of SCI (Priebe et al., 2007). The mainstay therapy for SCI remains surgical decompression of the spinal cord and physical rehabilitation. High dose methylprednisolone is the only widely-used pharmacologic treatment approach to SCI (Bracken, 2002; Baptiste and Fehlings, 2007) yet its efficacy remains controversial (Hugenholtz, 2003) and thus has not been approved by the Food and Drug administration (FDA). A small number of clinical trials focusing on neuroprotection and regeneration are underway (Hall and Springer, 2004; Sykova et al., 2006; Faden and Stoica, 2007; Alper, 2009). Due to limited therapeutic options beyond supportive care, there is an urgent need for novel treatment approaches that tackle multiple aspects of SCI pathophysiology.

The primary injury in SCI leads to axonal damage and mechanical disruption of the blood vessels within and surrounding the spinal cord (Mautes et al., 2000). Hemorrhage occurs immediately after SCI (Nelson et al., 1977). In addition, the blood-spinal cord barrier (BSCB) is further compromised due to the release of inflammatory cytokines (e.g. IL-1 β , TNF α , and IL-6) by activated central nervous system (CNS) cells (e.g. astrocytes and microglia) (Jones et al., 2005; Tian et al., 2007). These inflammatory cytokines cause local edema and signal the intravasation of neutrophils from the systemic vasculature into the parenchyma.

This process is partly mediated by increased expression of adhesion molecules (e.g. ICAM and VCAM) on the surface of vascular endothelial cells that facilitate diapedesis, chemotaxis, and attachment of neutrophils via their cell surface integrins (Carlos and Harlan, 1994). Neutrophils cause cellular damage via the release of free oxygen radicals that lead to lipid peroxidation, cell death, and further inflammation (Carlson et al., 1998; Juurlink and Paterson, 1998; Fleming et al., 2006). This cascade of molecular and cellular events that follows the primary injury is collectively termed “secondary injury” (Anderson and Hall, 1993) and causes tissue damage away from the site of injury and prevents recovery of neurological function (Coleman and Perry, 2002; Gimenez y Ribotta et al., 2002; Hagg and Oudega, 2006). The majority of SCI treatments target the secondary injury events in order to retard or prevent the downstream sequelae.

Role of Vascular Permeability in Spinal Cord Injury

A myriad of vascular events occur after SCI, each of which contributes to the evolving pathology. The primary trauma causes mechanical damage to blood vessels, resulting in hemorrhage primarily in gray matter (Amar and Levy, 1999). The BSCB breaks down, leading to inflammation, scar formation, and other sequelae (Mautes et al., 2000). Popovich et al. and Noble et al. previously showed that the BSCB remains compromised up to 28 days post-SCI and that this disruption extends both caudally and rostrally beyond the site of injury (Noble and Wrathall, 1989; Popovich et al., 1996). Studies from our laboratory, based on dynamic contrast-enhanced magnetic resonance imaging (DCE-MRI), have

confirmed these observations and demonstrated that the permeability remains elevated two months after injury even when the tissue appears normal on conventional MRI (Cohen et al.). Protracted BSCB disruption may exacerbate cellular injury and hinder neurobehavioral recovery.

The BSCB is a specialized structure at the level of capillaries that protects the spinal cord from potentially toxic agents found in the systemic circulation. Some of the components of the BSCB include: tight junction proteins between adjacent vascular endothelial cells, a basal lamina, a layer of smooth muscle/pericyte cells that sheathe the vascular endothelium, and a negatively-charged glycocalyx. Studies from our laboratory have identified a significant correlation between reduced BSCB permeability and improved open field locomotor scores in our rat model of SCI (Cohen et al.), suggesting the potential importance of restoring barrier integrity in SCI.

Angiopoietin-1

Angiopoietin-1 (Ang1) is a soluble ligand secreted by pericytes, astrocytes, mast cells, and stromal cells (Acker et al., 2001; Sundberg et al., 2002; Hori et al., 2004; Nakayama et al., 2004). Ang-1 binds to and phosphorylates Tie-2, a receptor tyrosine kinase on endothelial cells (Davis et al., 1996). Activation of Tie-2 promotes endothelial cell survival via the phosphoinositide 3-kinase (PI3K) survival pathway (Peters et al., 2004). Tie-2 phosphorylation also activates A-20 binding inhibitor of nuclear factor-kappa B (NF- κ B) activation (ABIN-2), which reduces the expression of adhesion molecules on the vascular endothelial cell surface (Tadros

et al., 2003). Selective inactivation of NF- κ B has been shown to improve neuromotor recovery in rat and mouse models of SCI (Brambilla et al., 2005; Rafati et al., 2007). Ang-1 is believed to reduce vessel permeability by a host of mechanisms, including increased pericyte coverage and tight junction protein upregulation in vascular endothelium (Liu et al., 2000; Iizasa et al., 2002; Stoeltzing et al., 2003; Zhu et al., 2006). In short, Ang-1 activation of Tie-2 stabilizes blood vessels by reducing vascular permeability (Papapetropoulos et al., 1999; Thurston et al., 1999; Thurston et al., 2000).

Human Ang1 has 89% homology with rat Ang1 and is cross-reactive with rat Tie-2 receptor. Recombinant human Ang1 was shown to reduce vessel leakiness and inflammation in a dose-dependent manner in rat models of diabetic retinopathy (Joussen et al., 2002) and in hCG-induced testicular inflammation (Haggstrom Rudolfsson et al., 2003). The vascular changes in these disease models are similar to those observed in the secondary injury of SCI (e.g. increased vessel permeability and inflammation). Ang1 has been shown to reduce the permeability of adult vasculature (Thurston et al., 2000) and central nervous system (CNS) vasculature, specifically the blood-brain barrier (Zacharek et al., 2007) and BSCB (Han et al., 2010). However, it should be noted that Ang1 has been demonstrated to act on other components of the nervous system as well, namely neurons. For instance, Ang1 has been shown to induce neurite outgrowth in cultured dorsal root ganglion cells (Kosacka et al., 2005; Kosacka et al., 2006). Thus, although the effects of Ang1 are known to be primarily mediated through the endothelial-specific

Tie-2 receptor, other CNS cells expressing Tie-2 may be affected by exposure to Ang1.

Angiopoietin-1 in Spinal Cord Injury

At present, there is only one published study that has investigated the role of Ang1 in experimental SCI, in a mouse T9 contusion model (Han et al.). This investigation demonstrated effects of Ang1 at the injury epicenter, including significantly increased vascularity and significant attenuation of vascular permeability, locomotor deficits, white matter loss, CD3-positive T cell infiltration, and inflammation (Han et al.). However, understanding of the role of Ang1 beyond the lesion site is lacking. In addition, the longitudinal effects of Ang1 administration after SCI remain unclear. Further study is warranted to better understand the potentially beneficial and detrimental roles, if any, of Ang1 in SCI.

Central Hypothesis

I hypothesize that Ang1 attenuates the severity of three secondary injuries of SCI (compromised BSCB, SCI lesion, and axonal damage) and improves neurobehavioral recovery after the injury.

Specific Aims

In order to test this hypothesis, three specific aims are proposed in an experimental rat model of thoracic level seven (T7) contusion SCI. Animals will be divided into two cohorts, experimental (Ang1-treated) and control (vehicle-treated).

Specific Aim 1: Investigate the effect of acute administration of Ang1 on BSCB permeability in the acute (2 days post-SCI), subacute (7 and 14 days post-SCI), and chronic (28, 42, and 56 days post-SCI) phases of injury. Blood-spinal cord barrier permeability will be quantified in the epicenter and perilesional regions based on *in vivo* DCE-MRI. Using an established two-compartment pharmacokinetic model, DCE-MRI data will be used to quantify BSCB permeability (Bilgen and Narayana, 2001; Bilgen et al., 2002; Cohen et al., 2009). DCE-MRI will allow for non-invasive spatial tracking of changes in BSCB permeability. *I hypothesize that, compared to the control cohort, decreased BSCB permeability will be observed in the Ang1 cohort.*

Specific Aim 2: Investigate the effect of acute administration of Ang1 on spinal cord lesion size in the acute (2 days post-SCI), subacute (7 and 14 days post-SCI), and chronic (28, 42, and 56 days post-SCI) phases of injury. Lesion size will be quantified in the epicenter and perilesional regions based on *in vivo* high-resolution rapid acquisition relaxation enhancement (RARE) MRI scans. A new histogram-based approach will be used to objectively assess lesion size and this approach will be evaluated against results from human raters. *I hypothesize that, compared to the control cohort, decreased SCI lesion size will be observed in the Ang1 cohort.*

Specific Aim 3: Investigate the effect of acute administration of Ang1 on axonal integrity in the subacute (7 and 14 days post-SCI) and chronic (28, 42, and 56 days post-SCI) phases of injury and on neurobehavioral outcomes in the acute (2 days post-SCI), subacute, and chronic phases of injury. Fiber

tract integrity in the epicenter and perilesional regions will be quantified based on *in vivo* diffusion tensor imaging (DTI) scans. Neurobehavioral outcomes will be evaluated based on standard assessments. *I hypothesize that, compared to the control cohort, increased axonal integrity and improved neurobehavioral recovery will be observed in the Ang1 cohort, and that these measures will be correlated with each other.*

Significance

There is considerable evidence that compromised vasculature plays an important role in initiating pathophysiological events that lead to secondary injury in SCI. There is also some evidence that Ang1 plays an important role in stabilizing vasculature and promoting neuroprotection. The outcome of any treatment is traditionally assessed using invasive techniques such as histology. Such studies provide invaluable information about the injury and mechanism. However, they are not directly applicable to humans, especially in the context of disorders of the central nervous system. The strength of the current studies is their noninvasive and multi-modal nature. For these studies I employed (1) MRI to determine the effects of Ang1 on BSCB compromise, lesion size, and axonal integrity and (2) neurobehavioral assessment to determine the effects of Ang1 on locomotion, axial stability, coordination, sensory-motor integration, rearing behavior, and persistent mechanical allodynia. Both types of methodologies (i.e., MRI and neurobehavioral evaluation) are non-invasive and serially use the animals as their own control, and could be adapted for human SCI patients in the assessment of promising

treatments. Overall, these studies are hypothesized to provide evidence to support a role for Ang1 as a potential therapeutic agent in the management of SCI.

CHAPTER 2:

MATERIALS AND METHODS

Ethics

The protocol employed in these studies was approved by the institutional Animal Welfare Committee. All animal procedures were performed according to the NIH Guide for the Care and Use of Laboratory Animals.

Overview

These studies investigate the role of Ang1, administered acutely after injury, on various aspects of SCI pathology (e.g., compromised BSCB, SCI lesion, and reduced axonal integrity) and neurobehavioral recovery. In order to longitudinally evaluate changes in these pathologies and functional outcomes, animals were serially assayed by MRI and neurobehavioral testing, respectively.

Justification for number of animals

Forty-three male Sprague-Dawley rats were used in these studies (n=40 for experimental investigation and n=3 to provide baseline data for DCE-MRI analysis). Table 2.1 summarizes the animals used for each component of these studies. Based on preliminary studies in our laboratory, power analysis was performed to determine the number of animals required to achieve statistical significance in the proposed studies ($\alpha=0.05$) with power = 0.8. In order to detect changes in MRI metrics (lesion size from anatomical MRI scans, K_{ps} parameter from DCE-MRI scans, and metrics from diffusion tensor imaging (DTI) scans), n=8 animals/treatment were required. In order to detect changes in neurobehavioral scores, n=12 animals/treatment were required. It would be ideal to scan the

animals daily; however, anesthetizing them everyday would lead to an unacceptably high mortality rate. It is our experience that scanning during the acute phase of SCI leads to an extremely high mortality rate; this is one reason why studies were separated into acute studies at a single time point and serial studies. The aim of this study was to evaluate the effect of acutely administered Ang1 in experimental SCI; thus all animals in SCI studies (single study and serial study) received a T7 contusion SCI, and a sham group was not necessary.

Group	No. Animals	Spinal Cord Manipulation	Intraspinal Microinjection	Purpose	Measurements
1, single study	8	SCI, RF coil implantation	Vehicle	Treatment control	MRI scans and neurobehavioral assessment at 2 days post-SCI
2, single study	8		Ang1	Effect of single dose in acute phase	
3, serial study	12		Vehicle	Treatment control	MRI scans and neurobehavioral assessment at 7, 14, 28, 42, and 56 days post-SCI
4, serial study	12		Ang1	Effect of single dose in acute phase	
5	3	Uninjured, RF coil implantation	None	Uninjured control for DCE-MRI analysis	MRI scans 7 days post-implantation

Table 2.1 - Experimental design. Ang1 = angiopoietin-1, DCE = dynamic contrast-enhanced, MRI = magnetic resonance imaging, RF = radiofrequency, SCI = spinal cord injury

Spinal cord injury

All surgical procedures were performed as described previously (Herrera et al., 2009). Male Sprague-Dawley rats (N=40, 300-350 g) were anesthetized with spontaneous inhalation of isoflurane (4%). They were then intubated and maintained under anesthesia by mechanical ventilation with 2-2.5% isoflurane,

30% oxygen and 67.5-68% air through a rodent ventilator (Model 683, Harvard Apparatus, Holliston, MA). The vertebral processes of the sixth and seventh thoracic vertebrae (T6 and T8) were secured to stabilize the vertebral column (Figure 2.1). The spinal cord at the level of T7 was exposed by removing the T7 spinous process and the corresponding laminae. A moderately severe contusion injury (150 kdynes force, 1 sec dwell time) was produced using the Infinite Horizon Impactor (Precision Systems and Instrumentation, LLC, Lexington, KY).

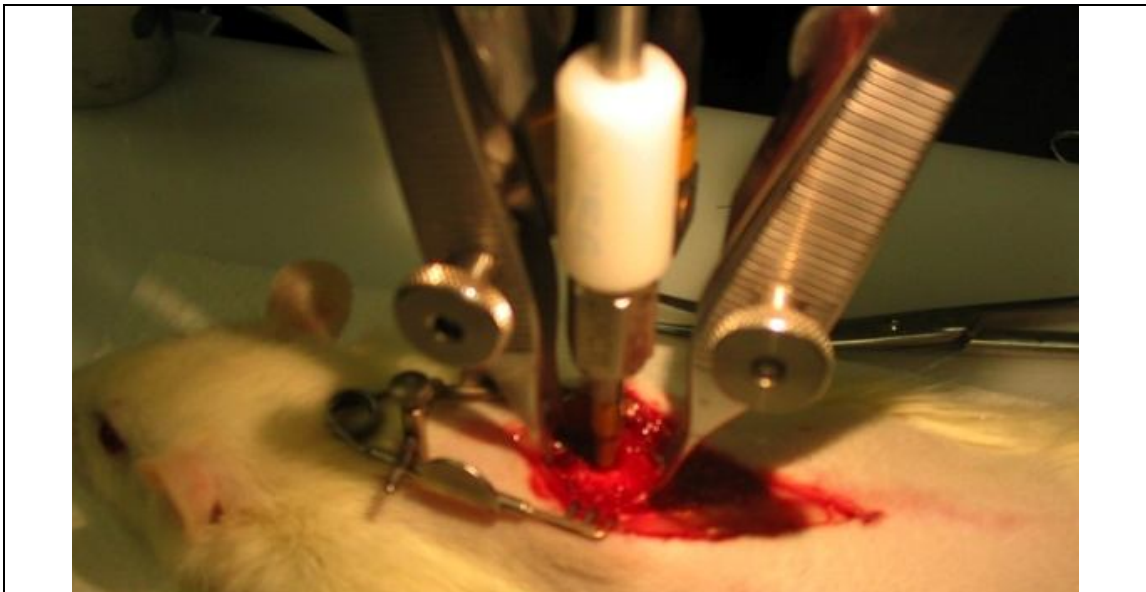


Figure 2.1 – Stabilization of vertebral column at T6 and T8 prior to spinal cord injury. The impactor tip is shown placed directly above the exposed T7 level of the spinal cord.

SCI animals were divided into two groups (n=16 single study and n=24 serial study) and each group was further divided in half (n=8 single study, Ang1 treatment; n=8 single study, vehicle treatment; n=12 serial study, Ang1 treatment; n=12 serial study, vehicle treatment). These animals received a single microinjection (1.5 μ L) of either purified rat albumin (1 μ g/ μ L, Pel-Freez Biologicals,

Rogers, AR) or carrier-free recombinant human Ang1 diluted in 0.1% rat albumin (0.67 $\mu\text{g}/\mu\text{L}$, R&D Systems, Minneapolis, MN) into the lesion site immediately after SCI, at a depth of 1.2 mm and a rate of 0.5 $\mu\text{L}/\text{min}$ through a 70 μm -diameter glass pulled-tip pipette driven by a picospritzer (Parker Hannafin Corp., Fairfield, NJ). The Ang1 dose of 1 μg was selected based on previous results from other studies of blood-organ barrier in immune privileged sites (retina and testis) in rat, which found this dose of Ang1 has led to measurably decreased vascular permeability (Joussen et al., 2002; Haggstrom Rudolfsson et al., 2003). Concerns regarding Cain et al.'s finding of a therapeutic effect of serum albumin treatment in SCI (Cain et al., 2007) are allayed by the fact that the dose of albumin we employed as vehicle control is 133-fold less than that used by Cain et al.

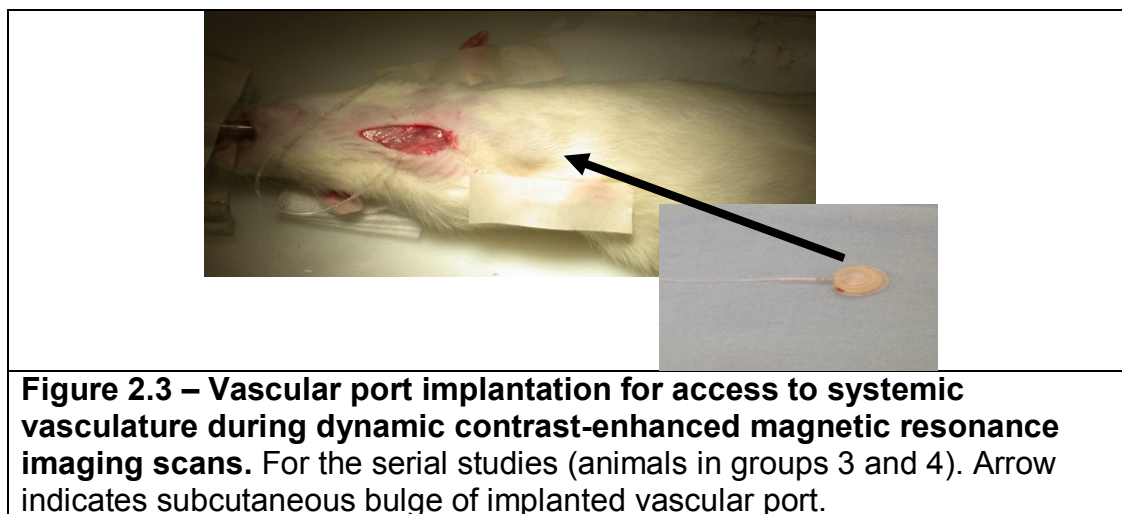
For improved signal-to-noise ratio (SNR) of MRI scans, a radiofrequency (RF) coil (35 mm length x 11 mm width x 7 mm height) was implanted subcutaneously over the injury site without touching the spinal cord (Fenyves and Narayana, 1998) (Figure 2.2). The coils had been coated with a biologically inert, biomedical grade silicone elastomer (Silastic[®] MDX4-4210, Dow Corning, Midland, MI) to electrically isolate it from the tissue and were then sterilized in a gas sterilizer (AN74i Anoprolene Gas Sterilization, Andersen Sterilizers, Inc., Haw River, NJ) prior to implantation. The Larmor frequency for the 7 T field strength of the MRI magnet used is 300 MHz and the resonating frequency of the implanted coil was designed to function at this frequency. The dorsal wound was closed in two layers (paraspinal muscles interiorly and skin exteriorly).



Figure 2.2 – Implantation of radiofrequency coil after spinal cord injury.
The coil improves signal-to-noise ratio on magnetic resonance imaging scans.

For intravenous delivery of gadodiamide (Gd, trademarked as Omniscan, GE Healthcare, Princeton, NJ) during the DCE-MRI scans in animals in groups 1 and 2, the right jugular vein was cannulated and silicone tubing (Instech Solomon, Plymouth Meeting, PA) was implanted and the incisions were closed. The silicone tubing was extended outside of the animal's neck area in order to allow vascular access for delivery of the contrast agent during the DCE-MRI scan. For animals in groups 3 and 4 (serial studies), the right jugular vein was cannulated, and a vascular port with silicone tubing (Instech Solomon, Plymouth Meeting, PA) was implanted (Figure 2.3), and the incisions were closed. To ensure patency of the jugular port and connected tubing over the 8-week duration of the serial studies, 0.2 mL of 0.9% saline was injected into the port before and after each scan. If resistance on the plunger of the syringe was felt during administration of the saline bolus, the port or tubing was assumed to be blocked and the animal was excluded

from further MRI scanning. Final confirmation of patency of the jugular port was assessed after the DCE-MRI scan, in which contrast agent could be readily observed in the vasculature.



Post-SCI animal care

Animals were allowed to recover in warmed cages and saline was administered subcutaneously. Animals also received subcutaneous cefazolin (15 mg/kg, West-Ward Pharmaceuticals, Eatontown, NJ) twice daily for 7 days, Buprenex (0.01 mg/kg, Hospira Inc., Lake Forest, IL) twice daily for 5 days, and 0.9% saline (3-5 mL, Hospira Inc., Lake Forest, IL) twice daily for 5 days. Urinary bladders were manually expressed twice daily until spontaneous return of urination. Zinc oxide ointment (E. Fougera & Co., Melville, NY) was applied if the skin appeared to be irritated. Triple antibiotic ointment (Alpharma USPD Inc., Baltimore, MD) was applied on wounds or broken skin. When necessary, rats were gently bathed with hypoallergenic shampoo (HydroSurge, Carlsbad, CA) and warm water.

Neurobehavioral assessment

From a clinical perspective, regaining neuromotor function and the ability to perform activities of daily living are the most tangible benefits of SCI therapy (Estores, 2003). In order to assess the effects of Ang1 on neurobehavioral recovery post-SCI, five neurobehavioral assays were performed. All assays were performed by two independent observers who were blinded to the treatment groups. The neurobehavioral assessments were performed prior to injury, and prior to each MRI scan (i.e., post-SCI neurobehavioral data was recorded on the same day of MRI scans) to reduce any potentially interfering effects of the anesthesia using during the scans.

In group 1-4 animals, open field locomotion was assessed using the Basso-Beattie-Bresnahan (BBB) scale (range of scores: 0-21) (Basso et al., 1995). To perform the BBB assessment, the animal was placed in an open field and encouraged to continuously move. If no hindlimb movement was observed, a score of zero was given; if a slight movement of one or two joints was seen, then a score of one was assigned. The scores increased as the animal displayed greater stability, coordination, and functional recovery. The highest score of 21 was given if the rat displayed “coordinated gait, consistent toe clearance, parallel paw position throughout stance, consistent trunk stability, and a consistently lifted tail.”

Although group 1-2 animals only underwent the BBB assay, group 3-4 animals received additional neurobehavioral assessments. Once the BBB score was ≥ 5 (this usually occurred by 7-14 days post-SCI and indicates “slight movement of two joints *and* extensive movement of the third”), axial stability and

postural control was tested with the inclined plane test (Rivlin and Tator, 1977). Animals were placed on an inclined plane whose angle of elevation could be adjusted. The maximum angle of incline for which the rat could maintain his position for 5 sec without slipping was recorded.

Once the BBB score was ≥ 9 (this usually occurred by 14-28 days post-SCI and indicates “plantar placement of the paw with weight support in stance only (i.e., when stationary); or occasional, frequent, or consistent weight supported dorsal stepping and no plantar stepping”), mechanical allodynia was assayed with the vonFrey hair filament test (Peng et al., 2006). Fifteen minutes prior to evaluation, rats were placed in clear Plexiglas boxes on an elevated platform with mesh surface, for acclimation. After this period, an electronic vonFrey anesthesiometer (IITC Life Science, Inc., Woodland Hills, CA) was used to probe forepaw sensitivity. The filament was alternatingly applied to the plantar surface of each forepaw and the maximum pressure required to elicit paw withdrawal was recorded. This process was performed five times and the highest and lowest pressure recordings for each paw were discarded; data analysis was carried out on the remaining three values for each forepaw. Based on previous work in our lab (Sundberg, 2009), chronic pain was defined as mean threshold values at days 28, 42, and 56 post-SCI being lower than that at baseline (pre-SCI), for both forepaws.

Once the BBB score was ≥ 12 (this usually occurred by 14-28 days post-SCI and indicates “frequent to consistent weight supported plantar steps and occasional forelimb-hindlimb coordination”), animals were assessed for forelimb-hindlimb coordination, sensory-motor integration, and fine motor control with the

grid walk test (Bresnahan et al., 1987). Animals were placed on a walkway grid with 2 cm x 2 cm wide gaps. Animals had to correctly place their limbs on the grid bars in order to traverse the walkway. A minimum of 30 steps was counted and the number of errors (i.e. footfalls) of either the hindlimb or forelimb was also counted during that time. The data from the grid walk test was analyzed as a ratio of footfalls to total steps and reported as the percent of footfalls.

Starting with the 2-week post-SCI time point, computerized activity boxes were used to assess fine motor movements, ambulation, and rearing. Animals were placed in activity chambers for 15-minute testing periods and data were collected using the software and hardware provided by the Photobeam Activity System (PAS) with Flexfield (San Diego Instruments, Inc., San Diego, CA). The PAS acquired data reflecting the animal's movements within the activity chamber by recording the number of times photobeams were obstructed in a x-, y-, and z-axis oriented grid system (Mills et al., 2001). Measures from the computerized activity boxes included gross motor movement, fine motor movement, and rearing activity.

Animal preparation for MRI scans

Animals underwent MRI scans on the days specified in Table 2.1. On the day of MRI scan, animals were anesthetized with an induction dose of 4% isoflurane and were then intubated and mechanically ventilated with 2-2.5% isoflurane, 30% oxygen and 67.5-68% air through a rodent ventilator (Model 683, Harvard Apparatus, Holliston, MA) for the duration of the scan (approximately 2.5

hours). Silicone tubing (Instech Solomon, Plymouth Meeting, PA) attached to a syringe containing Gd at a concentration of 0.1 mmol/kg body weight (0.2 mL/kg body weight) was attached to the tubing protruding from the animal's neck (for animals in groups 1 and 2) or to the subcutaneous vascular port (for animals in groups 3 and 4).

Animals were placed in the supine position on a Plexiglas bed and a 35 mm x 40 mm coil that was inductively coupled to the implanted RF coil was placed under the rat. The respiratory rate and rectal temperature were monitored throughout the experiment with a MRI-compatible physiologic monitoring unit (Model 1025, SA Instruments, Inc., Stonybrook, NY). A pulse oximeter (Model 8600V, Nonin Medical Inc., Plymouth, MN) was used to monitor heart rate and oxygen levels. For the duration of the experiments, a heating system (Model 11007B, SA Instruments, Inc., Stonybrook, NY) was used to maintain the body temperature at 36 °C.

MRI data acquisition

All MR studies were performed on a 7 Tesla Bruker scanner (70/30 USR Bruker Biospec, Karlsruhe, Germany) using a 116 mm shielded gradient insert that is capable of producing maximum gradient amplitude of 400 mT/m with 80 μ s rise time. Prior to performing each MRI scan, a quality assurance scan that included SNR and magnetic field homogeneity assessment was performed, as described elsewhere (Cohen et al., 2009). After initially shimming the magnet using the

manufacturer's autoshim routine (ParaVision, Bruker Biospec, Karlsruhe, Germany), manual adjustment of the X, Y, Z, and Z^2 shims was performed.

Following the acquisition of a tri-pilot scan (for locating the spinal cord), either anatomical imaging (group 1 and 2 animals) or diffusion tensor imaging (DTI, group 3 and 4 animals) was performed. DTI scans were not performed in group 1 and 2 animals because of the concerns about high mortality rate due the long scan times. In addition, the poor tissue contrast at this acute time point precludes meaningful analysis of axonal integrity in the injured area. DTI data were acquired using an echo planar imaging (EPI) readout sequence with 4 shots, repetition time (TR) = 3000 ms, echo time (TE) = 39.73 ms, receiver bandwidth of 200 kHz, 42 gradient directions (using a rotationally invariant encoding scheme with 21 positive and 21 negative encoding directions that were balanced and unbiased (Madi et al., 2005)), acquisition matrix of 128x128, square field of view (FOV) of 2.62 cm x 2.62 cm, 25 contiguous 1-mm-thick slices, and b-factor = 842 sec/mm^2 (gradient amplitude = 386 mT/m, gradient pulse duration δ = 2 ms and gradient pulse separation Δ = 22 ms). DTI images were reconstructed to 256x256. The DTI scan lasted approximately 35 minutes.

The high-resolution anatomical images were acquired with a dual-echo rapid acquisition relaxation enhancement (RARE) scan using TR = 3200 ms, TE = 21.2 ms and 63.6 ms, acquisition matrix = 256x256, FOV = 2.62 cm x 2.62 cm, and 35 contiguous 1-mm-thick slices. The RARE scan lasted approximately 15 minutes.

Finally, the DCE-MRI scan was performed (Cohen et al., 2009; Patel et al., 2009). Two repetitions of pre-contrast T1-weighted spin echo, axial images were acquired using TR = 500 ms, TE = 10.4 ms, acquisition matrix = 256x128 (zero-filled to 256x256), FOV = 2.62 cm x 2.62 cm, and 35 contiguous 1-mm-thick slices). Then, without moving the animal, a bolus of Gd was injected in less than 5 seconds into the cannulated jugular vein via the silicone tubing (group 1 and 2 animals) or vascular port (group 3 and 4 animals). Immediately following the administration of Gd, T1-weighted images were continuously acquired for an additional 18 repetitions, each with a temporal resolution of 4 minutes, as part of the DCE-MRI scan. The DCE-MRI scan lasted approximately 80 minutes.

Animal handling after MRI scans

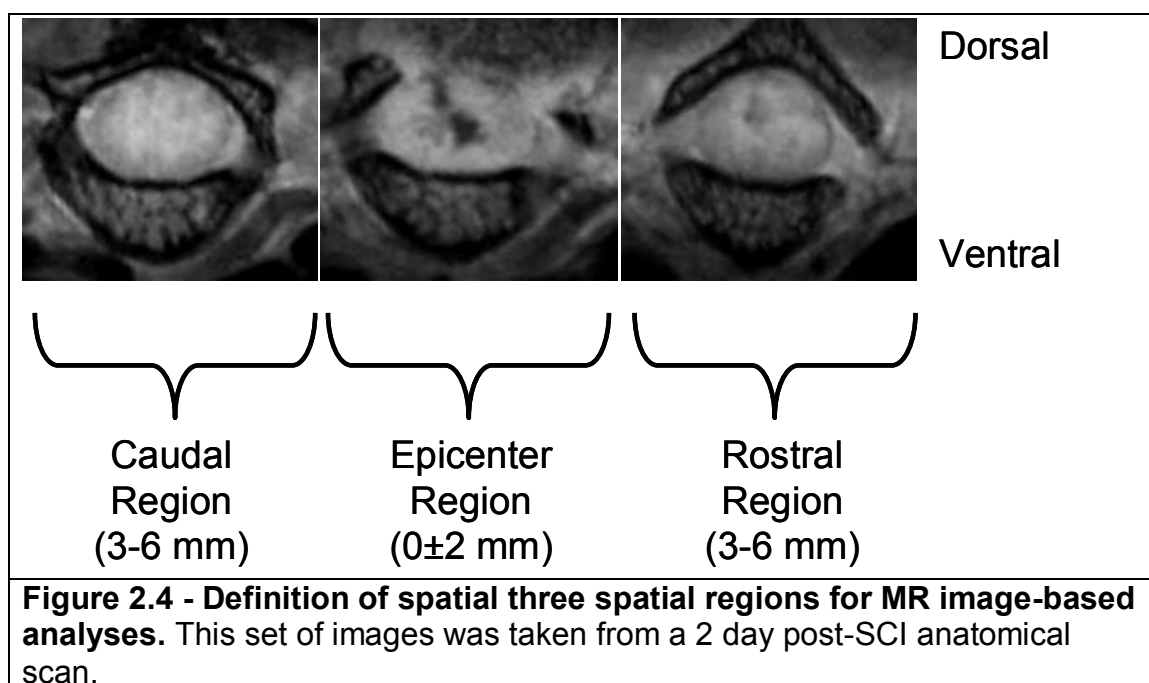
After the MRI scans, rats were weaned off of the ventilator and anesthesia, until they breathed spontaneously. They were then extubated and placed under a heating lamp for 15 minutes.

MRI data analysis: inclusion/exclusion criteria and definition of spatial regions

Data were excluded if the SCI injury was too severe and resulted in observable illness (e.g. lack of appetite) or abnormal pathology on MRI as indicated by extended spatial spread of injury on RARE scans (loss of gray-white matter contrast in >10 slices at 2 days post-SCI or in >15 slices at 7 days post-SCI). In addition, data were excluded based on neurobehavioral criteria. An injury

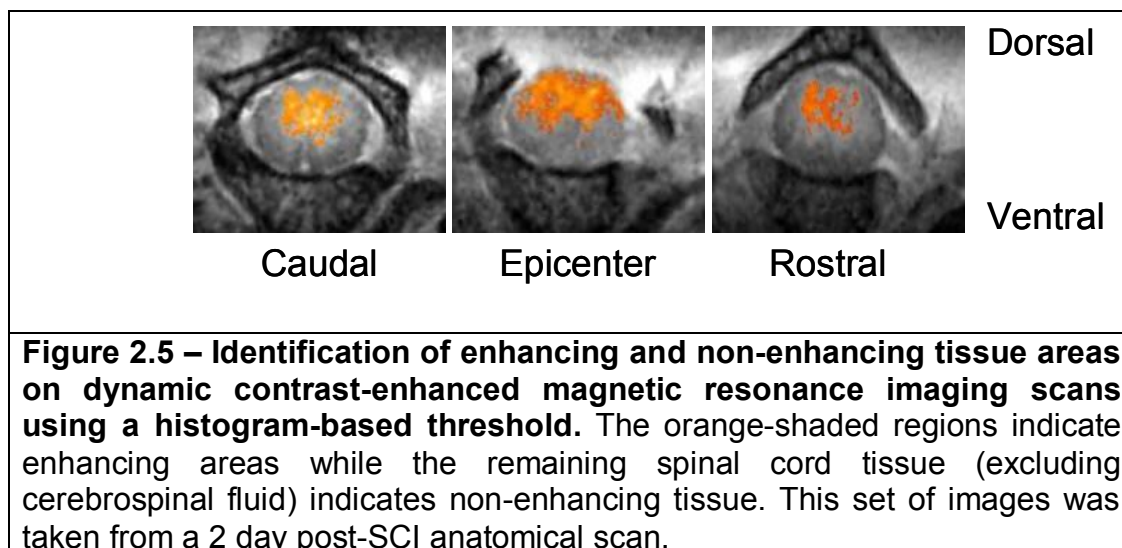
was considered too light if the BBB score was >5 at 3 days post-SCI and too severe if the BBB score was <5 at 14 days post-SCI.

In regards to MRI-based identification of spinal cord spatial regions, the first step entailed identification of the MRI epicenter slice. This slice was verified by two independent trained observers as the single slice containing the largest lesion (RARE scan) and greatest extravasation of Gd into the spinal cord parenchyma (DCE-MRI scan). If the observers' choice of epicenter slice did not match, the observers conferred until the epicenter slice was agreed upon. Next, the length of the spinal cord was divided into three spatial regions: epicenter region (SCI epicenter slice, 2 slices immediately caudal to the epicenter slice, and 2 slices immediately rostral to the epicenter slice), caudal region (slices 3-6 mm caudal to the epicenter slice), and rostral region (slices 3-6 mm rostral to the epicenter slice), as indicated in Figure 2.4. The size of the regions corresponds to those of previously published reports (Cohen et al., 2009; Patel et al., 2009).



MRI data analysis: DCE-MRI scans (BSCB compromise and permeability)

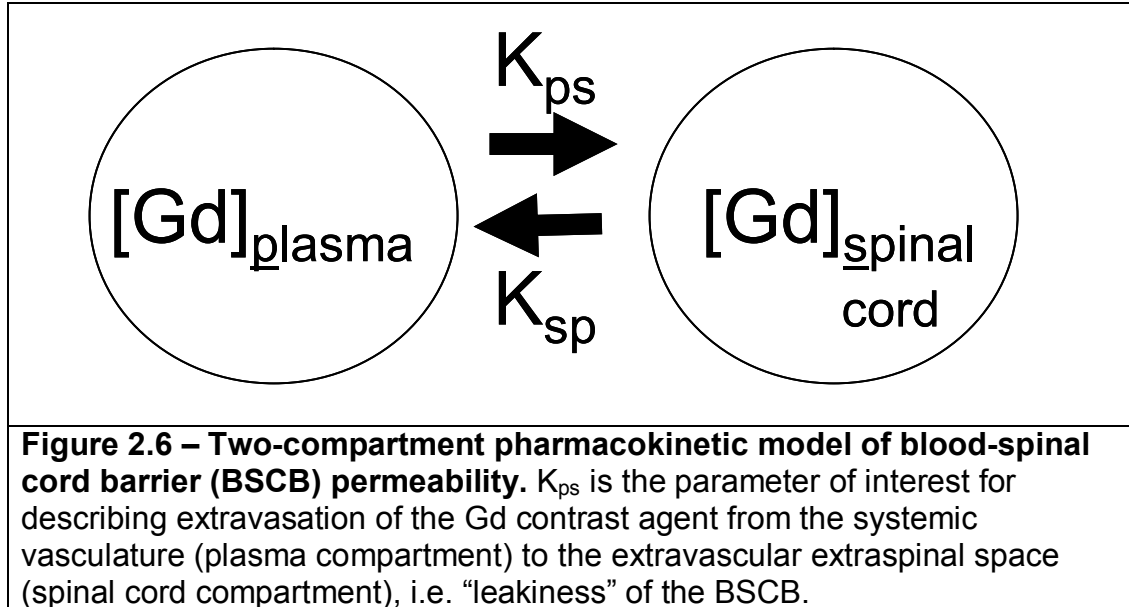
Frank enhancement in tissue on post-contrast DCE-MRI scans represents areas of compromised BSCB that allow for extravasation of Gd from systemic vasculature into the spinal cord parenchyma. Data were separately analyzed for enhancing and normal-appearing tissue areas. Unlike previous studies that relied on objective segmentation of these regions from the DCE-MRI scans (Cohen et al., 2009; Patel et al., 2009) based on what was visually observable, these studies employed a slice-by-slice objective technique that is solely dependent on the signal intensity distribution (SID) of the total spinal cord cross sectional area. First, a region of interest (ROI) enclosing the entire spinal cord, but excluding peripheral cerebrospinal fluid (CSF), was drawn. Next, the SID was obtained. Enhancing tissue areas were defined as pixels in the entire spinal cord ROI whose signal intensity was above the 35% threshold, or in other words, in the upper 65% of the SID (Figure 2.5). This threshold was determined by two independent and trained observers as the threshold that best corresponded to visual areas of frank contrast enhancement on the DCE-MRI scans.



After application of the SID-based threshold in a given slice, if enhancing tissue areas was detected, then the corresponding normal-appearing tissue area for that slice was defined as the difference between the total spinal cord area and the enhancing areas. If no enhancing areas were detected in a slice, then the normal-appearing area for that slice was the entire spinal cord area. Thus, it was possible for a single slice of the spinal cord to simultaneously contain enhancing and normal-appearing tissue areas. In each slice, gross BSCB compromise (expressed as a percent) was defined as the ratio of the area of the enhancing ROI to the area of the spinal cord cross-section. For reporting of gross BSCB compromise by spatial region, the gross compromise for each slice in the region was averaged.

The mathematical model for analyzing the DCE-MRI data in rat spinal cord has been previously described (Bilgen and Narayana, 2001). For quantification of Gd leakage through the compromised BSCB, a two-compartment model was employed (Figure 2.6). One compartment represents the systemic circulation (intravascular) and the second compartment represents the extravascular extracellular space (EES) within the spinal cord. The adequacy of a two-compartment model in spinal cord has been demonstrated in (Bilgen et al., 2001; Bilgen et al., 2002; Cohen et al., 2009; Patel et al., 2009). The concentration of Gd in the spinal cord EES at each time point t , $(Gd(t)_{EES})$, was estimated according to the following equation (Cohen et al., 2009):

$$[Gd(t)_{EES}] = K_{ps} \times \left(\left(\frac{0.4}{0.6 - K_{sp}} + \frac{0.16}{0.04 - K_{sp}} \right) e^{-K_{sp}t} - \left(\frac{0.4}{0.6 - K_{sp}} \right) e^{-0.6t} - \left(\frac{0.16}{0.04 - K_{sp}} \right) e^{-0.04t} \right)$$

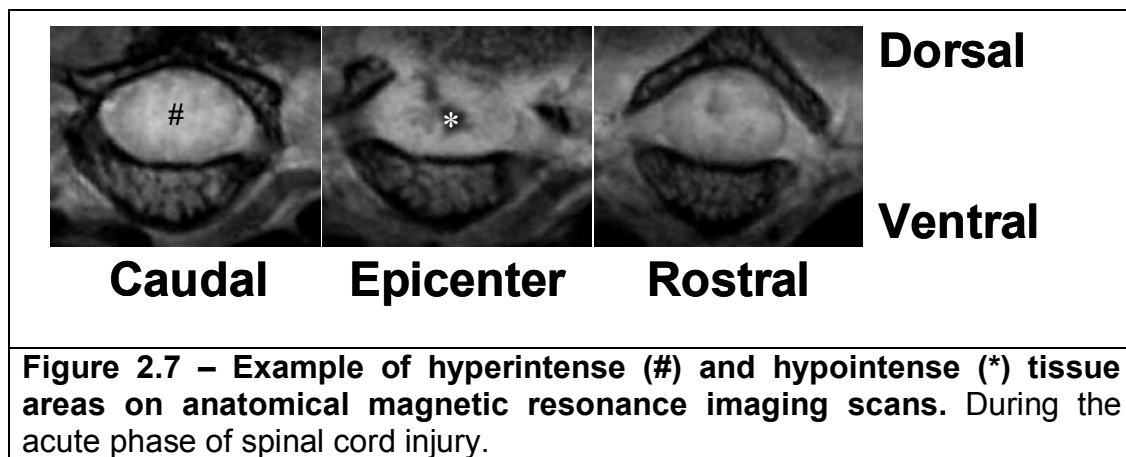


The parameter K_{ps} represents the transfer rate of Gd from systemic circulation to the EES of the spinal cord. The rate of influx of Gd from the systemic circulation into the EES is $K_{ps} * [Gd(t)]_{\text{Systemic Circulation}}$. The values of $Gd(t)_{\text{EES}}$ at each time point (based on DCE-MRI data) were fitted to the above equation using a nonlinear least squares method in Matlab (MathWorks, Inc., Natick, MA) to estimate K_{ps} . Because of the uncertainty in the exact time of Gd injection and because it improved the ability of the model to fit the data, the time of contrast injection (t_0) was also estimated as a part of the curve fitting routine.

MRI data analysis: RARE scans (lesion size)

For SCI lesion analysis, the second echo of the dual-echo RARE MRI sequence provides important information about the pathological tissue changes (e.g., hemorrhage and necrosis). Acutely after SCI, hypointense (dark) areas on

these images represent hemorrhage while hyperintense (bright) areas represent edema (Weirich et al., 1990) (Figure 2.7). Hyperintense, hypointense, and total (hyperintense + hypointense) lesion sizes were calculated for each slice in the three spatial regions. Data were separately analyzed for hyperintense and hypointense lesions. Unlike previous studies that have relied on hand-drawn segmentation (Nout et al., 2009) or objective segmentation of these lesions based on absolute pixel intensity thresholds (Sundberg, 2009; Qian et al., 2010), the current studies employed a slice-by-slice objective technique based on the probability density function (PDF) of pixel intensity in each slice (histogram-based approach).



Images of the second echoes of the 35-slice RARE scan were exported from Paravision software (Bruker Biospec, Karlsruhe, Germany) in *analyze* format. The images were processed to reduce the field inhomogeneity using in-house developed software (Hui et al., submitted). Using ImageJ software (NIH, Bethesda, MD), a ROI encompassing the entire spinal cord but excluding peripheral CSF was

drawn for each slice within the 13 slices under investigation (this represents a span of 13 mm centered at the SCI epicenter). Next, the PDF of pixel intensity that represents the normalized pixel intensity distribution (unit area under the curve) was generated for each slice. Finally, the area of the SCI lesion as a fraction of the spinal cord cross-sectional area was determined in an objective way. On a slice-by-slice basis, pixels whose intensity was less than or equal to $\mu_{\text{pixel intensity}} - n \cdot \sigma_{\text{pixel intensity}}$ (μ represents mean and σ represents standard deviation of the mean) were considered to compose the hypointense lesion and pixels whose intensity was greater than or equal to $\mu_{\text{pixel intensity}} + n \cdot \sigma_{\text{pixel intensity}}$ were considered to compose the hyperintense lesion, $n \in \{1, 1.5, 2, 2.5, 3\}$. For example, assuming a normal distribution, a threshold of $n=2$ represents an area under the curve of 2.28% at the end of each tail, resulting in 95.4% of all pixels being rejected upon application of the threshold. For each slice, the total lesion area was defined as the sum of the hyperintense and hypointense lesion areas.

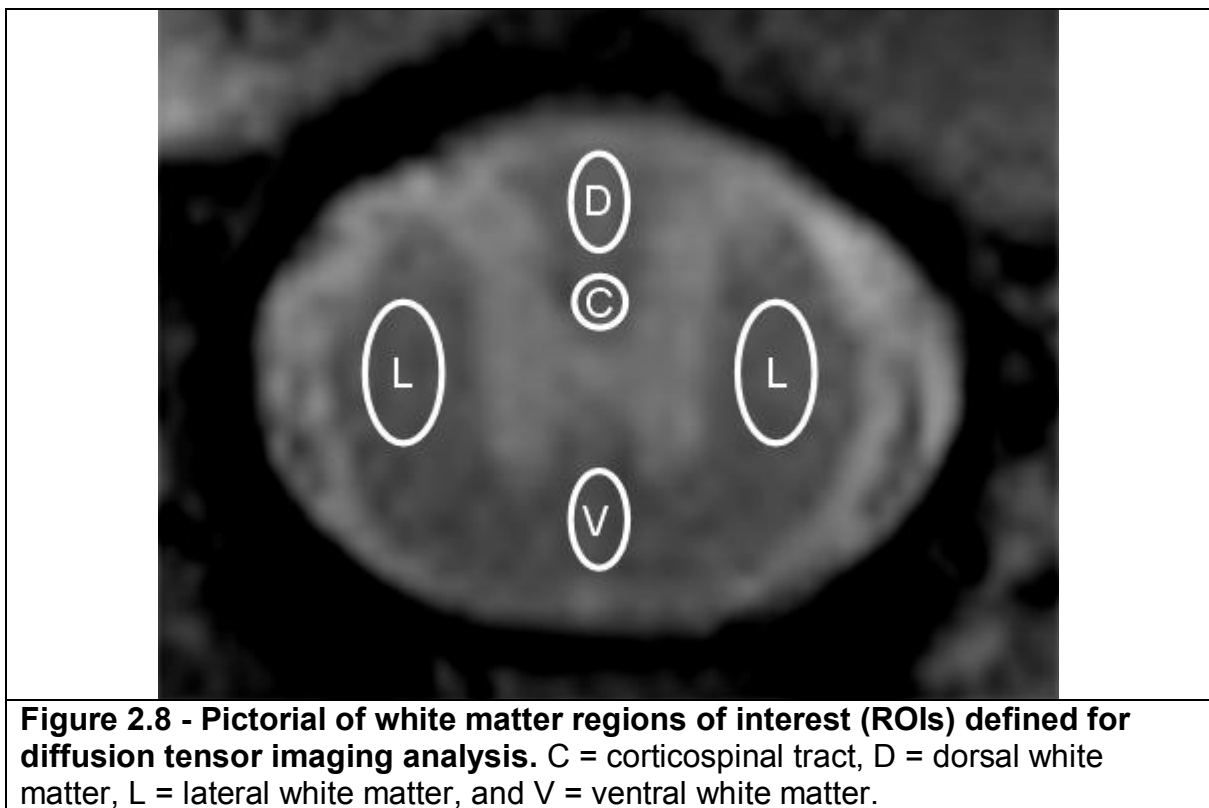
Because there is no gold standard for quantitating SCI lesion size on MRI scans (most approaches employ human raters) and histological approaches tend to overestimate lesion size (Ditor et al., 2008), the validity of the histogram-based approach described above was evaluated using the majority voting rule on segmentations of human raters. Four independent experienced raters segmented (using ImageJ) the hyperintense and hypointense lesion from a random series of 16 anatomical MRI slices representing the heterogeneity of time points and spatial regions under study. The raters were instructed to limit their segmentation to the spinal cord parenchyma, excluding the bordering CSF. The raters were blinded to

each other's segmentations and were proctored by the same investigator, who did not provide any guidance during the approximately 30-minute segmentation period. The raters' segmentations were individually saved using the ROI manager in ImageJ and the hyperintense and hypointense lesion sizes in each slice were calculated for each rater. For each slice, the reference image was defined on a pixel-by-pixel basis, assigning a value of 1=yes when the majority of raters (>2) assigned a value of 1=yes to that pixel. All other pixels in the reference image were assigned a value of 0=no. Next, the histogram-based segmentation was applied to the 16 rater-segmented slices, $\forall n$. The n-value of the histogram-based approach that yielded the most comparable performance with rater-based hyperintense and hypointense lesion sizes (based on measures including sensitivity and specificity) was defined as the optimal histogram-based approach n-value. This n-value was used for the quantification of hyperintense, hypointense, and total lesion area in the Ang1 and vehicle groups.

MRI data analysis: DTI scans (axonal integrity)

All DTI data were analyzed using procedures described elsewhere (Madi et al., 2005). In these studies, fractional anisotropy (FA) was targeted as the measure of anisotropy because it is less susceptible to noise (Hasan et al., 2004). In order to improve pathologic specificity for fiber tract integrity, transverse diffusivity (λ_T), longitudinal diffusivity (λ_L), and mean diffusivity (MD) were also determined from DTI data (Deo et al., 2006; Herrera et al., 2007). Decoding and diagonalization was performed using in-house developed software (Hasan and Narayana, 2003) that

was implemented under IDL 6.1 (ITT Visual Information Solutions, Boulder, CO). DTI Studio (Department of Radiology, Johns Hopkins School of Medicine) was used to calculate the value of the DTI measures within each ROI (e.g. dorsal white matter [WM]). The specific WM ROIs are displayed in Figure 2.8. In addition to the evaluation of DTI measures in the lateral, dorsal, and ventral WM ROIs (Deo et al., 2006), a dorsal corticospinal tract (CST) ROI was also evaluated. The placement of the ROIs in these areas, particularly the CST, facilitated longitudinal correlation analysis between the DTI measures and measures from neurobehavioral assays.



Statistics

Data and statistical analysis was performed using Intercooled Stata version 9.2 (StataCorp LP, College Station, TX). At least 6 animals per treatment group per

time point were included for analysis of all primary outcome measures, which included:

- BBB score, angle of maximum incline tolerated, footfalls (%), prevalence of chronic pain, gross motor movement, fine motor movement, and rearing activity from neurobehavioral assays (at time points indicated in the “Neurobehavioral assessment” section of this chapter)
- K_{ps} metric (min^{-1}) in enhancing and non-enhancing areas, and frank contrast enhancement (%) from DCE-MRI scans (at 2, 7, 14, 28, 42, and 56 days post-SCI)
- Hyperintense and hypointense lesion size (percent of spinal cord cross-sectional area) and specificity/sensitivity of rater- and histogram-based approaches for lesion segmentation from RARE MRI scans (at 2, 7, 14, 28, 42, and 56 days post-SCI)
- FA, MD, λ_T , and λ_L values in white matter ROIs from DTI scans (at 7, 14, 28, 42, and 56 days post-SCI)

Statistical analyses were performed to determine (1) if, compared to vehicle, administration of Ang1 acutely after SCI affected any of these parameters and (2) whether there were any correlations between (a) BBB score and RARE and DTI measures and between (b) RARE and DTI measures. Wilcoxon rank-sum analysis was used to test for significant differences between treatment groups at each time point.

For analysis of longitudinal data, the generalized estimating equation (GEE) approach was used. The GEE technique has been widely used for the analysis of

repeated measurement data due to flexibility in modeling nonuniform correlational structures of repeated measurements and in handling the unequal number of observations for each experimental unit. GEE was used to examine the pair-wise association of MRI metrics and neurobehavioral measures.

All values are reported as mean \pm standard error of the mean (SEM) unless otherwise stated. Statistical significance was defined as $\alpha = 0.05$, with corrections for multiple comparisons based on the multiple spatial regions and time points (Bonferroni adjustment).

CHAPTER 3:

EFFECT OF SINGLE ACUTE ANG1 DOSE ON BLOOD-SPINAL CORD BARRIER COMPROMISE AND PERMEABILITY

INTRODUCTION

Following the primary mechanical damage from contusive injury to the spinal cord, various secondary pathobiological processes ensue. The secondary injury is the therapeutic target for improving long-term outcome. Compromise of the BSCB is a secondary mechanism that plays an important role in SCI (Noble and Maxwell, 1983; Noble and Wrathall, 1987, 1988, 1989; Popovich et al., 1996; Tator and Koyanagi, 1997; Mautes et al., 2000; Pan et al., 2001; Bilgen et al., 2002; Pan et al., 2003; Whetstone et al., 2003; Sharma, 2005; Maikos and Shreiber, 2007; Pan and Kastin, 2008; Cohen et al., 2009). Studies investigating the acute mitigation of BSCB breakdown have reported neuroprotective, anti-inflammatory, and locomotor recovery benefits in SCI animal models (Sharma, 2000; Pan et al., 2001; Noble et al., 2002; Nyberg and Sharma, 2002; Kaptanoglu et al., 2003; Sharma, 2003, 2006; Sharma et al., 2006a; Sharma et al., 2007). However, some experimental therapies have required high doses that may be inappropriate in human SCI patients due to harmful side effects.

Angiopoietin-1 is an essential protein (Suri et al., 1996) that plays a role in vascular development and remodeling, specifically in the stabilization of blood vessels (Hayes et al., 1999; Thurston et al., 1999; Thurston et al., 2000; Koh et al., 2002; Uemura et al., 2002; Baffert et al., 2006), via activation of the Tie-2 receptor tyrosine kinase expressed on endothelial cells (Davis et al., 1996). Ang1's effects have been studied *in vitro*, suggesting mechanisms of action that include increased endothelial cell survival (Papapetropoulos et al., 2000; Harfouche et al., 2002; Tadros et al., 2003), reduced inflammation (Hughes et al., 2003; Imhof and

Aurrand-Lions, 2006), upregulation of tight junction proteins (Iizasa et al., 2002; Hori et al., 2004; Wang et al., 2007), and neuroprotection (Valable et al., 2003). Ang1 is thought to have therapeutic potential in reducing blood-brain barrier breakdown after brain injury (Nourhaghighi et al., 2003) and has been shown to reduce vascular permeability in experimental models of CNS vascular disease (Zhang et al., 2002; Valable et al., 2005; Ohab et al., 2006; Chen et al., 2008; Childs et al., 2008; Cui et al., 2008a; Cui et al., 2008b; Onda et al., 2008). Recently, daily administration of Ang1 post-SCI was shown to reduce vascular permeability and CD3-positive T cell infiltration after experimental SCI in a mouse model (Han et al., 2010). Compared to other therapies that may reduce BSCB permeability, Ang1 has been shown to be tolerated at high circulating levels (Thurston et al., 2000).

Dynamic contrast-enhanced MRI is a powerful noninvasive technique for quantifying BSCB permeability *in vivo* in SCI (Runge et al., 1997; Bilgen et al., 2001; Bilgen and Narayana, 2001; Cohen et al., 2009; Patel et al., 2009). In DCE-MRI, T1-weighted magnetic resonance images are serially acquired following intravenous administration of paramagnetic contrast agents such as gadodiamide (Gd, molecular weight (MW) = 0.573 kDa) (Tofts et al., 1999). In the absence of SCI, the intact BSCB strictly regulates entry of molecules from the systemic vasculature into the spinal cord. However, when the BSCB is compromised due to SCI, these molecules leak out from the vasculature into the spinal cord parenchyma (Baldwin et al., 1998). When a contrast agent (e.g., Gd) extravasates

into the injured spinal cord via the compromised BSCB, it renders the surrounding tissue area hyperintense on T1-weighted MRI scans.

In the acute phase of SCI, frank enhancement of tissue is observed due the mechanical trauma-induced BSCB disruption in the epicenter region (Bilgen et al., 2001) and spreads to the adjacent regions (Bilgen et al., 2000). However, recent studies have demonstrated that the so-called “normal appearing” non-enhancing tissue areas, those with no visual contrast enhancement, also exhibit compromised BSCB (Kobiler et al., 2001; Cohen et al., 2009; Patel et al., 2009). Using an appropriate pharmacokinetic model (Bilgen and Narayana, 2001), the temporal changes in the contrast agent-induced signal increase observed with DCE-MRI can be quantitatively related to the BSCB permeability (Bilgen et al., 2001; Bilgen and Narayana, 2001; Bilgen et al., 2002; Bilgen et al., 2007; Cohen et al., 2009; Patel et al., 2009).

In the present studies we used DCE-MRI to investigate the effects of a single dose of Ang1 (administered intraspinally immediately after experimental SCI) on the temporal and spatial evolution of frank BSCB compromise and BSCB permeability. For each time point assessed (days 2, 7, 14, 28, 42, and 56 post-SCI), at least 6 animals were studied in each group.

RESULTS

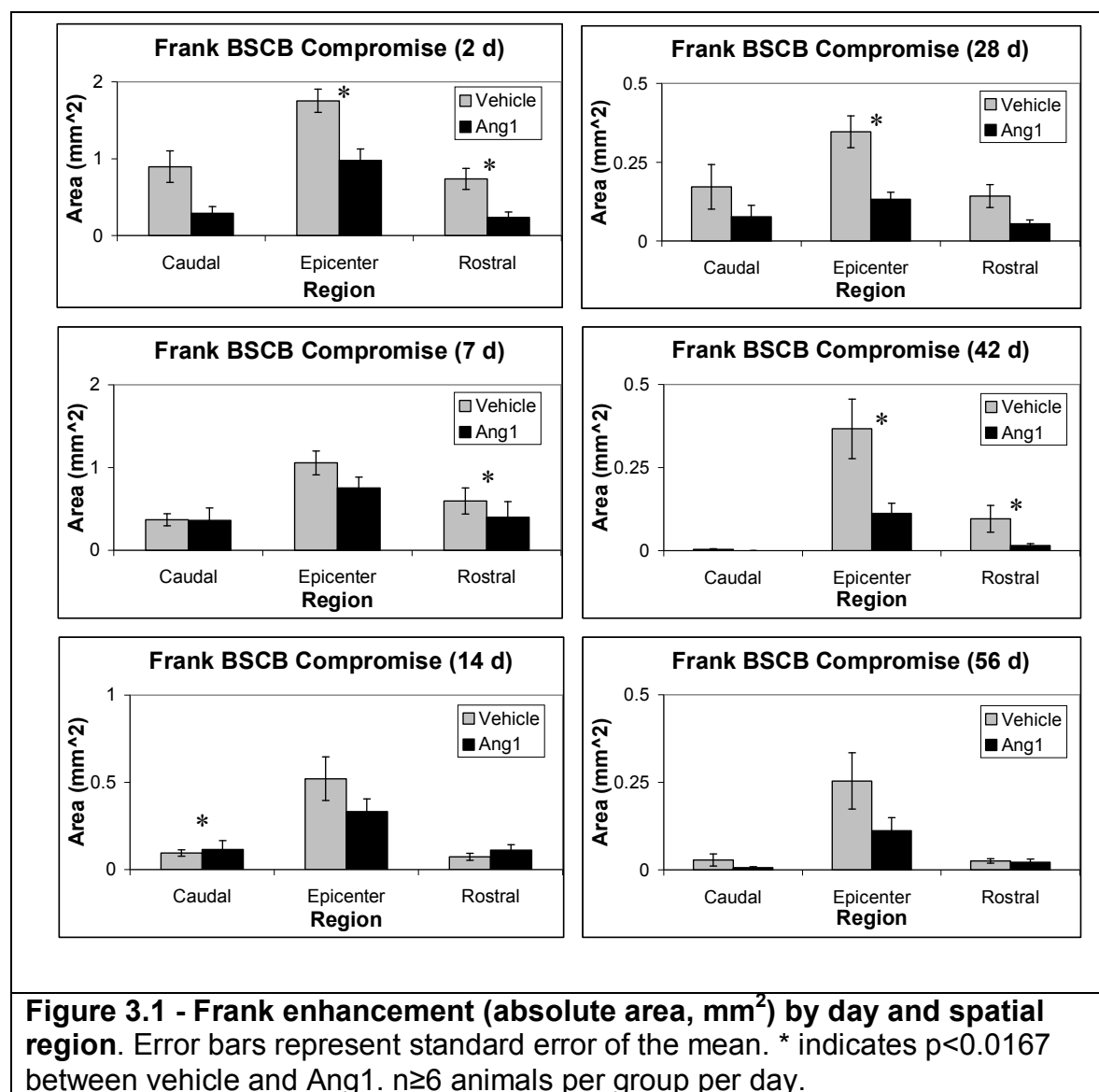
Frank enhancement (absolute area)

Frank enhancement on DCE-MRI scans is a result of gross BSCB compromise. Figure 3.1 displays the frank enhancement in absolute area (mm^2 , defined as the area of spinal cord tissue with contrast-enhancement on DCE-MRI scans above the 35% threshold) by day and spatial region, while Figure 3.2 displays the data longitudinally. Compared to vehicle, Ang1 treatment resulted in a significant increase in frank enhancement in the caudal region at day 14 post-SCI, while it resulted in a significant decrease in the epicenter region at days 2, 28, and 42 post-SCI, and in the rostral region at days 2, 28, and 42 post-SCI.

Figure 3.3 displays the data by time period. Compared to vehicle, Ang1 treatment resulted in a significant decrease in frank enhancement (absolute area) in the acute phase (epicenter and rostral regions), subacute phase (caudal and rostral regions), and chronic phase (epicenter and rostral regions).

Table 3.1 summarizes, for each group, the significant spatial and temporal differences in frank enhancement after SCI. In all three regions and in each group, there was a significant reduction at days 42 and 56 compared to day 2 post-SCI, indicating reduced frank enhancement over time in both groups. In the caudal region, there was a significant decrease from day 28 post-SCI to day 42 post-SCI in both groups, with a further reduction at day 56 post-SCI in the Ang1 group only, indicating continued restoration of the BSCB in this region. At all time points in both groups, the epicenter region contained significantly greater frank enhancement than the adjacent caudal and/or rostral region. In addition, the rostral region

contained significantly greater frank enhancement compared to the caudal region in the chronic phase, indicating a spatial asymmetry in restoration of the BSCB after SCI.



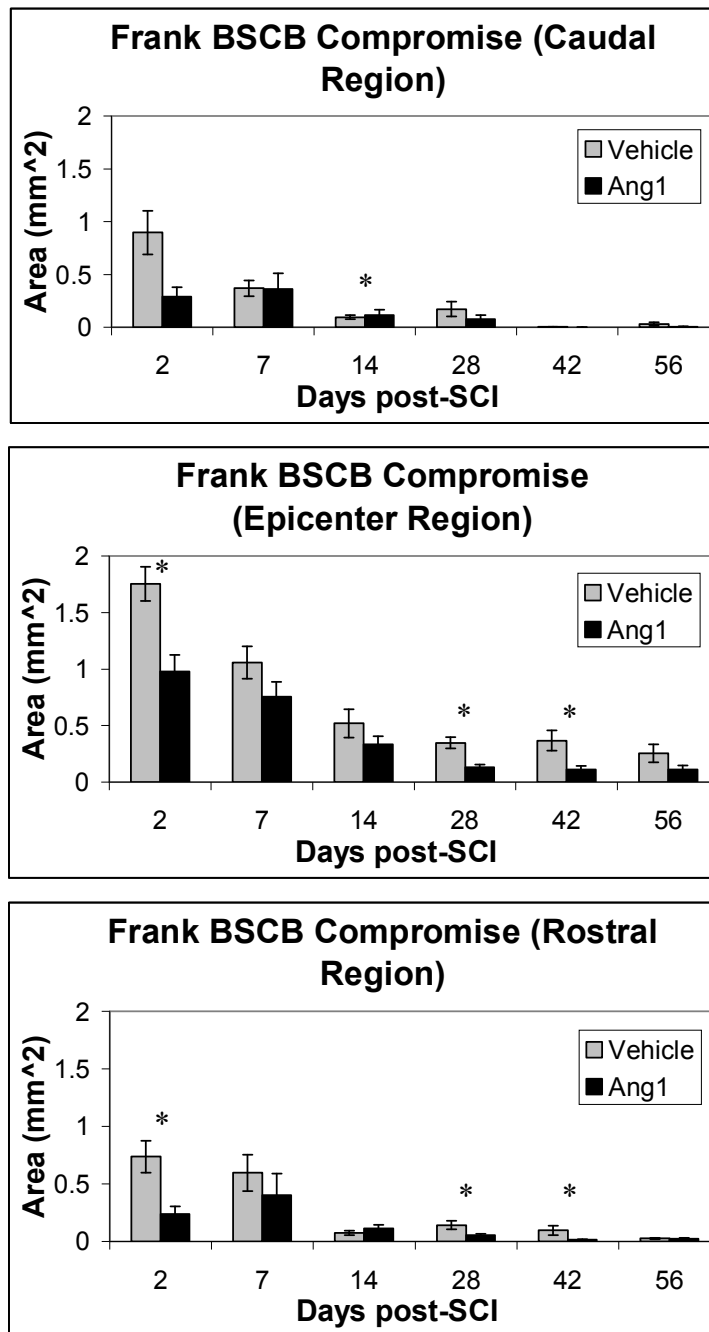


Figure 3.2 - Frank enhancement (absolute area, mm²) by day and spatial region (temporal view). Error bars represent standard error of the mean. * indicates $p < 0.0167$ between vehicle and Ang1. $n \geq 6$ animals per group per day.

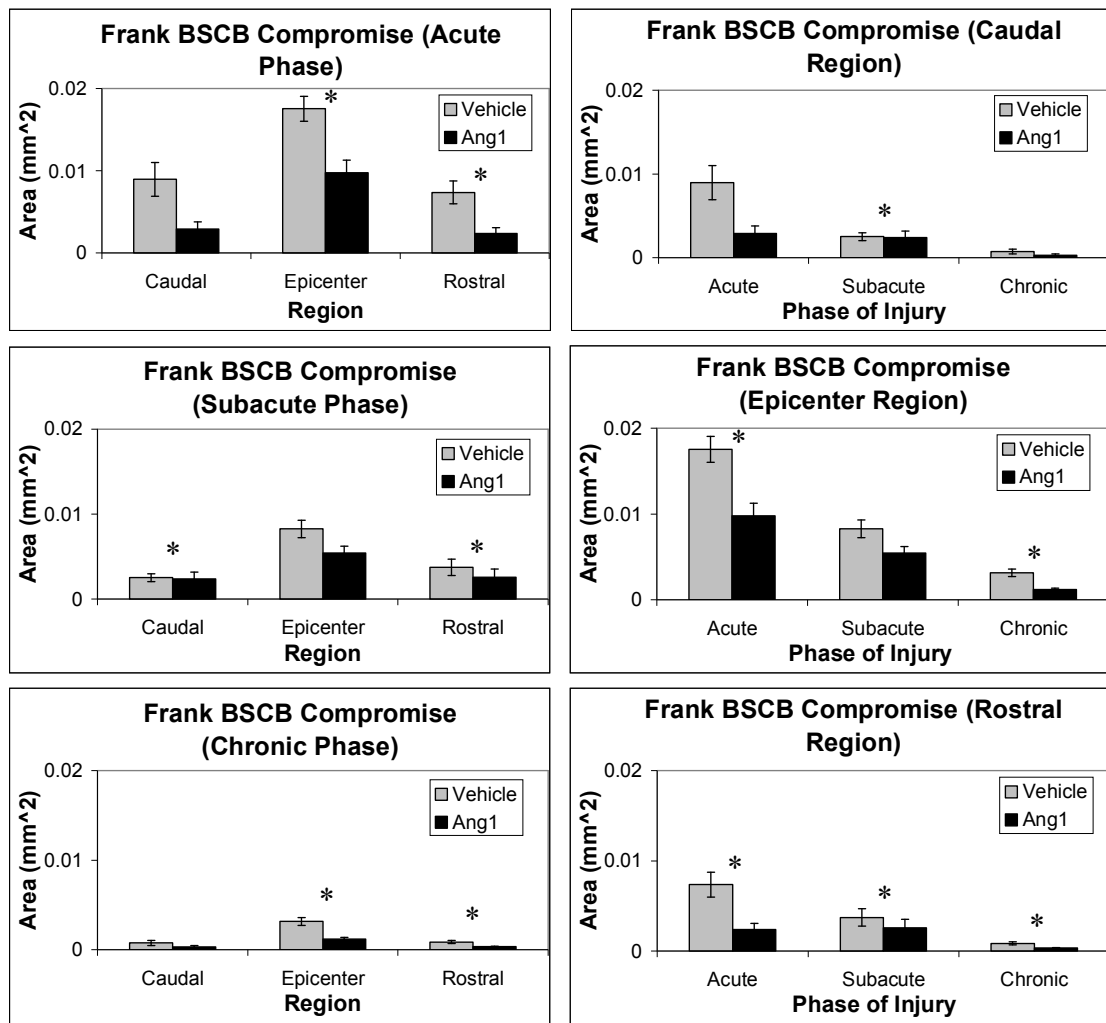


Figure 3.3 - Frank enhancement (absolute area, mm²) by phase of injury and spatial region (including temporal view). Error bars represent standard error of the mean. * indicates p<0.0167 between vehicle and Ang1. n≥6 animals per group per phase.

Temporal comparisons of frank enhancement (absolute area), by region						
Group	Caudal Region		Epicenter Region		Rostral Region	
Vehicle	d2 > d{14, 28, 42, 56}		d2 > d{7, 14, 28, 42, 56}		d2 > d{14, 28, 42, 56}	
	d7 > d{28, 42, 56}		d7 > d{28, 42, 56}		d7 > d{14, 42, 56}	
	d14 > d{42, 56}					
	d28 > d42		d28 > d56			
	pA > {pS, pC}		pA > {pS, pC}		pA > {pS, pC}	
	pS > pC		pS > pC		pS > pC	
Angiopietin-1	d2 > d{28, 42, 56}		d2 > d{14, 28, 42, 56}		d2 > d{42, 56}	
	d7 > d{42, 56}		d7 > d{14, 28, 42, 56}			
	d14 > d{42, 56}					
	d28 > d{42, 56}					
	pA > {pS, pC}		pA > {pS, pC}		pA > {pS, pC}	
	pS > pC		pS > pC			
Spatial comparisons of frank enhancement (absolute area), by days post-SCI						
Group	d2	d7	d14	d28	d42	d56
Vehicle	rE > r{C, R}	rE > r{C, R}	rE > rR	rE > r{C, R}	rE > r{C, R}	rE > rC
					rR > rC	
Angiopietin-1	rE > r{C, R}	rE > r{C, R}	rE > r{C, R}	rE > r{C, R}	rE > r{C, R}	rE > rC
					rR > rC	
Spatial comparisons of frank enhancement (absolute area), by phase of SCI						
Group	Acute Phase		Subacute Phase		Chronic Phase	
Vehicle	rE > r{C, R}		rE > r{C, R}		rE > r{C, R}	
					rR > rC	
Angiopietin-1	rE > r{C, R}		rE > r{C, R}		rE > r{C, R}	
					rR > rC	

Table 3.1 - Spatial and temporal differences in frank enhancement (absolute area) after spinal cord injury (SCI). Only significant differences shown (p<0.0033 for inter-day comparisons in a given spatial region; p<0.0167 for inter-phase comparisons in a given spatial region; p<0.0167 for spatial region comparisons on a given day post-SCI or phase of injury). d = days post-SCI, pA = acute phase, pC = chronic phase, pS = subacute phase, rC = caudal region, rE = epicenter region, rR = rostral region. n≥6 animals per group per day (or phase).

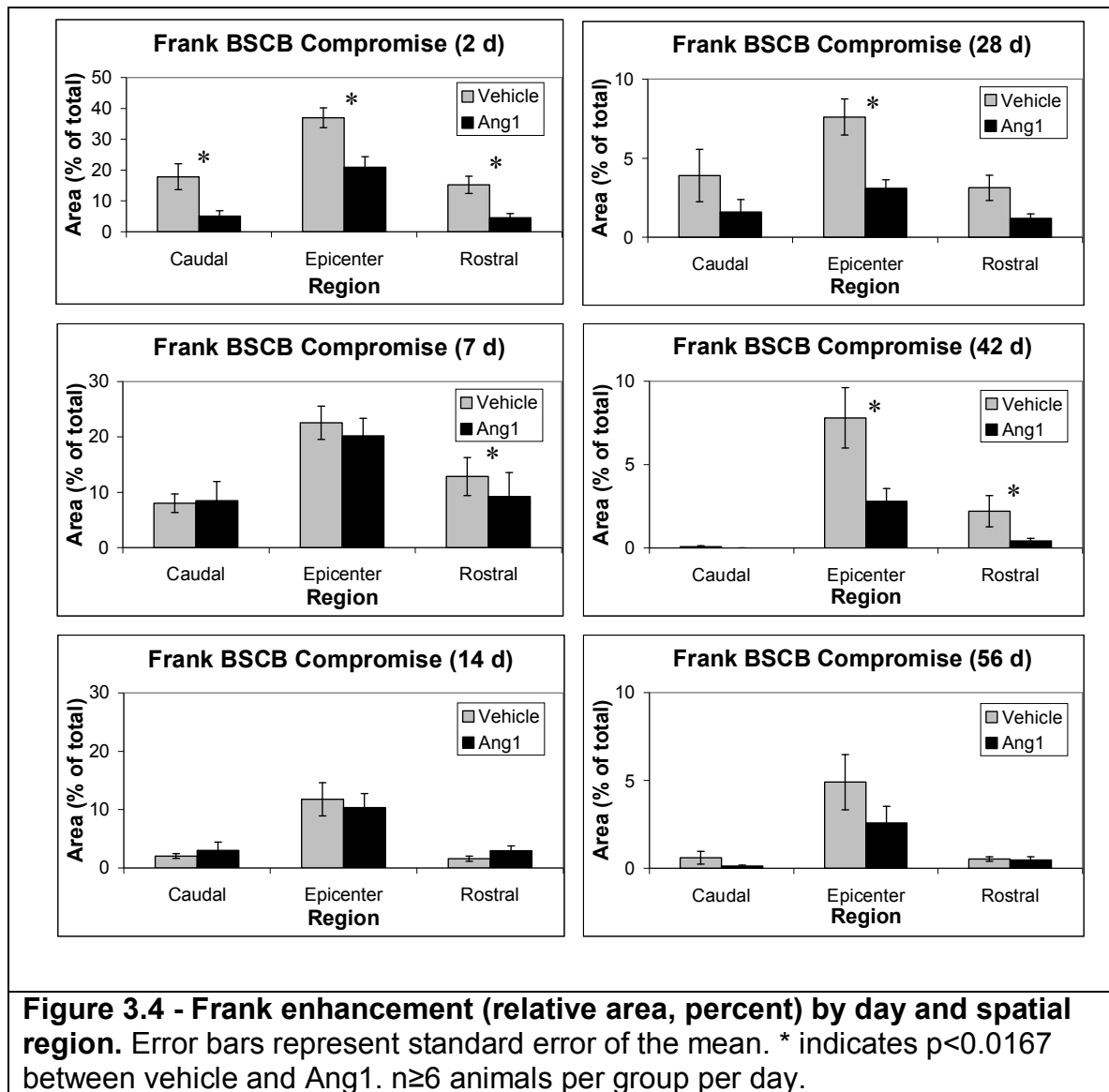
Frank enhancement (relative area)

Because the spinal cord cross-sectional area may change after SCI (e.g., due to atrophy (Deng et al., 2007)), we normalized the frank enhancement (absolute area) as frank enhancement (relative area). The latter parameter was defined for each slice as the area of spinal cord tissue with contrast-enhancement on DCE-MRI scans (i.e., above the 35% threshold) divided by the spinal cord cross sectional area. These results are shown in Figure 3.4, by day and spatial region. Figure 3.5 displays this data longitudinally. Compared to vehicle, Ang1 treatment resulted in a significant decrease in frank enhancement in the caudal region at day 2 post-SCI, in the epicenter region at days 2, 28, and 42 post-SCI, and in the rostral region at days 2, 7, and 42 post-SCI.

Figure 3.6 displays the data by time period. Compared to vehicle, Ang1 treatment resulted in a significant decrease in frank enhancement (relative area) in the acute phase (all three regions), subacute phase (caudal and rostral regions), and chronic phase (epicenter and rostral regions).

Table 3.2 summarizes, for each group, the significant spatial and temporal differences in frank enhancement after SCI. In all three regions and in each group, there was a significant reduction at days 42 and 56 compared to day 2 post-SCI, indicating reduced frank enhancement over time in both groups. In the caudal region, there was a significant decrease from day 28 post-SCI to day 42 post-SCI in both groups, with a further reduction at day 56 post-SCI in the Ang1 group only, indicating continued restoration of the BSCB in this region. At all time points in both groups, the epicenter region contained significantly greater frank enhancement

than the adjacent caudal and/or rostral region. In addition, the rostral region contained significantly greater frank enhancement compared to the caudal region in the chronic phase, indicating a spatial asymmetry in restoration of the BSCB after SCI.



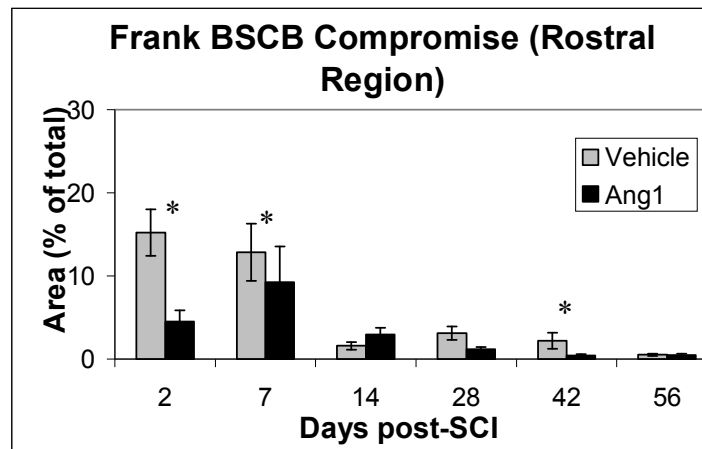
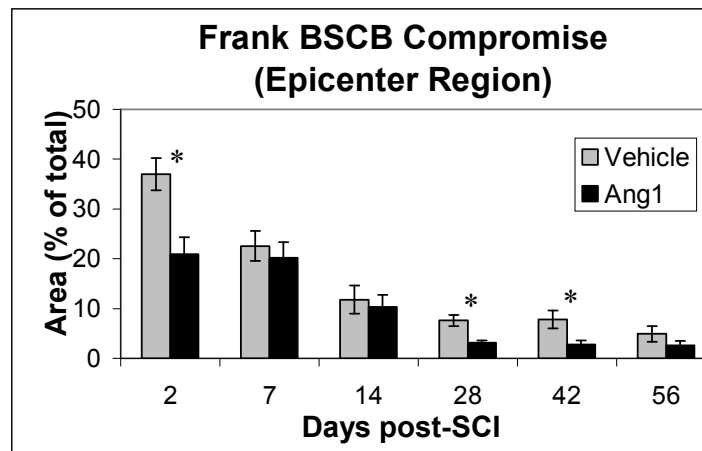
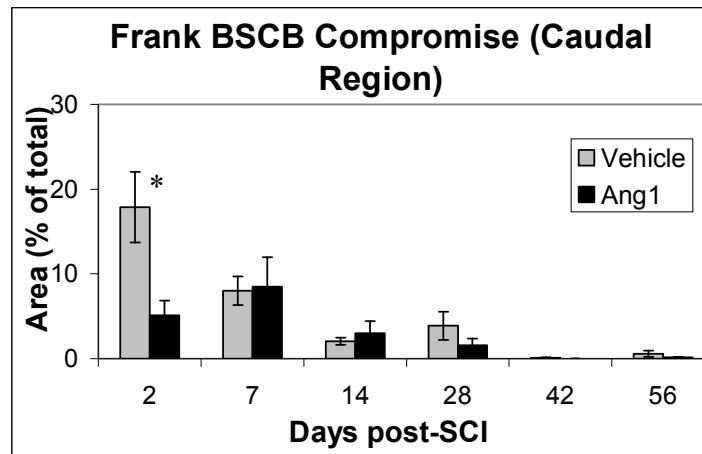
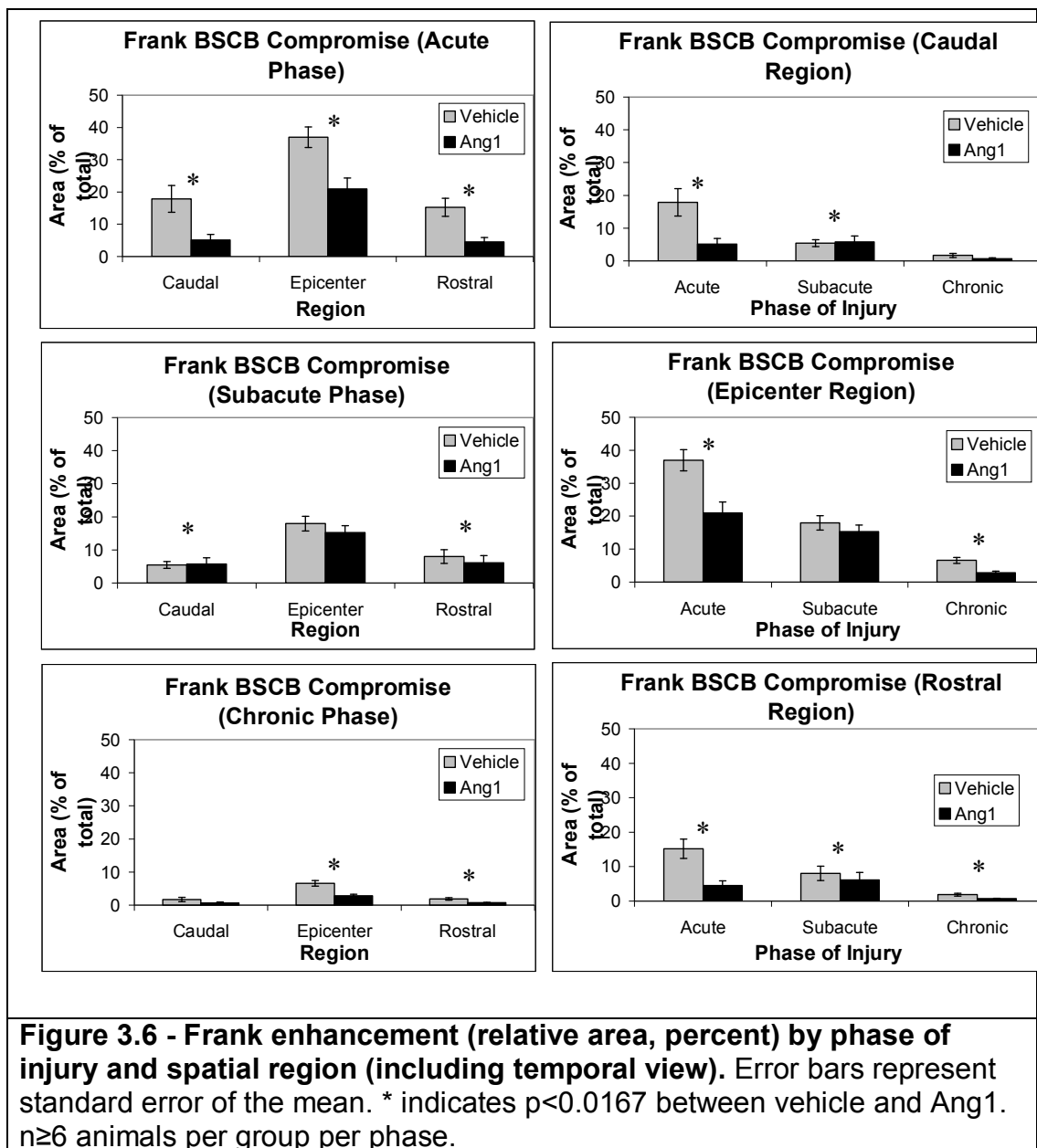


Figure 3.5 - Frank enhancement (relative area, percent) by day and spatial region (temporal view). Error bars represent standard error of the mean. Error bars represent standard error of the mean. * indicates $p < 0.0167$ between vehicle and Ang1. $n \geq 6$ animals per group per day.



Temporal comparisons of frank enhancement (relative area), by region						
Group	Caudal Region		Epicenter Region		Rostral Region	
Vehicle	d2 > d{14, 28, 42, 56}		d2 > d{7, 14, 28, 42, 56}		d2 > d{14, 28, 42, 56}	
	d7 > d{28, 42, 56}		d7 > d{28, 42, 56}		d7 > d{14, 56}	
	d14 > d{42, 56}					
	d28 > d42		d28 > d56		d28 > d56	
	pA > p{S, C}		pA > p{S, C}		pA > p{S, C}	
	pS > pC		pS > pC		pS > pC	
Angiopietin-1	d2 > d{42, 56}		d2 > d{14, 28, 42, 56}		d2 > d{42, 56}	
	d7 > d{42, 56}		d7 > d{14, 28, 42, 56}			
	d14 > d{42, 56}		d14 > d56			
	d28 > d{42, 56}					
	pA > pC		pA > pC		pA > pC	
	pS > pC		pS > pC			
Spatial comparisons of frank enhancement (relative area), by days post-SCI						
Group	d2	d7	d14	d28	d42	d56
Vehicle	rE > r{C, R}	rE > r{C, R}	rE > r{C, R}	rE > r{C, R}	rE > r{C, R}	rE > rC
					rC < rR	
Angiopietin-1	rE > r{C, R}	rE > r{C, R}	rE > r{C, R}	rE > r{C, R}	rE > r{C, R}	rE > rC
					rC < rR	
Spatial comparisons of frank enhancement (relative area), by phase of SCI						
Group	Acute Phase		Subacute Phase		Chronic Phase	
Vehicle	rE > r{C, R}		rE > r{C, R}		rE > r{C, R}	
					rC < rR	
Angiopietin-1	rE > r{C, R}		rE > r{C, R}		rE > r{C, R}	
					rC < rR	

Table 3.2 - Spatial and temporal differences in frank enhancement (relative area) after spinal cord injury (SCI). Only significant differences shown (p<0.0033 for inter-day comparisons in a given spatial region; p<0.0167 for inter-phase comparisons in a given spatial region; p<0.0167 for spatial region comparisons on a given day post-SCI or phase of injury). d = days post-SCI, pA = acute phase, pC = chronic phase, pS = subacute phase, rC = caudal region, rE = epicenter region, rR = rostral region. n≥6 animals per group per day (or phase).

BSCB permeability in tissue areas exhibiting contrast enhancement

Next, the established two-compartment pharmacokinetic model for determination of BSCB permeability (defined as K_{ps} , the rate constant of leakage from the systemic vasculature into the extravascular extracellular space of the spinal cord) was employed. Figure 3.7 displays the BSCB permeability in spinal cord tissue exhibiting contrast-enhancement (K_{ps} -enhancing) on DCE-MRI scans (i.e., above the 35% threshold), by day and spatial region, while Figure 3.8 displays the data longitudinally. There was no inter-group difference in K_{ps} -enhancing at any day post-SCI or in any region, indicating that the permeability in tissue areas with compromised BSCB was not affected by Ang1. Figure 3.9 displays the data by time period. Again, the effects of Ang1 on the permeability of tissue with compromised BSCB were indistinguishable from those of vehicle, for all regions and time periods.

Table 3.3 summarizes, for each group, the significant spatial and temporal differences in K_{ps} -enhancing after SCI. In the vehicle-treated animals, there was a significant reduction at day 14 post-SCI compared to day 2 post-SCI and in the subacute phase compared to the acute phase (epicenter region) and a significant increase in the chronic phase compared to the subacute phase (rostral region). In addition to these differences, others were identified in the Ang1-treated animals: a significant reduction at day 7 post-SCI compared to day 2 post-SCI and in the subacute phase compared to the acute phase (caudal region), a significant reduction at day 7 post-SCI compared to day 2 post-SCI and a significant increase in the chronic phase compared to the subacute phase (epicenter region), and a

significant reduction in the subacute phase compared to the acute phase (rostral region). These findings reflect the effect of Ang1 on reducing K_{ps} -enhancing during the acute and subacute phases, to an extent greater than that of vehicle. In both groups the significant increase in the chronic phase compared to the subacute phase in the rostral region (a reversal of the significant difference between the acute and subacute phases) without a concomitant increase in the caudal region during the same time frame further suggests a spatial asymmetry that was detectable during the chronic phase of SCI.

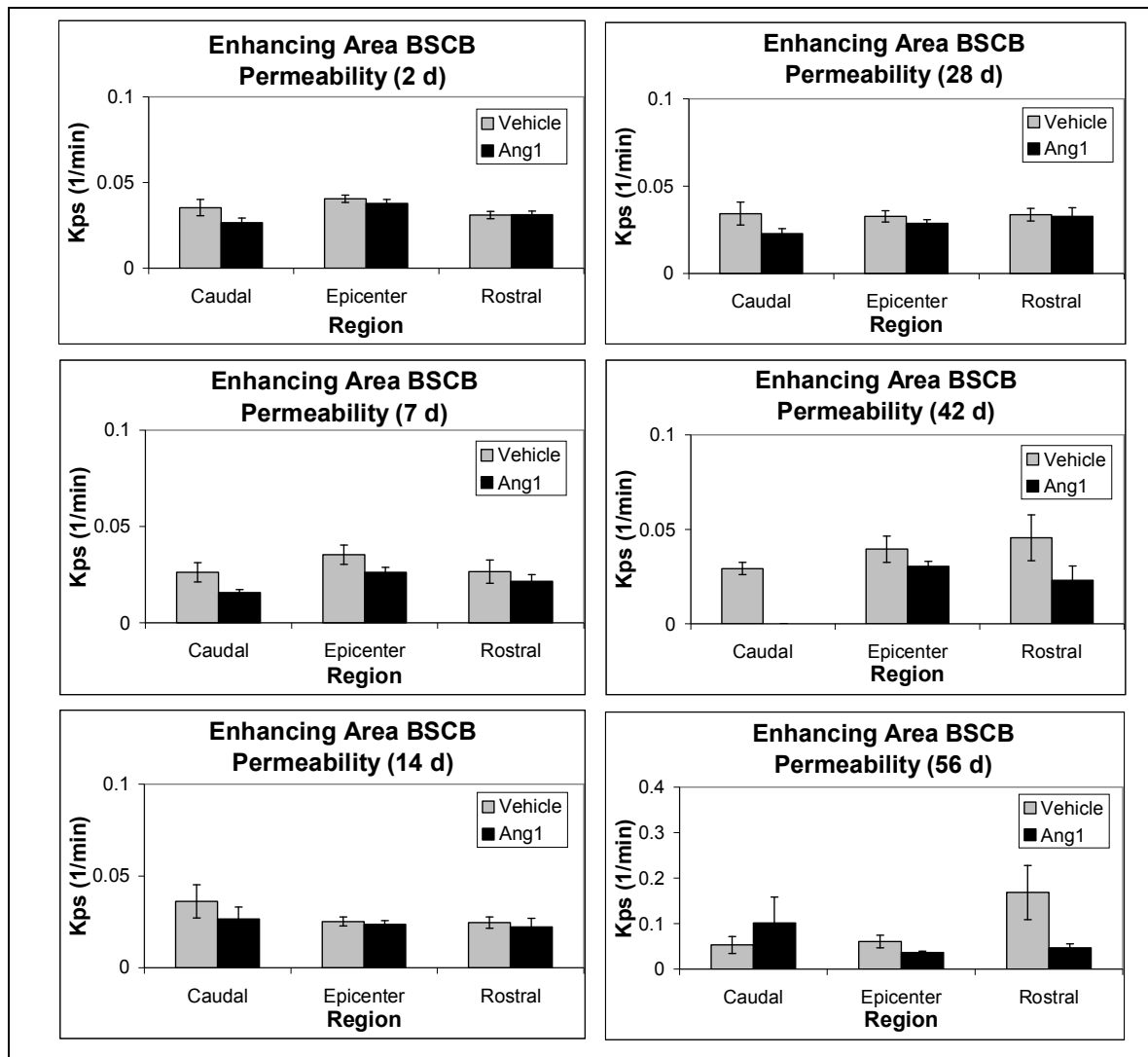


Figure 3.7 - Blood-spinal cord barrier (BSCB) permeability in spinal cord tissue areas exhibiting contrast enhancement, by day and spatial region.

K_{ps} indicates the permeability/leakiness of the BSCB. Error bars represent standard error of the mean. $n \geq 6$ animals per group per day.

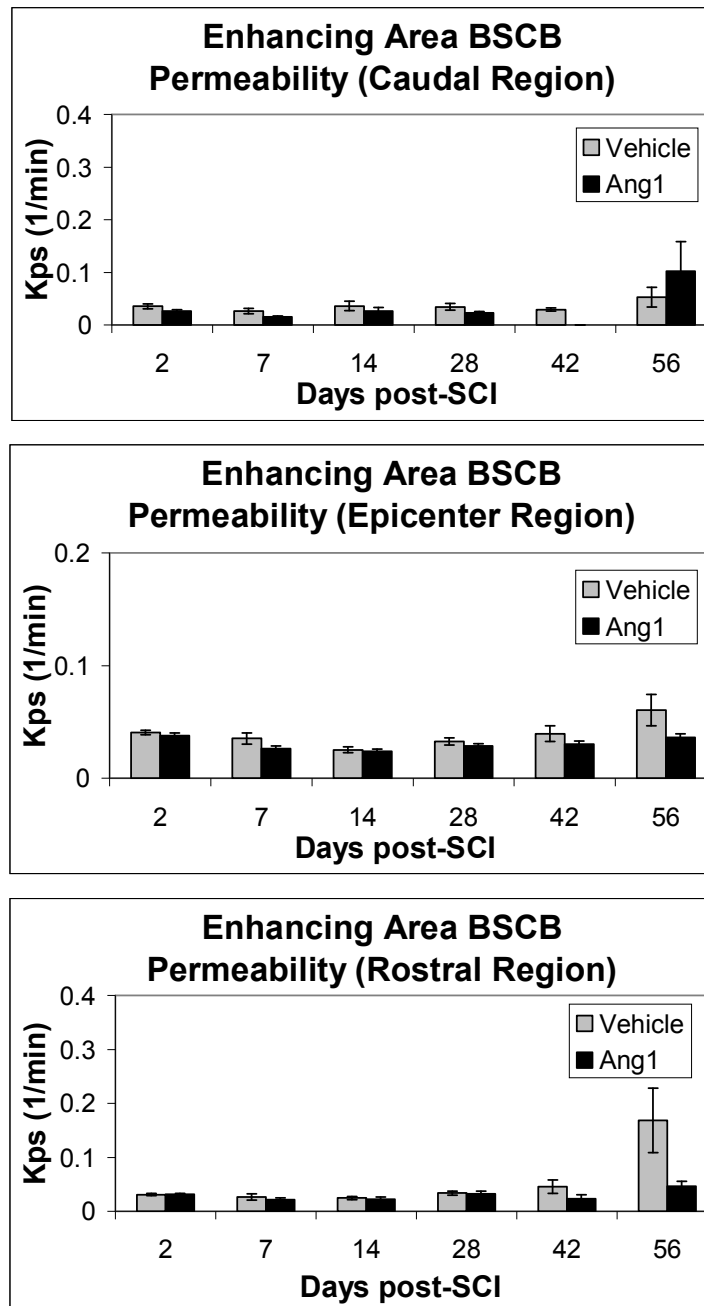


Figure 3.8 - Blood-spinal cord barrier (BSCB) permeability in spinal cord tissue areas exhibiting contrast enhancement, by day and spatial region (temporal view). K_{ps} indicates the permeability/leakiness of the BSCB. Error bars represent standard error of the mean. $n \geq 6$ animals per group per day.

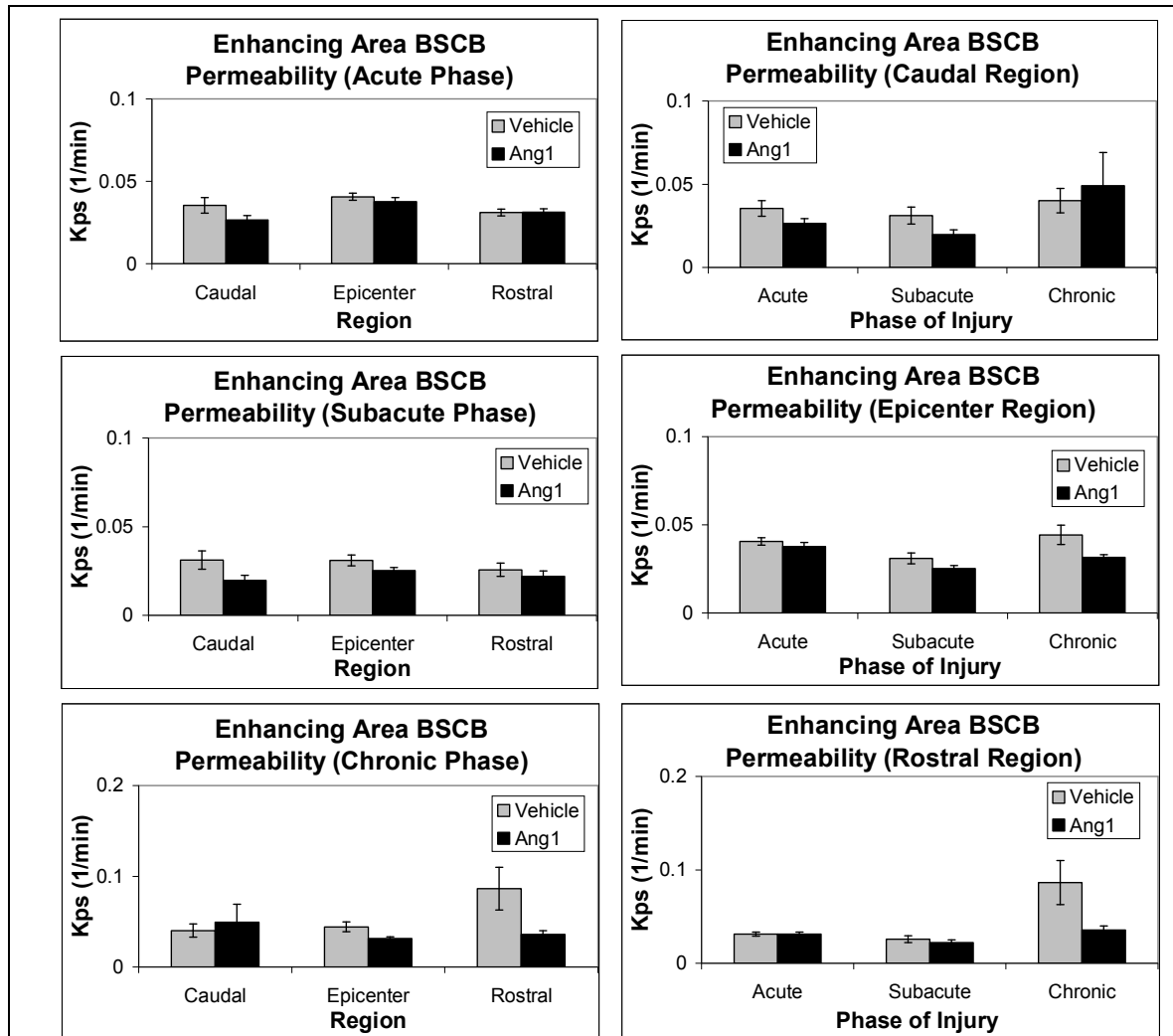


Figure 3.9 - Blood-spinal cord barrier (BSCB) permeability in spinal cord tissue areas exhibiting contrast enhancement, by phase of injury and spatial region (including temporal view). K_{ps} indicates the permeability/leakiness of the BSCB. Error bars represent standard error of the mean. $n \geq 6$ animals per group per phase.

Temporal comparisons of BSCB permeability (enhancing tissue areas), by region						
Group	Caudal Region		Epicenter Region		Rostral Region	
Vehicle			d2 > d14			
			pA > pS			
					pS < pC	
Angiopietin-1	d2 > d7		d2 > d{7, 14}			
	pA > pS		pA > pS		pA > pS	
			pS < pC		pS < pC	
Spatial comparisons of BSCB permeability (enhancing tissue areas), by days post-SCI						
Group	d2	d7	d14	d28	d42	d56
Vehicle	rE > r{C, R}					
Angiopietin-1	rC < rE	rC < rE				
Spatial comparisons of BSCB permeability (enhancing tissue areas), by phase of SCI						
Group	Acute Phase		Subacute Phase		Chronic Phase	
Vehicle	rE > r{C, R}					
Angiopietin-1	rC < rE		rC < rE			

Table 3.3 - Spatial and temporal differences in blood-spinal cord barrier (BSCB) permeability in enhancing tissue areas after spinal cord injury (SCI). Only significant differences shown (p<0.0033 for inter-day comparisons in a given spatial region; p<0.0167 for inter-phase comparisons in a given spatial region; p<0.0167 for spatial region comparisons on a given day post-SCI or phase of injury). d = days post-SCI, pA = acute phase, pC = chronic phase, pS = subacute phase, rC = caudal region, rE = epicenter region, rR = rostral region. n≥6 animals per group per day (or phase).

BSCB permeability in “normal appearing” tissue areas that do not exhibit contrast enhancement

Three uninjured animals underwent DCE-MRI scans 7 days after implantation of the radiofrequency coil and vascular port, to allow enough time for them to recover. Based on the analysis of data from these scans, the value for baseline BSCB permeability (K_{ps} -uninjured) was determined to be $0.00759 \pm 0.0007 \text{ min}^{-1}$.

In regards to the SCI animals, Figure 3.10 displays K_{ps} -normal-appearing by day and spatial region, while Figure 3.11 displays the data longitudinally. Compared to vehicle, Ang1 treatment resulted in significantly decreased K_{ps} -normal-appearing at day 2 post-SCI (in all three regions), day 7 post-SCI (in the

rostral region), day 28 post-SCI (in the epicenter region), and day 42 post-SCI (in the rostral region).

Figure 3.12 displays the data by time period. There was a significant reduction in K_{ps} -normal-appearing in the Ang1 group compared to the vehicle group during the acute (in all three regions), subacute (in the rostral region), and chronic (in the epicenter region) phases.

Table 3.4 displays, for each group, the significant spatial and temporal differences in K_{ps} -normal-appearing after SCI. In the caudal region, K_{ps} -normal-appearing was significantly reduced in the subacute phase (vehicle group) and chronic phase (Ang1 group) compared to in the acute phase, indicating its delayed reduction in the Ang1 group in this region. In the epicenter and rostral regions, K_{ps} -normal-appearing was significantly reduced in both the subacute and chronic phases in both groups. Treatment with Ang1 delayed the reduction of K_{ps} -normal-appearing after the acute phase in the caudal region compared to the rostral region, while treatment with vehicle did not maintain the reduced K_{ps} -normal-appearing in the caudal region after the subacute phase. In the acute phase, K_{ps} -normal-appearing was significantly reduced in the caudal (but not rostral) region compared to the epicenter region in both groups. In the subacute phase, K_{ps} -normal-appearing was significantly reduced in the rostral (but not caudal) region in the Ang1 group only. In the chronic phase, K_{ps} -normal-appearing was significantly reduced in both the caudal and rostral regions compared to the epicenter region in the Ang1 group only. This, coupled with the findings of Figure 3.2, could suggest that as the effects of Ang1 extend spatially with increasing time post-SCI (i.e., in

the chronic phase), the effect of reduced perilesional K_{ps} -normal-appearing is pronounced.

Table 3.5 summarizes the phenomenon of persistent elevated BSCB permeability in normal-appearing tissue. Compared to the value of K_{ps} -normal-appearing in uninjured animals, the value of K_{ps} -normal-appearing in both groups was significantly increased in all three regions during all three phases of injury, with one exception: in the Ang1 group rostral region during the subacute phase ($p < 0.06$).

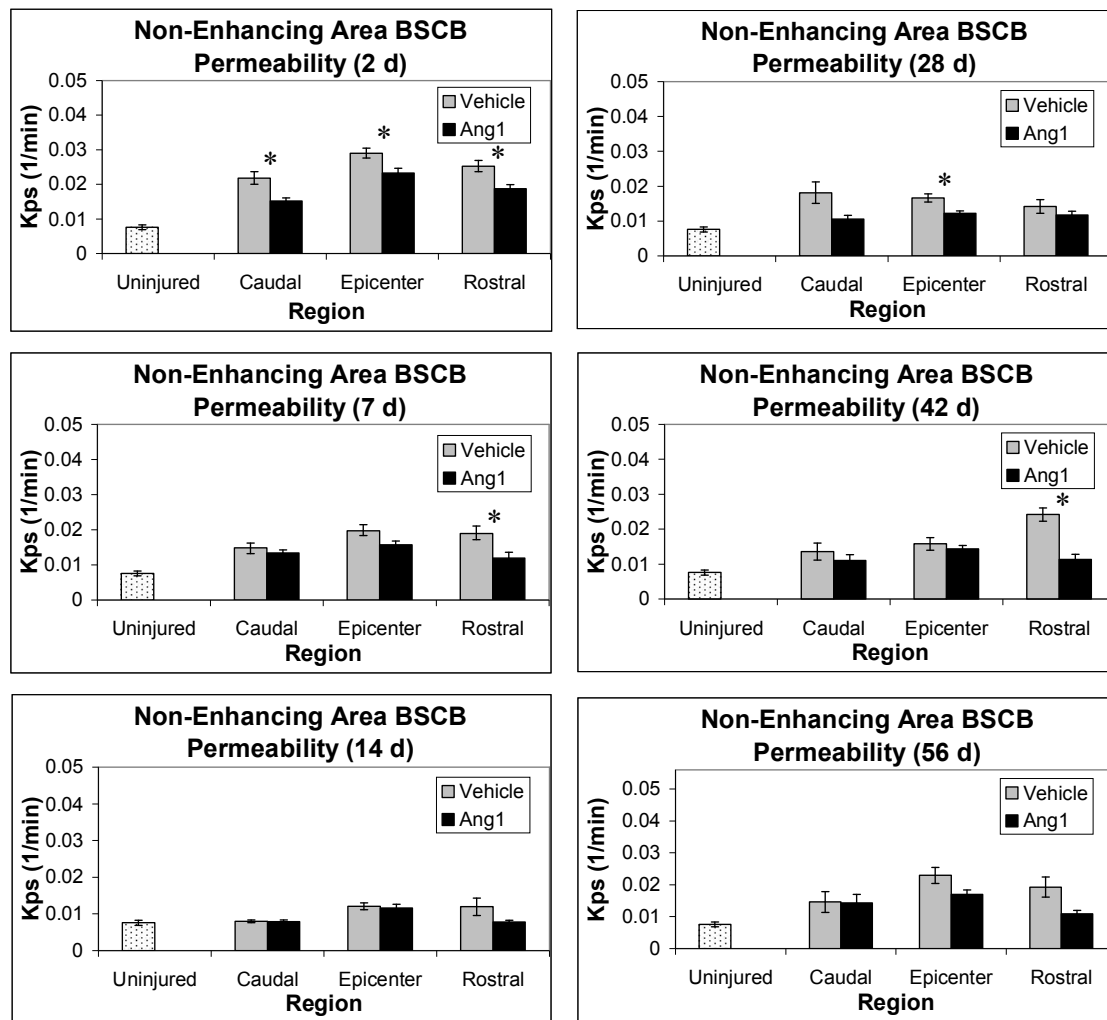


Figure 3.10 - Blood-spinal cord barrier (BSCB) permeability in non-enhancing spinal cord tissue areas, by day and spatial region. K_{ps} indicates the permeability/leakiness of the BSCB. Error bars represent standard error of the mean. * indicates $p < 0.0167$ between vehicle and Ang1. $n \geq 6$ animals per group per day.

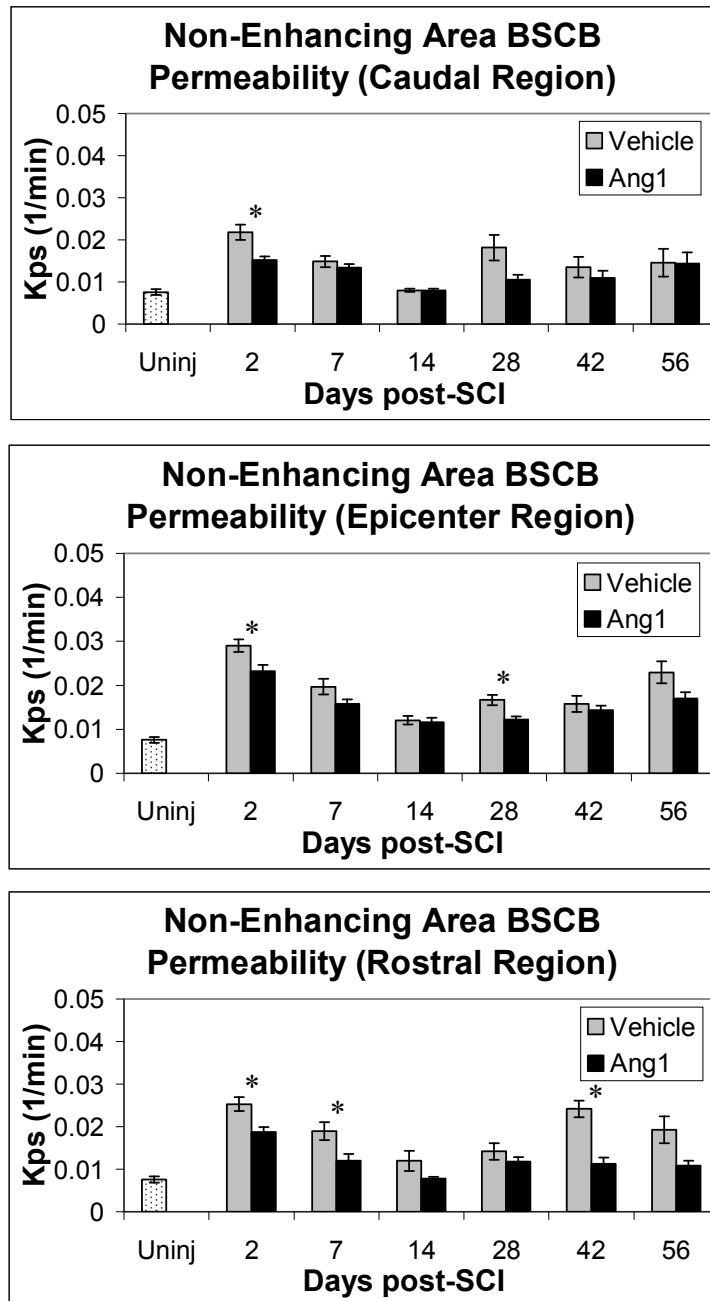


Figure 3.11 - Blood-spinal cord barrier (BSCB) permeability in non-enhancing spinal cord tissue areas, by day and spatial region (temporal view). K_{ps} indicates the permeability/leakiness of the BSCB. Error bars represent standard error of the mean. Uninj = uninjured. * indicates $p < 0.0167$ between vehicle and Ang1. $n \geq 6$ animals per group per day.

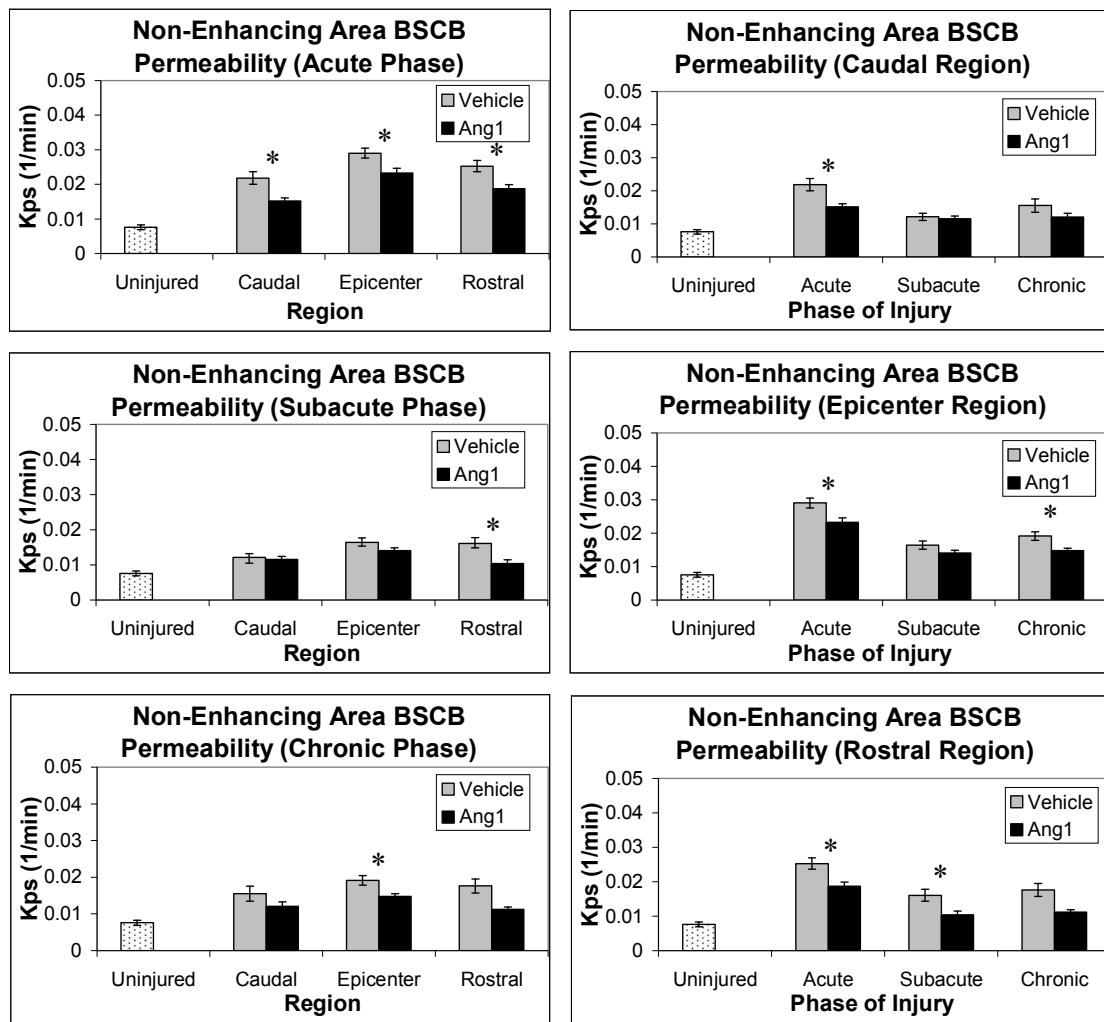


Figure 3.12 - Blood-spinal cord barrier (BSCB) permeability in non-enhancing spinal cord tissue areas, by phase of injury and spatial region (including temporal view). K_{ps} indicates the permeability/leakiness of the BSCB. Error bars represent standard error of the mean. * indicates $p < 0.0167$ between vehicle and Ang1. $n \geq 6$ animals per group per phase.

Temporal comparisons of BSCB permeability (non-enhancing tissue areas), by region						
Group	Caudal Region		Epicenter Region		Rostral Region	
Vehicle	d2 > d{14, 56}		d2 > d{7, 14, 28, 42}		d2 > d{14, 28}	
	d7 > d14					
	pA > pS		pA > p{S, C}		pA > {S, C}	
Angiopietin-1	d2 > d{14, 42}		d2 > d{7, 14, 28, 42, 56}		d2 > d{7, 14, 28, 42, 56}	
	d7 > d14					
	pA > pC		pA > p{S, C}		pA > p{S,C}	
Spatial comparisons of BSCB permeability (non-enhancing tissue areas), by days post-SCI						
Group	d2	d7	d14	d28	d42	d56
Vehicle	rC < rE		rC < rE			rC < rE
Angiopietin-1	rC < rE					rE > rR
Spatial comparisons of BSCB permeability (non-enhancing tissue areas), by phase of SCI						
Group	Acute Phase		Subacute Phase		Chronic Phase	
Vehicle	rC < rE					
Angiopietin-1	rC < rE		rE > rR		rE > r{C, R}	

Table 3.4 - Spatial and temporal differences in blood-spinal cord barrier (BSCB) permeability in non-enhancing tissue areas after spinal cord injury (SCI). Only significant differences shown ($p<0.0033$ for inter-day comparisons in a given spatial region; $p<0.0167$ for inter-phase comparisons in a given spatial region; $p<0.0167$ for spatial region comparisons on a given day post-SCI or phase of injury). d = days post-SCI, pA = acute phase, pC = chronic phase, pS = subacute phase, rC = caudal region, rE = epicenter region, rR = rostral region. $n\geq 6$ animals per group per day (or phase).

Group	Region	Days post-SCI						Phase of injury		
		2	7	14	28	42	56	Acute	Subacute	Chronic
Vehicle	Caudal	+	+		+			+	+	+
	Epicenter	+	+		+	+	+	+	+	+
	Rostral	+	+					+	+	+
Ang1	Caudal	+	+					+	+	+
	Epicenter	+	+		+	+	+	+	+	+
	Rostral	+			+			+		+

Table 3.5 - Evaluating persistently increased blood-spinal cord barrier (BSCB) permeability in normal-appearing tissue after spinal cord injury (SCI). Ang1 = angiotensin-1. + indicates that the BSCB permeability for the post-SCI temporal-region combination was greater than the BSCB permeability in uninjured animals ($p < 0.0167$).

DISCUSSION

Although not a causal relationship, we have previously identified a significant correlation between decreased BSCB permeability in normal-appearing areas and improved locomotor scores in experimental SCI (Cohen et al., 2009). Decreasing the BSCB permeability acutely after SCI may mitigate the severity of extravascular secondary pathologies. Using spatiotemporal analysis, the primary aim of these studies was to determine if a single dose of Ang1 delivered by microinjection directly into the lesion immediately post-SCI would result in reduced BSCB compromise and permeability.

Frank Enhancement

Due to the variability of spinal cord tissue preservation and atrophy after injury (Weirich et al., 1990; Deng et al., 2007), normalization of the area of tissue exhibiting contrast enhancement to the total cross-sectional area provided for meaningful comparisons between the groups. Although this approach is semi-quantitative, it has been shown to be correlated with quantitative analysis in a human study (Galbraith et al., 2002). The reduction in frank enhancement attributable to Ang1 began at 2 days post-SCI and lasted up to 42 days post-SCI in the epicenter and rostral regions, but was limited at 2 days post-SCI in the caudal region. Yet in the caudal region, a significant reduction in frank enhancement from day 28 post-SCI to day 56 in the Ang1 group (but only to day 42 in the vehicle group) may indicate prolonged restoration of the BSCB in this region after exposure to Ang1. This complements the finding that in both groups during the

chronic phase, frank enhancement was significantly greater in the rostral region compared to the caudal region.

BSCB permeability in tissue areas exhibiting contrast enhancement

Given that tissues with contrast-enhancement reflect extravasation of the contrast agent from the systemic vasculature through the compromised BSCB into the spinal cord, we did not expect to detect inter-group differences in K_{ps} -enhancing. Indeed, this was the case and it confirmed our previous findings of no differences in K_{ps} -enhancing after experimental SCI with a different vehicle (saline) and experimental treatment (vascular endothelial growth factor) (Patel et al., 2009). Although K_{ps} -enhancing was significantly decreased in the caudal region compared to the epicenter region in both groups during the acute phase, this difference was extended into the subacute phase in the Ang1 group only, indicating a possible effect of Ang1 in mediating the delay of normalization of K_{ps} -enhancing between these two regions (i.e., loss of significant difference) during this phase of injury.

BSCB permeability in “normal appearing” tissue areas that do not exhibit contrast enhancement

The value of K_{ps} -uninjured in this study ($0.00759 \pm 0.0007 \text{ min}^{-1}$) is comparable to that previously reported as a baseline value ($0.00698 \pm 0.0019 \text{ min}^{-1}$) (Cohen et al., 2009), indicating the reliability of the two-compartment pharmacokinetic model employed. Compared to vehicle, Ang1 resulted in a significant reduction in K_{ps} -normal-appearing in all three regions during the acute

phase; however, the reduction was maintained only in the rostral region during the subacute phase and in the epicenter region during the chronic phase. In a different murine model of SCI (T9 contusion in mouse), Han et al. administered Ang1 daily starting with the day of injury (with a delay of 4 hours between SCI and first Ang1 dose) (Han et al., 2010). They evaluated BSCB permeability histologically by injecting luciferase 30 min prior to sacrifice and then quantifying the amount that extravasated into the spinal cord at 24 hours and 72 hours post-SCI. Compared to vehicle, they detected a significant reduction in BSCB permeability due to Ang1 in the epicenter region (the same as the epicenter region defined in the current study, 5 mm centered about the lesion site) at 72 hours, but not 24 hours, post-SCI (Han et al., 2010). Our findings at 2 days post-SCI confirm Han et al.'s findings and provide evidence for an effect of Ang1 that extends farther, up to 6 mm rostral and 6mm caudal to the site of injury. Furthermore, our data show that a single injection of Ang1 administered immediately after SCI can reduced BSCB permeability in the chronic phase of injury (28-56 days post-SCI), specifically up to 42 days post-SCI.

We have previously shown that “normal appearing” areas on post-contrast DCE-MRI scans, i.e. those tissue areas that do not exhibit contrast enhancement, undergo dynamic changes in BSCB permeability (Cohen et al., 2009; Patel et al., 2009). In the current study we found that BSCB permeability in normal-appearing areas was elevated compared to uninjured K_{ps} -normal-appearing values in both groups, in all three regions, in all three phases, with one exception: the Ang1 group in the rostral region during the subacute phase. This was due to the fact that K_{ps} -normal-appearing was significantly reduced in the subacute phase in rostral region

compared to the epicenter region in the Ang1 group only. Most previous studies of BSCB permeability in SCI have employed *ex vivo* histological methods using macromolecular tracers (e.g., albumin (Noble and Maxwell, 1983; Sharma et al., 1998; Pan and Kastin, 2001; Sharma et al., 2006b), IgG (Baldwin et al., 1998), and horseradish peroxidase (Noble and Maxwell, 1983; Noble and Wrathall, 1987, 1988, 1989)) whose sizes range from 40-150 kDa. An advantage of *in vivo* DCE-MRI investigations is the ability to spatiotemporally evaluate changes in BSCB compromise in the same cohort of animals at serial time points. As with *in vivo* studies, post-mortem studies are susceptible to altered tissue microstructure. For example, Popovich et al. found that the BSCB is compromised for as long as 28 days post-SCI and is completely restored thereafter (tracer: ^{14}C -labeled α -aminoisobutyric acid, MW = 0.117 kDa) (Popovich et al., 1996) while Whetstone et al. observed restoration of the BSCB between 7-14 days post-SCI (tracer: luciferase, MW = 61 kDa) (Whetstone et al., 2003).

Contrary to the findings of Popovich et al. (Popovich et al., 1996) and Whetstone et al. (Whetstone et al., 2003), based on DCE-MRI studies we have found that the BSCB remains compromised even at 56 days post-SCI (Cohen et al., 2009; Patel et al., 2009). This may be due to the size of the contrast agent used in the DCE-MRI studies (Gd, molecular weight = 0.573 kDa) (Tofts et al., 1999), which due to its small size would be expected to leak into epicenter and perilesional regions during times when the BSCB has been restored to the point of prohibiting larger molecules, i.e. during the chronic phase of injury. Interestingly, Popovich et al. used a tracer smaller than Gd yet concluded restoration of the

BSCB to be one month earlier than what we have determined; this highlights the different conclusions that may be drawn from post-mortem versus *in vivo* studies, respectively, even when comparably small tracers are used to probe the integrity of the BSCB. Future DCE-MRI studies may determine that BSCB permeability to Gd in normal-appearing tissue persists in the ultrachronic (>2 months post-SCI) phase of injury. In regards to method of treatment delivery, we postulate that repeated administration of Ang1 may result in a more potent and longer-lasting reduction in BSCB compromise compared the effects observed in this study. Such administration could take the form of daily injections of Ang1 protein administered intravenously through the same vascular port used to administer the contrast agent during DCE-MRI scans. Alternatively, sustained-release methods such as gene-based delivery (Abdellatif et al., 2006) or mini-pump implantation could be considered (Lee et al., 1999). In the former, administration of the agent in some other form during the acute phase of injury may be necessary to compensate for the delay (on the order of days (Boulis et al., 1999)) in the commencement of gene expression, while in the latter, catheter patency, cord compression, and scarring may hinder successful therapy long-term (Jones and Tuszynski, 2001).

Strengths

This study provides proof of principle that Ang1 reduces BSCB compromise after experimental SCI, both in terms of the amount of tissue containing frank enhancement and the permeability of the barrier. Despite a single administration of Ang1 protein at the injury epicenter, differences compared to vehicle were

observed in the perilesional area and at subacute and chronic time points. Further evidence for the caudal-rostral asymmetry post-SCI was also demonstrated. The persistently elevated BSCB permeability observed at all time periods and in all regions in the vehicle group confirms our earlier findings in untreated SCI animals (Cohen et al., 2009) and supports further investigation into delayed treatments for spinal cord injury (Novikova et al., 2000; Lynskey et al., 2006; Hejcl et al., 2008), many of which are delivered intravenously and therefore must cross the compromised BSCB in order to exert their effects (Wrathall et al., 1997; Huang et al., 2007; Mann et al., 2008; Fleming et al., 2009).

Limitations

The results of this study should be considered in the context of its limitations. First, a rigorous analysis of the distribution of the treatment (neither vehicle nor Ang1) after spinal microinjection was not performed. Second, the treatments were delivered intraspinally immediately after SCI, a scenario that is not clinically translatable due to the delay involved in transit from site of injury to tertiary care center and relative inaccessibility to the spinal cord unless surgical decompression is warranted. Third, histological assessment was not performed as part of this study, which could have validated the DCE-MRI results and provided possible clues into the mechanism of action underlying the observed effects. Fourth, the optimal dose and administration regimen of Ang1 is unknown because a dose-response assessment was not performed.

CHAPTER 4:

EFFECT OF SINGLE ACUTE ANG1 DOSE ON SPINAL CORD ATROPHY AND SCI LESION SIZE

INTRODUCTION

Sparing of tissue has been shown to be associated with improved neuromotor recovery after spinal cord injury (Noble and Wrathall, 1985; Behrmann et al., 1992; Basso, 2000). The growing lesion after spinal cord injury spreads to gray matter and white matter, hindering recovery (Nishi et al., 2007). T2-weighted anatomical MRI can identify hyperintense (bright) and hypointense (dark) lesions that correlate with pathology (Weirich et al., 1990). In the acute phase of injury, hyperintense lesions represent edema and hypointense lesions represent hemorrhage, while in the chronic phase of injury, hyperintense lesions represent demyelination and hypointense lesions represent necrosis.

The traditional histological approach (i.e., method of Cavalieri) employed to measure the lesion after spinal cord injury has been shown to be an overestimate relative to that determined from MRI (Ditor et al., 2008). Even with MRI-based visualization of the spinal cord *in vivo*, lesion analysis of MR images involves the application of user-defined absolute thresholds for identifying hyper- and hypointense lesions (Nout et al., 2009; Sundberg, 2009; Qian et al., 2010).

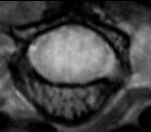
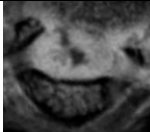
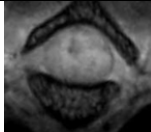
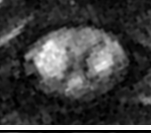





The quantification of lesion size is further complicated by atrophy of the spinal cord parenchyma over time (Olby and Blakemore, 1996; Deng et al., 2007). High-resolution anatomical MR imaging has previously been used to quantify the extent of atrophy. (Deng et al., 2007). In order to remove the confounder of atrophy from reporting of lesion size, it may be appropriate to normalize the size of the lesion by the cross-sectional area of the parenchyma on a slice-by-slice manner.

The purpose of these studies was to evaluate the role of acutely administered Ang1 on atrophy and lesion size after traumatic SCI. An objective histogram-based method for lesion segmentation that can be easily implemented in freeware software (ImageJ, Bethesda, MD) is described and evaluated against segmentations from human raters.

RESULTS

Rater-based segmentation

Sixteen high-resolution anatomical MRI slices were randomly chosen for rater-based segmentation and representative images are shown in Figure 4.1. The slices were derived from a cross-section of anatomical regions (caudal, epicenter, and rostral) and time points (acute, subacute, and chronic phase). During the acute phase of injury, hyperintense (bright) areas are representative of edema and hypointense (dark) areas are representative of hemorrhage. In the late subacute and chronic phases, the hyperintense areas represent demyelination and the hypointense regions indicate necrosis (Weirich et al., 1990).

	Caudal region	Epicenter region	Rostral region
Acute phase			
Subacute phase			
Chronic phase			
Figure 4.1 – Representative sample of anatomical images segmented by human raters. This set of images represents the heterogeneity hyperintense and hypointense lesions seen over time and space. From a total of 16 images. Orientation: ventral on top, dorsal on bottom.			

Four experienced raters with >1 year of experience assessing and analyzing high-resolution anatomical MRI scans segmented the hyperintense and

hypointense lesions from the set of 16. An example of the segmentation of the four raters for a single slice is shown in Figure 4.2.

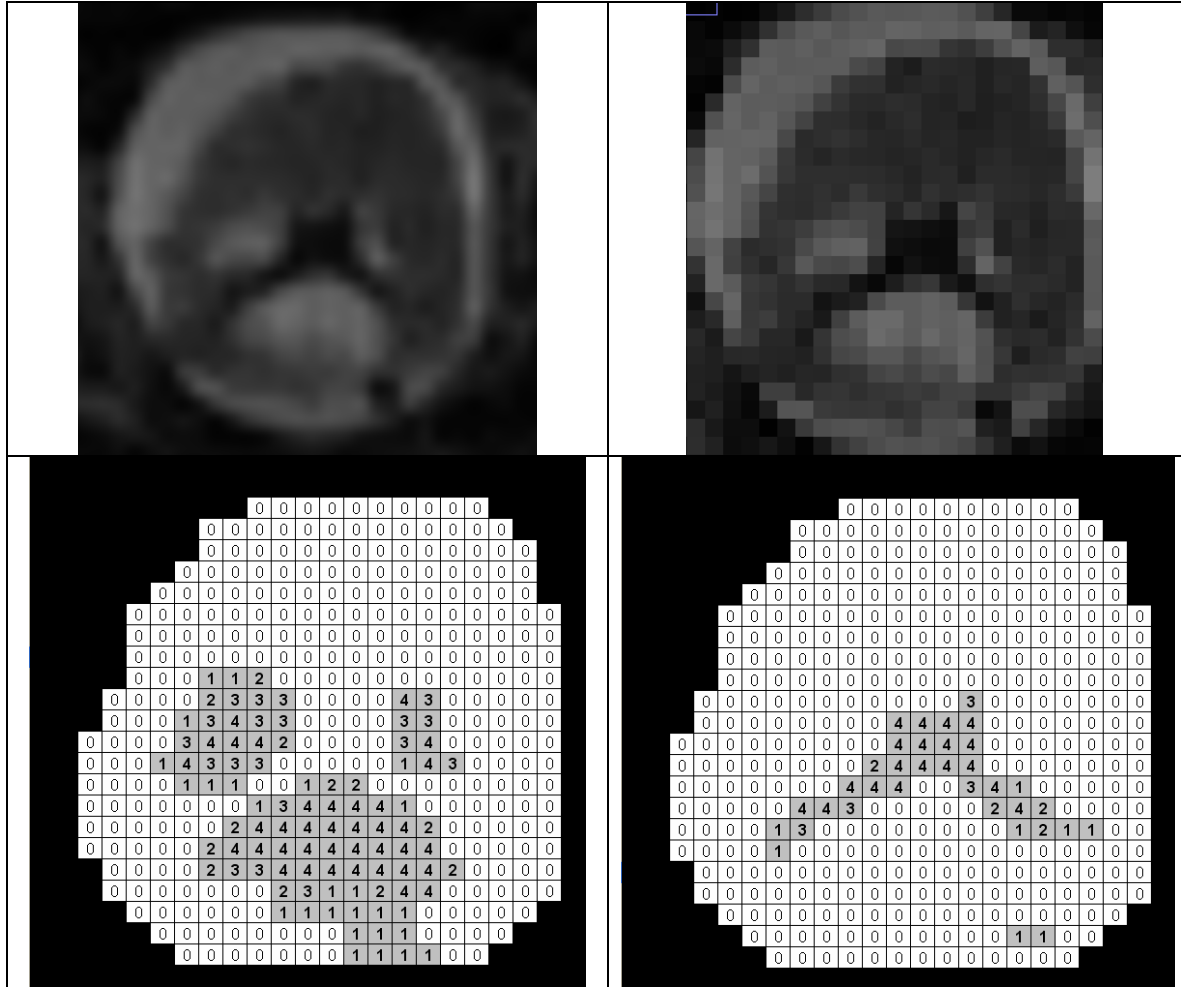


Figure 4.2 Rater segmentation (four raters) in a slice containing both hyperintense and hypointense lesion. The numbers in each pixel refer to the number of raters that classified the pixel as hyperintense or hypointense. Upper left: high-resolution image, upper right: zoomed-in view, lower left: raters' segmentation of hyperintense (bright) lesion, lower right: raters' segmentation of hypointense (dark) lesion.

For each slice, the “truth” or reference image was defined by the majority voting rule, i.e. a pixel was considered to be part of lesion if more than two raters classified it as containing lesion. In the event of a tie (i.e. 2 raters with the same

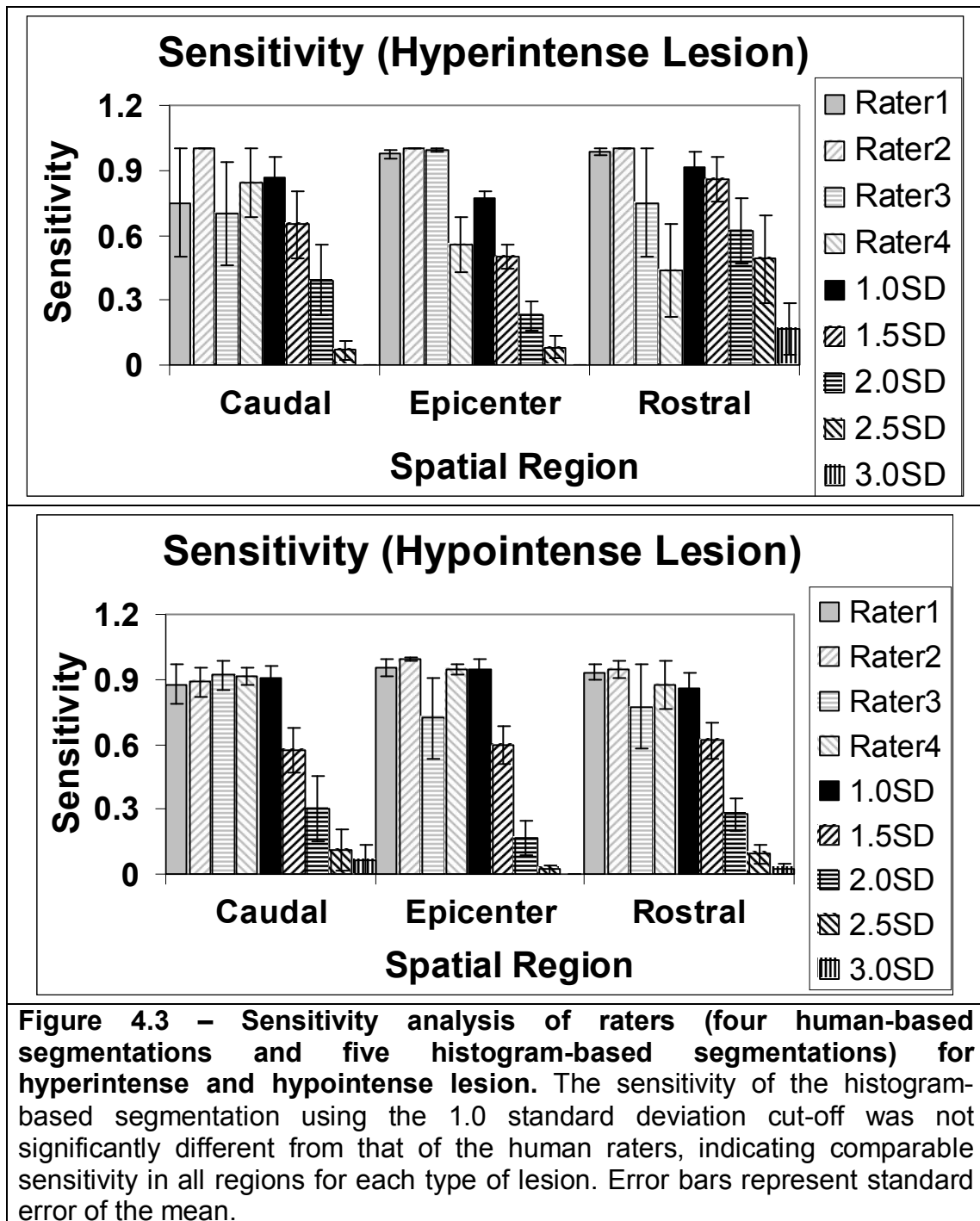
classification), the pixel was not considered to be part of the lesion. The segmentations from the histogram-based method (described in the Materials and Methods chapter), as well as those from the human raters, were evaluated against the reference image for each slice. The segmentation of a particular pixel was considered to be a true positive (TP, if both the segmented and reference images agreed that it belongs to a lesion), false positive (FP, if the segmented image determined that the pixel belongs to a lesion, but the reference image did not), true negative (TN, if the both the segmented and reference images determined that the pixel is not part of the lesion), or false negative (FN, if the segmented image determined that a pixel belongs to a lesion, but the reference image did).

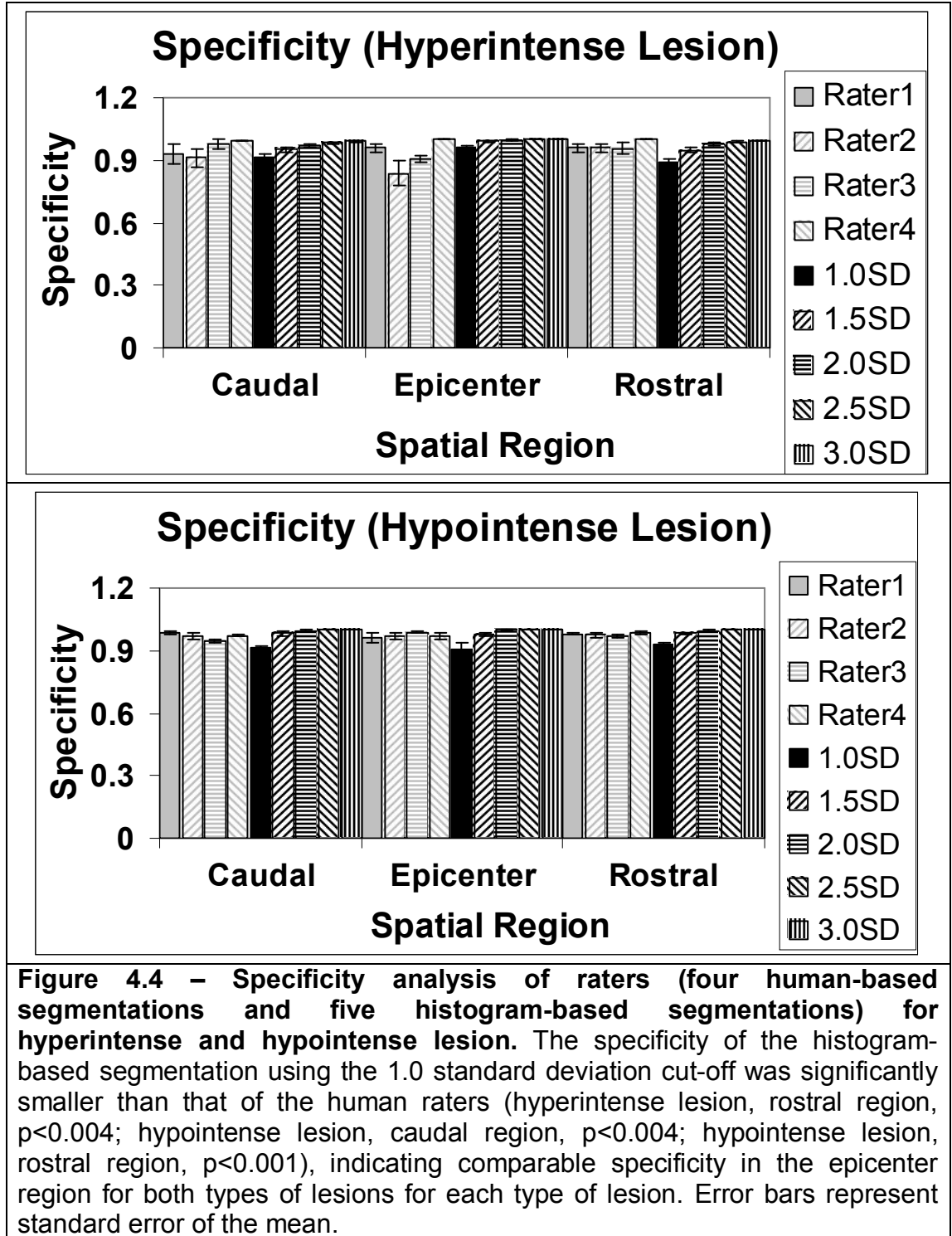
Evaluation of objective histogram-based approach for lesion segmentation

Because the slices represented a heterogeneous cross-section of pathology seen over the course of the study, evaluation of the performance of the human raters and histogram-based method is presented by spatial region. Performance measures included sensitivity ($TP / [TP + FN]$, see Figure 4.3), specificity ($TN / [TN + FP]$, see Figure 4.4), positive predictive value ($TP / [TP + FP]$, see Figure 4.5), negative predictive value ($TN / [TN + FN]$, see Figure 4.6), and Dice similarity coefficient ($2*TP / [(FP + TP) + (TP + FN)]$, see Figure 4.7). Beyond a comparison of the lesion area determined by each segmentation method, these performance measures provide information regarding the degree of spatial overlap between pixels considered to contain hyperintense or hypointense lesion. Greater sensitivity indicates a smaller FN detection rate while greater specificity indicates a smaller

FP rate. Greater PPV indicates that if a rater classifies a pixel as being located in a lesion, the likelihood that the pixel is actually located in a lesion is increased. Likewise, great NPV indicates that if a rater classifies a pixel as not being located in a lesion, the likelihood that the pixel is not actually located in a lesion is increased. Given two sets of information, the DSC is essentially the ratio of twice the intersection of the sets to the union of the sets; thus, two completely overlapping sets would have a DSC of 1 while two sets that do not overlap at all would have a DSC of 0.

For the histogram-based approach, five different cut-offs were used: mean \pm 1.0*SD, mean \pm 1.5*SD, mean \pm 2.0*SD, mean \pm 2.5*SD, and mean \pm 3.0*SD. As can be seen from Figures 4.3 – 4.7, the 1.0*SD cut-off was superior to that of the other four histogram-based segmentations, as its performance measures were least often significantly different from those of the human raters. Thus, the 1.0*SD cut-off was used for determination of lesion size in these studies.





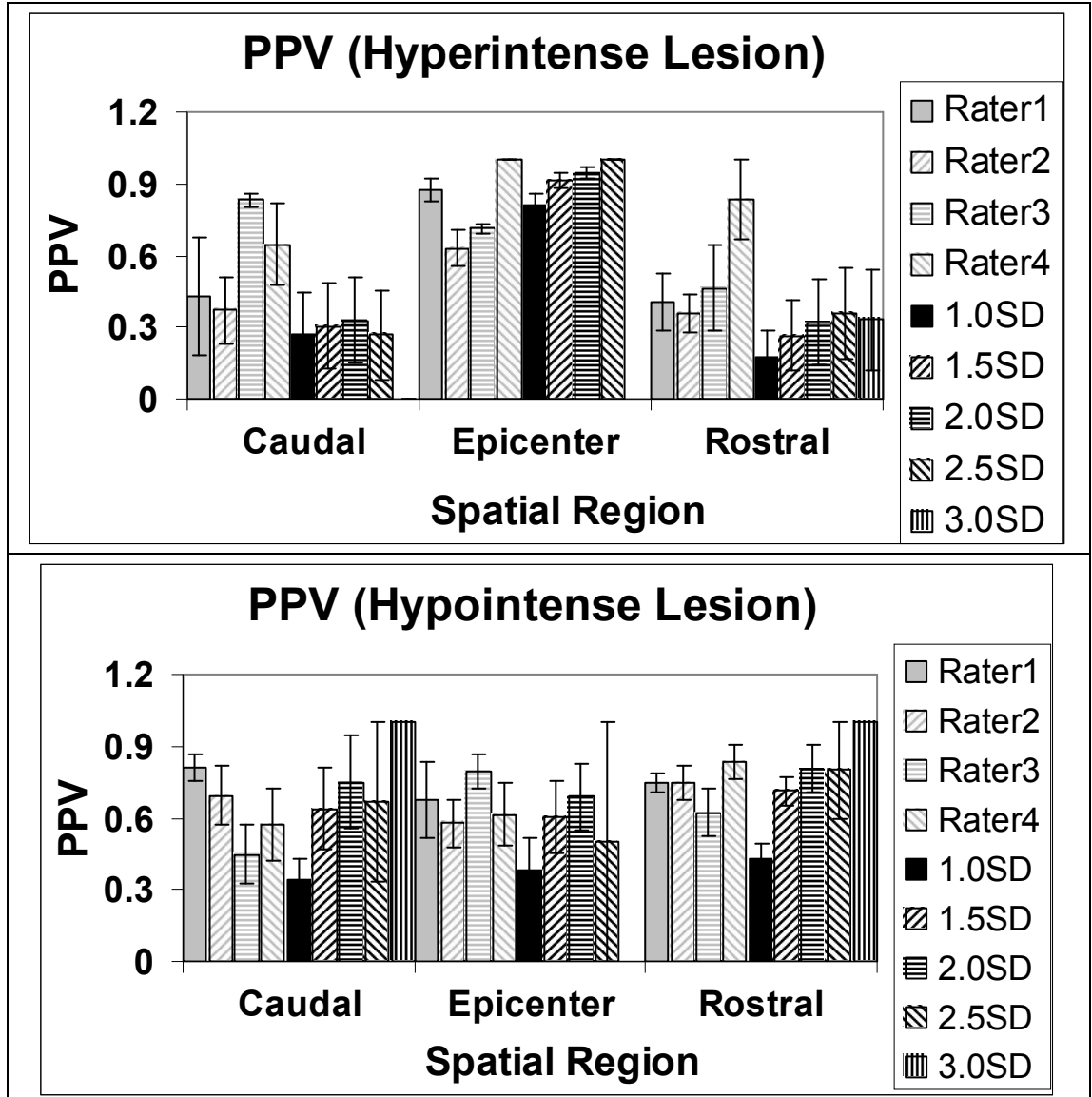
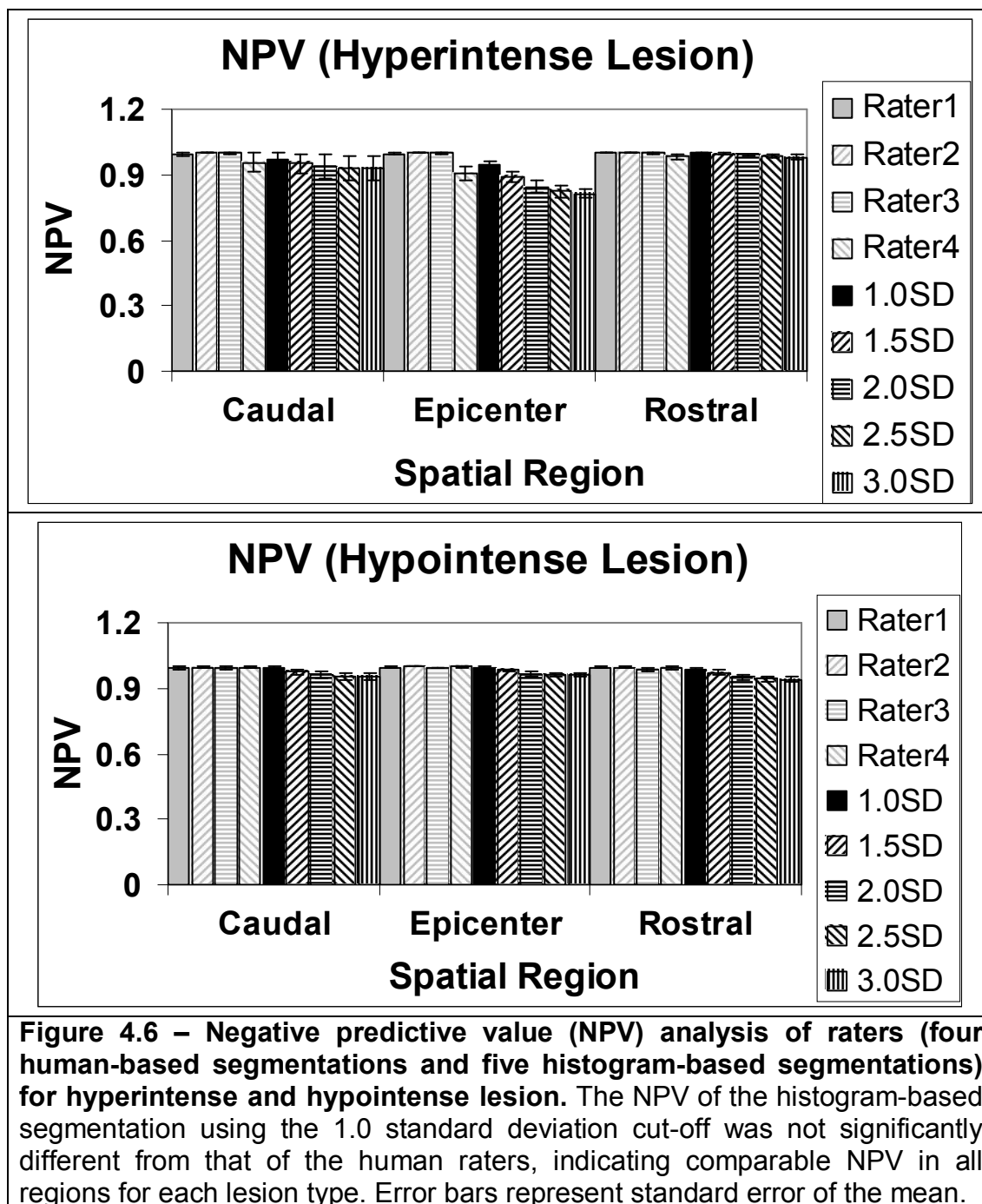
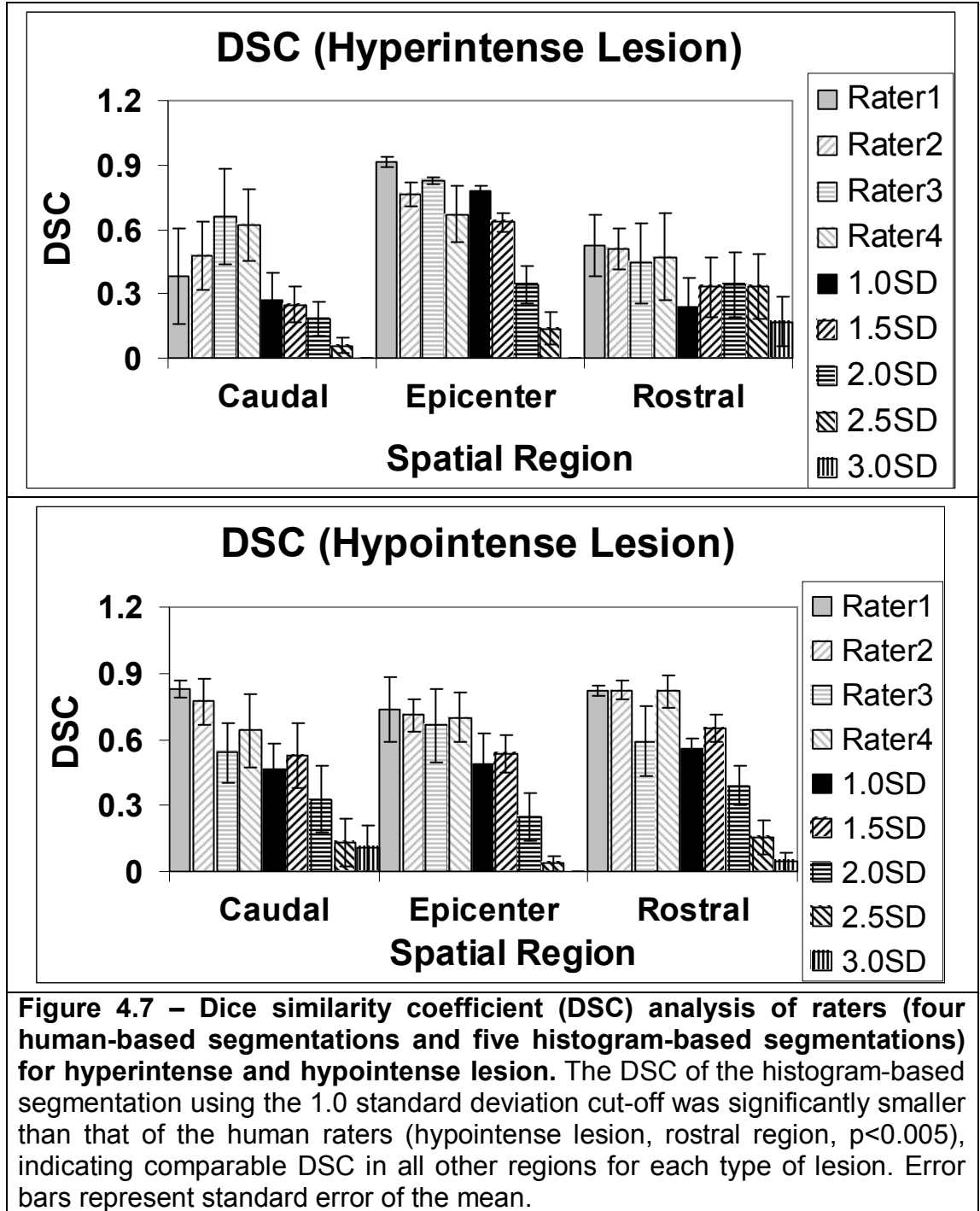


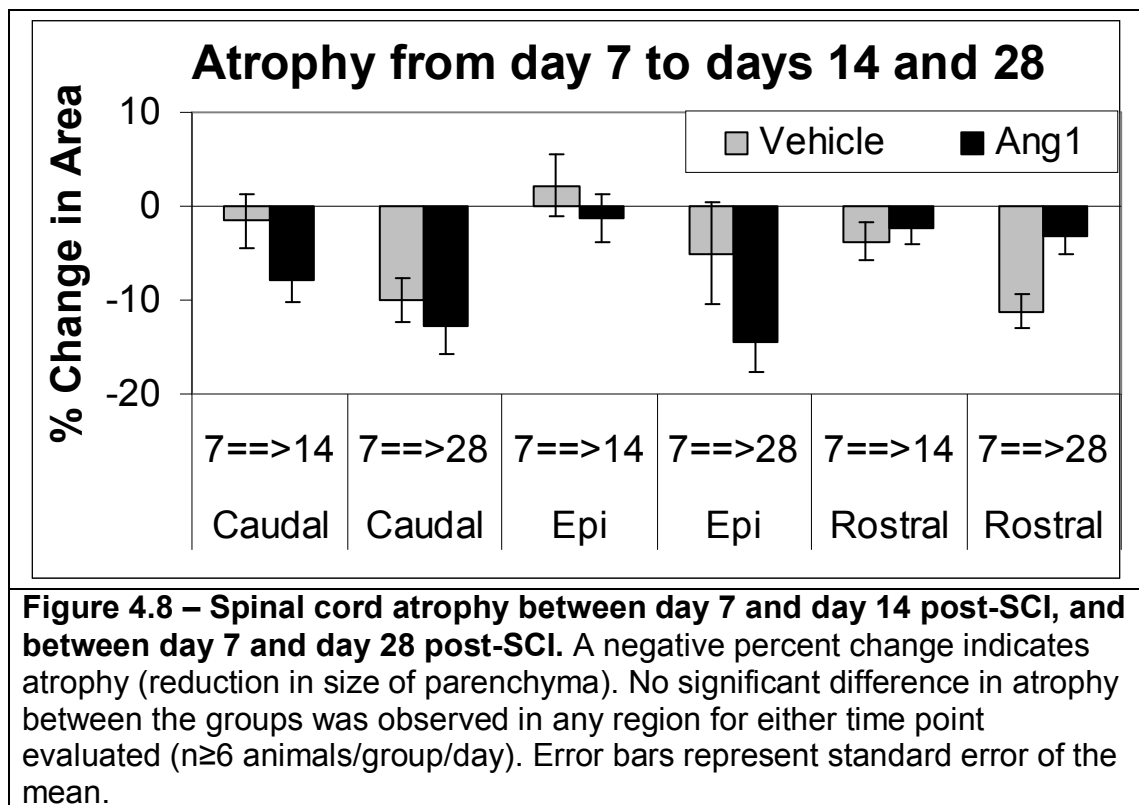
Figure 4.5 – Positive predictive value (PPV) analysis of raters (four human-based segmentations and five histogram-based segmentations) for hyperintense and hypointense lesion. The PPV of the histogram-based segmentation using the 1.0 standard deviation cut-off was significantly smaller than that of the human raters (hypointense lesion, rostral region, $p < 0.003$), indicating comparable PPV in all other regions for each type of lesion. Error bars represent standard error of the mean.





Atrophy

In order to understand the effects of Ang1 on atrophy after spinal cord injury, on a slice-by-slice basis, the percent difference in cord cross-sectional area between day 7 post-SCI and days 14 and 28 post-SCI was calculated. This analysis was performed on an intra-animal rather than intra-group basis, in order to ensure that the analysis was based on the exact same subgroup of animals ($n \geq 6$ animals per group). The results are presented in Figure 4.8 and indicate that, compared to vehicle, Ang1 did not have an effect on atrophy. Atrophy was greatest in the epicenter region and increased from day 14 post-SCI to day 28 post-SCI. In the Ang1 group but not the vehicle group, atrophy significantly increased between days 7-14 post-SCI and days 7-28 post-SCI ($p < 0.0005$) in the epicenter region. A temporal increase in atrophy was not observed in any other region for either group.



Lesion size

Applying the $1.0 \times \text{SD}$ cut-off, the hyperintense, hypointense, and total lesion sizes were determined as a fraction of the total cross-sectional area. The results are presented in Figure 4.9 (hyperintense lesion), Figure 4.10 (hypointense lesion), and Figure 4.11 (total lesion). A significant decrease in the lesion size (both hyperintense and total) was observed at the epicenter region at day 28 post-SCI in the Ang1 group compared to the vehicle group.

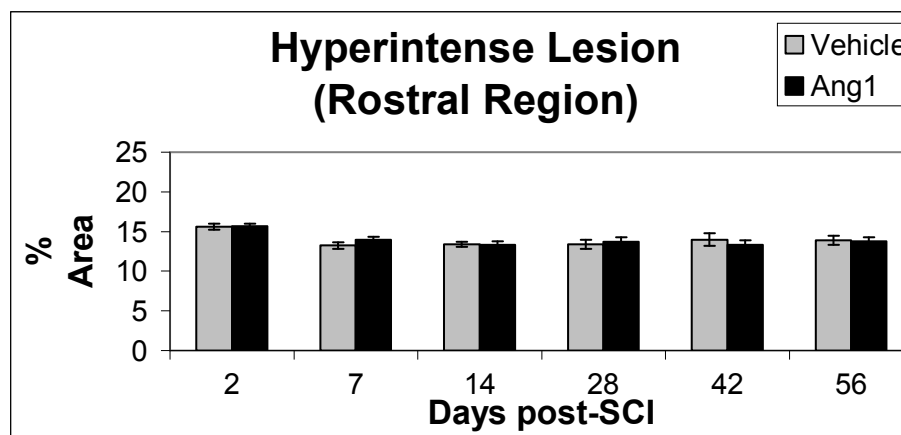
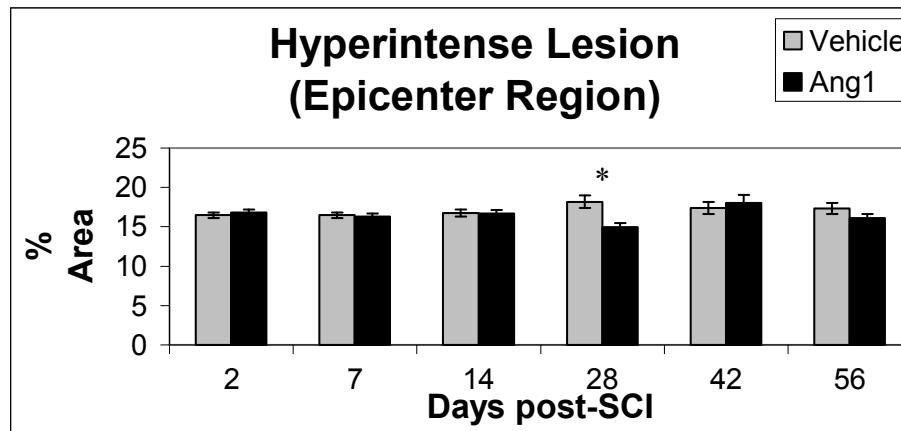
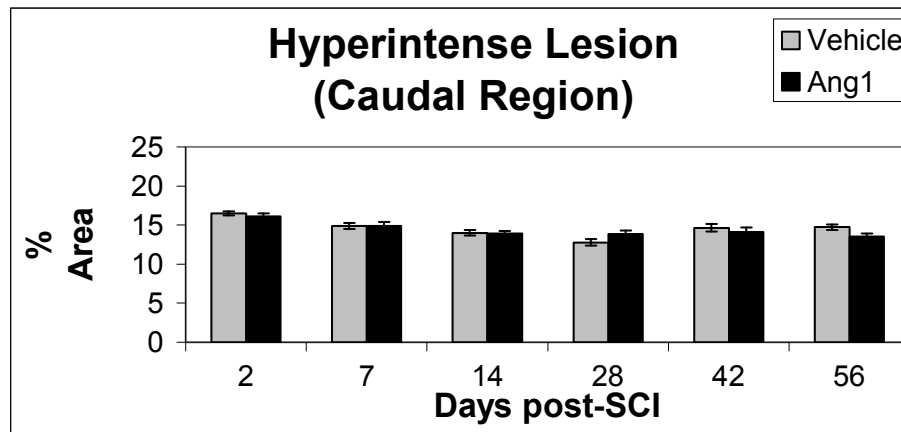


Figure 4.9 – Hyperintense lesion determined by objective histogram-based approach (1.0*standard deviation cut-off). *p<0.003. (n≥6 animals/group/day). Error bars represent standard error of the mean.

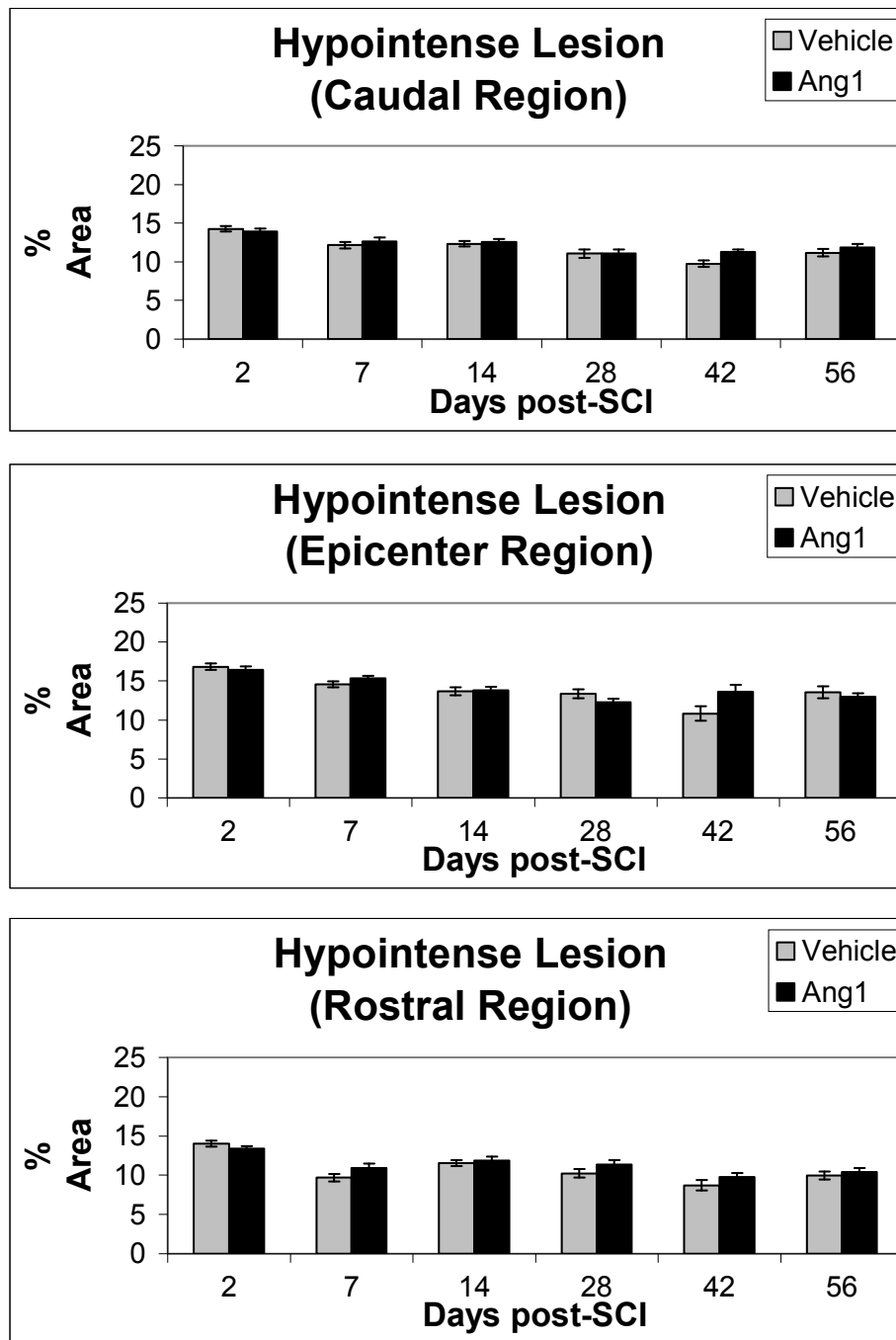


Figure 4.10 – Hypointense lesion determined by objective histogram-based approach (1.0*standard deviation cut-off). ($n \geq 6$ animals/group/day). Error bars represent standard error of the mean.

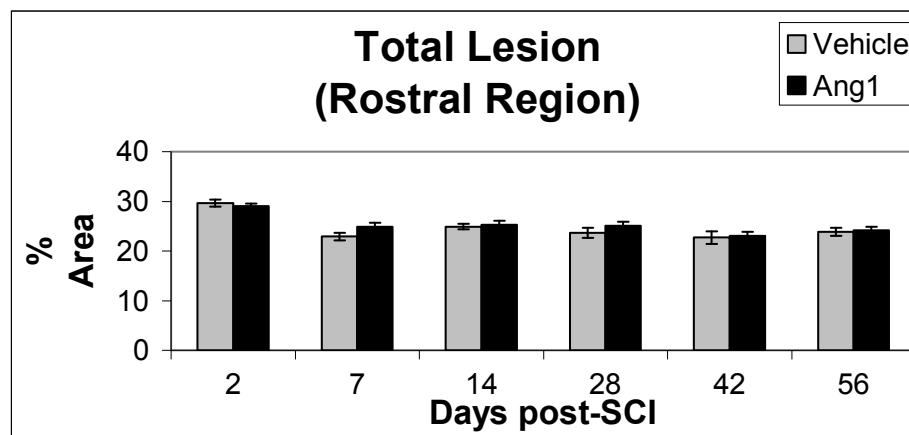
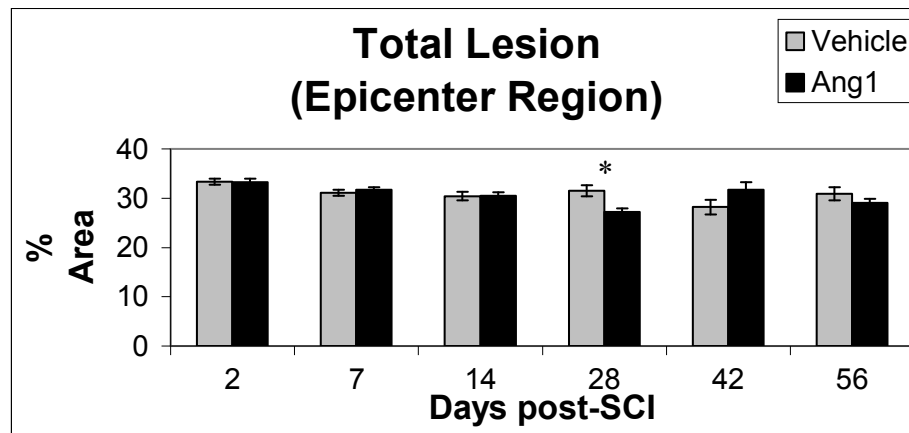
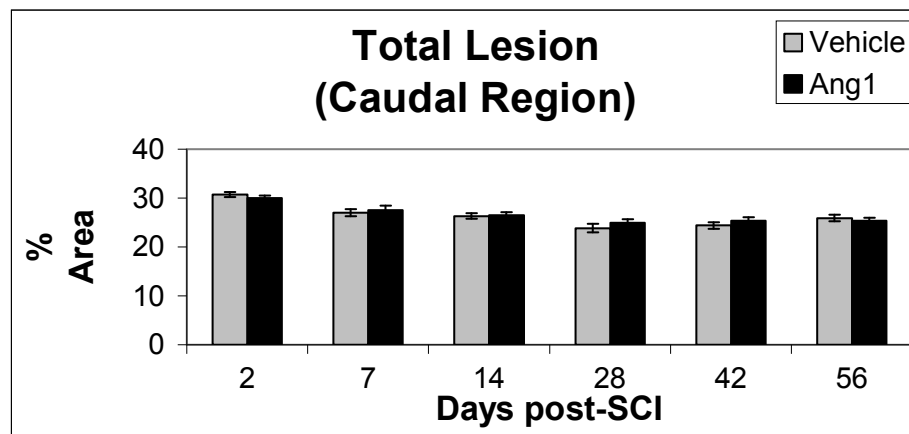


Figure 4.11 – Total lesion determined by objective histogram-based approach (1.0*standard deviation cut-off). * $p < 0.003$. ($n \geq 6$ animals/group/day). Error bars represent standard error of the mean.

DISCUSSION

In the absence of a ground truth for determining the lesion size in SCI, hyperintense and hypointense lesions are manually segmented with (Sundberg, 2009; Qian et al., 2010) or without (Nout et al., 2009) the assistance of objective absolute thresholds. Despite the best efforts to optimize the image quality, differences in SNR and signal intensity invariably are present from scan to scan, necessitating animal-, spatial region-, and time-specific absolute thresholds. This introduces some bias to the evaluation of lesion size. A histogram-based approach can consistently and objectively identify pixels whose signal intensity is above or below a relative threshold, which is based on the mean and standard deviation of signal intensity, on a slice-by-slice basis. Evaluation of the performance of the histogram-based approach compared to segmentation by human raters revealed comparable performance. However, the reference image used in these studies was obtained from the majority voting rule, which assumes that each rater is equally good at segmenting lesions and thus assigns a weight of $\frac{1}{4}$ to each. Newer methods, such as simultaneous truth and performance level estimation (STAPLE), allow for the generation of a reference segmentation in the absence of a ground truth (Warfield et al., 2004). Briefly, the STAPLE technique iteratively estimates the sensitivity and specificity of various image segmentations that are entered into the algorithm, with the end result of identifying each segmentation's sensitivity and specificity against a hidden ground truth. Use of this approach in future studies may reveal even more comparable performance between the histogram-based technique using $1.0 \times \text{SD}$ cut-off and human raters.

A significant increase in atrophy was observed from days 7-14 post-SCI to days 7-28 post-SCI in the Ang1 group. Given that Ang1 has been shown to be neuroprotective (Onda et al., 2008; Bai et al., 2009; Han et al., 2010), the atrophy effect observed in this study may be attributable to the single dose of Ang1 that was administered immediately after SCI. Because the animals scanned at 2 days-post SCI were not scanned thereafter, we were not able to determine the effect of Ang1 on atrophy during the acute phase of injury, when the effects of such a dose may be expected to be significant. Previous studies have determined maximum atrophy to occur at 14 days post-SCI (Deng et al., 2007). However, in the current study, the maximum atrophy (based on the 28-day window studied) occurred at 28 days post-SCI in each region in both groups. An *ex vivo* MRI-based study of atrophy during the ultrachronic phase of injury determined that atrophy was maximal at 5 months post-SCI (Scholtes et al., 2008). This may indicate increased atrophy over time with evolving secondary pathologies (e.g., tissue scarring). *In vivo* MRI assessment of atrophy in the late chronic and ultrachronic phases of SCI will need to be performed in order to validate the post-mortem findings of Scholtes et al.

In regards to lesion size, an effect of Ang1 in reducing the hyperintense and total lesion was observed in the epicenter region at 28 days post-SCI. During this time point (transition from subacute to the chronic phase of injury), the hyperintense signal on the second echo of the RARE MRI scan represents a transition from edema to demyelination. Thus, a reduced hyperintense lesion at 28 day post-SCI may indicate preserved white matter. This is consistent with the finding of Han et

al., who reported significantly reduced white matter loss in Ang1-treated animals compared to vehicle-treated animals, in the same region (epicenter), at 42 days post-SCI (Han et al., 2010). However, they also reported an increase at 7 days post-SCI, which may have occurred due to the daily administration of Ang1 in their study (Han et al., 2010). Han et al. quantified lesion volume histologically and reported it to be decreased at 7 days post-SCI in the group of animals that received daily injections of C-16, a ligand for $\alpha\beta3$ integrin; similar results for the Ang1 group were not reported in their study (Han et al., 2010).

Taken together, the results of the atrophy and lesion size analysis indicate that the effects of an acute administration of Ang1 may not be realized until the subacute/chronic phase. This is in contrast to the findings in the previous chapter, in which the effects of Ang1 on reducing BSCB permeability were realized as early as 2 days post-SCI. This suggests that the established effects of Ang1 on vascular endothelium take place closer to the time of administration, while perhaps its indirect effects may not be realized until later. For example, Ang1 has been shown to reduce inflammation through inhibition of NF- κ B via ABIN-2 (Hughes et al., 2003). Although reduced inflammation may result in decreased demyelination indirectly and in a delayed fashion, the direct effects on vascular endothelium are more pronounced (Tadros et al., 2003). An alternate explanation for the delayed effect of Ang1 on reducing lesion size, despite reducing BSCB permeability as early as 2 days post-SCI, is that the dose of Ang1 was not sufficient for its anti-inflammatory effects to be significant in the acute phase of injury. Using daily injections of Ang1 after SCI, Han et al. demonstrated that an increased and

sustained dose of Ang1 can lead to a reduction in white matter loss (i.e., decreased lesion size) in both the acute and chronic phases of injury (Han et al., 2010).

As another example, Ang1 has been shown to reduce the expression of cell adhesion molecules, e.g. intercellular adhesion molecule 1 (ICAM-1), which facilitate the adhesion and subsequent transendothelial migration of leukocytes (Kim et al., 2001) into the injured cord. Studies that directly target ICAM-1, which has been shown to be endogenously upregulated in SCI (Isaksson et al., 1999), have demonstrated improved neurobehavioral recovery (Hamada et al., 1996; Farooque et al., 1999) and white matter preservation (Farooque et al., 2001) after injury. In the absence of histological assessment in the current studies, the effects of a single dose of Ang1 on ICAM-1 expression is unknown. Even if a role for Ang1-mediated reduction in ICAM-1 expression after SCI were to exist, the benefits of directly targeting ICAM-1 observed in previous studies was not observed in this study. This highlights the fact that, despite mitigating various known secondary pathologies of SCI, Ang1's most immediate effect in the current study was in the context of reducing vascular permeability.

In summary, the results indicate that, at 28 days post-SCI, a single acute dose of Ang1 reduces lesion size at the epicenter of injury. The methods used in these studies can be applied in other models of spinal cord injury, which may enable consistent reporting of results that will allow for meaningful comparative analysis across studies.

Limitations

The results of these studies should be considered in the context of its limitations. First, the STAPLE method was not used to establish the ground truth reference image based on the human rater segmentations. Although the STAPLE-based reference image may not be significantly different than the one used in these studies (due to the small number of pixels encompassed by the rat spinal cord), plans are underway to employ this approach and re-assess the performance of the histogram-based technique. Second, the analysis of lesion size was not completely automated because the CSF and surrounding tissue were manually stripped from the spinal cord prior to analysis. Although methods for automated stripping have been reported (Deng et al., 2007), they still require an initial human-based input (seed point). Nonetheless, full automation of the proposed method would further reduce any possible bias introduced by user intervention.

CHAPTER 5:

EFFECT OF SINGLE ACUTE ANG1 DOSE ON AXONAL INTEGRITY AND NEUROBEHAVIORAL RECOVERY AND LONGITUDINAL CORRELATION WITH LESION SIZE

INTRODUCTION

Reduced axonal integrity and demyelination are major consequences of spinal cord injury that affect motor function (Blight, 1985; Waxman, 1992; Hagg and Oudega, 2006; McDonald and Belegu, 2006). Therapeutic remyelination approaches have been studied in the context of spinal cord injury (Klussmann and Martin-Villalba, 2005; Sasaki et al., 2007; McTigue and Tripathi, 2008; Wu and Ren, 2009). In fact, the first study to receive FDA approval for the treatment of human SCI involves intraspinal injection of oligodendrocyte progenitor cells that are hypothesized to assist with the process of axonal remyelination (Couzin, 2009).

Diffusion tensor imaging, a MRI modality, allows for the evaluation of axonal integrity and has been applied in the context of spinal cord injury (Fenyes and Narayana, 1999; Madi et al., 2005; Deo et al., 2006). A high mean diffusivity (MD), defined as the average diffusivity in the three primary orthogonal directions (λ_1 , λ_2 , and λ_3), indicates a lack of structure that enables water molecules to diffuse in a non-preferential manner. Coupled with high MD, low fractional anisotropy (FA, an indicator of the diffusion anisotropy that reflects the orderliness of tissue structure) are indicative of poor axonal integrity. On the other hand, low MD in the presence of high FA is indicative of high axonal integrity. MD can be subdivided further into longitudinal diffusivity ($\lambda_L = \lambda_1$) and transverse diffusivity ($\lambda_T = 0.5*\lambda_2 + 0.5*\lambda_3$). Although λ_T and λ_L have been shown to be correlated with demyelination and axonal damage, respectively (Budde et al., 2007; Herrera et al., 2007), controversy remains in the literature regarding the specificity of these DTI measures for white matter pathology. Due to the highly organized nature of axons comprising the

fibers of white matter tracts and the impedance provided by myelin, $\lambda_L > \lambda_T$ (Hasan and Narayana, 2006).

In the assessment of white matter pathology after SCI, correlations between axonal integrity and measures from neurobehavioral assessments can be used to probe structure-function relationships. Such assessments include the open-field BBB locomotor assay (Basso et al., 1995), inclined plane test for evaluating axial muscle strength and control of posture (Rivlin and Tator, 1977), grid walk test for assessment of hindlimb-forelimb sensory and motor coordination (Bresnahan et al., 1987), and computerized activity box system for testing of gross motor movement (i.e., ambulation), fine motor movement, and rearing (Mills et al., 2001). Neurosensory assessment of mechanical allodynia is assessed with the von Frey filament (Peng et al., 2006).

The purpose of these studies was to evaluate the effects of acutely administered Ang1 on axonal integrity, neurobehavioral recovery, and neuropathic pain during the subacute and chronic phases of spinal cord injury, with additional assessment of possible correlations among neurobehavioral and MRI measures.

RESULTS

DTI measures

Table 5.1 summarizes the inter-group significant differences in mean diffusivity values in the four ROIs described in the methodology chapter (dorsal, CST, lateral, and ventral), by days post-SCI and spatial region. Mean diffusivity was significantly greater in the Ang1 group during the subacute phase but significantly greater in the vehicle group during the chronic phase.

ROI	Days post-SCI	Spatial Region	Vehicle	Operator	Ang1	p-value
Dorsal	7	Epicenter	0.00069± 0.000045	<	0.00088± 0.000054	p<0.003
	56	Epicenter	0.0017± 0.00014	>	0.00098± 0.000091	p<0.0008
CST	56	Caudal	0.00093± 0.00015	>	0.00050± 0.000044	p<0.007
	56	Epicenter	0.0017± 0.00016	>	0.00087± 0.000095	p<0.0003
Lateral	7	Epicenter	0.00069± 0.000030	<	0.00095± 0.000050	p<0.00001
	7	Rostral	0.00072± 0.000033	<	0.00092± 0.000057	p<0.016
	14	Epicenter	0.00069± 0.000043	<	0.00092± 0.000029	p<0.00001
	14	Rostral	0.00078± 0.000050	<	0.00093± 0.000025	p<0.0008
Ventral	14	Epicenter	0.00069± 0.000041	<	0.00096± 0.000038	p<0.00001

Table 5.1 – Summary of significant inter-group differences in mean diffusivity (units: mm²s⁻¹). Ang1 = angiopoietin-1, CST = corticospinal tract, SCI = spinal cord injury. (n≥6 animals/group/day). Data are presented as mean±standard error of the mean.

Table 5.2 summarizes the significant differences in fractional anisotropy between the two groups. Converse to the findings in MD, FA was significantly reduced in the Ang1 group during the subacute phase but significantly greater in the Ang1 group during the chronic phase. The findings in FA and MD are complementary in that reduced MD with concomitantly increased FA is indicative of higher axonal integrity, whereas increased MD with concomitantly reduced FA is indicative of poor axonal integrity. Taken together, in the Ang1 group compared to vehicle group, these findings indicate reduced axonal integrity during the subacute phase and increased axonal integrity during the chronic phase.

ROI	Days post-SCI	Spatial Region	Vehicle	Operator	Ang1	p-value
Dorsal	42	Epicenter	0.22±0.04	<	0.40±0.04	p<0.004
Lateral	7	Rostral	0.61±0.02	>	0.41±0.04	p<0.00001
	14	Epicenter	0.47±0.03	>	0.36±0.02	p<0.011
Ventral	7	Rostral	0.65±0.03	>	0.50±0.03	p<0.003
	14	Rostral	0.64±0.03	>	0.52±0.03	p<0.0165
Table 5.2 – Summary of significant inter-group differences in fractional anisotropy (unitless). Ang1 = angiopoietin-1, CST = corticospinal tract, SCI = spinal cord injury. (n≥6 animals/group/day). Data are presented as mean±standard error of the mean.						

Table 5.3 summarizes the significant differences in longitudinal diffusivity between the two groups. Consistent with the temporal pattern observed for MD in the Ang1 group, λ_L was significantly greater in the subacute phase and significantly reduced in the chronic phase.

ROI	Days post-SCI	Spatial Region	Vehicle	Operator	Ang1	p-value
Dorsal	7	Epicenter	0.00094± 0.00007	<	0.00120± 0.00010	p<0.002
	56	Epicenter	0.00203± 0.00016	>	0.00121± 0.00011	p<0.0004
CST	56	Caudal	0.00126± 0.00017	>	0.00077± 0.00004	p<0.012
	56	Epicenter	0.00202± 0.00017	>	0.00118± 0.00012	p<0.0003
Lateral	7	Epicenter	0.00104± 0.00007	<	0.00132± 0.00009	p<0.003
	14	Epicenter	0.00104± 0.00007	<	0.00132± 0.00006	p<0.0003
	14	Rostral	0.00131± 0.00009	<	0.00160± 0.00006	p<0.002
	56	Epicenter	0.00197± 0.00007	>	0.00164± 0.00009	p<0.006
Ventral	14	Epicenter	0.00099± 0.00008	<	0.00140± 0.00009	p<0.0008
Table 5.3 – Summary of significant inter-group differences in longitudinal diffusivity (units: mm²s⁻¹). Ang1 = angiotensin-1, CST = corticospinal tract, SCI = spinal cord injury. (n≥6 animals/group/day). Data are presented as mean±standard error of the mean.						

Table 5.4 summarizes the significant differences in transverse diffusivity between the two groups. As was the case with MD and λ_L in the Ang1 group, λ_T was significantly increased in the subacute phase and significantly reduced during the chronic phase.

ROI	Days post-SCI	Spatial Region	Vehicle	Operator	Ang1	p-value
Dorsal	7	Epicenter	0.00056± 0.00003	<	0.00073± 0.00005	p<0.004
	14	Caudal	0.00045± 0.00005	<	0.00061± 0.00005	p<0.016
	56	Epicenter	0.00146± 0.00014	>	0.00087± 0.00009	p<0.002
CST	56	Caudal	0.00076± 0.00015	>	0.00036± 0.00005	p<0.012
	56	Epicenter	0.00155± 0.00016	>	0.00072± 0.00009	p<0.0004
Lateral	7	Epicenter	0.00052± 0.00002	<	0.00076± 0.00004	p<0.00001
	7	Rostral	0.00042± 0.00002	<	0.00070± 0.00005	p<0.00001
	14	Epicenter	0.00051± 0.00004	<	0.00072± 0.00003	p<0.00001
Ventral	7	Epicenter	0.00050± 0.00003	<	0.00072± 0.00007	p<0.003
	14	Epicenter	0.00054± 0.00003	<	0.00075± 0.00003	p<0.00001
	14	Rostral	0.00049± 0.00006	<	0.00061± 0.00003	p<0.007
Table 5.4 – Summary of significant inter-group differences in transverse diffusivity (units: mm²s⁻¹). Ang1 = angiopoietin-1, CST = corticospinal tract, SCI = spinal cord injury. (n≥6 animals/group/day). Data are presented as mean±standard error of the mean.						

The results of analysis of the DTI measures indicate that a single administration of Ang1 in the acute phase of injury resulted in reduced axonal integrity during the subacute phase but improved axonal integrity during the

chronic phase. Functional correlates of WM integrity, i.e., neurobehavioral recovery, are presented in the next section.

Neurobehavioral assays

Figure 5.1 displays the BBB scores over time. The BBB score was significantly increased in the Ang1 group at 2 days post-SCI and 3 days post-SCI. These results provide evidence for an Ang1 treatment effect on neurobehavioral recovery in the acute phase of injury.

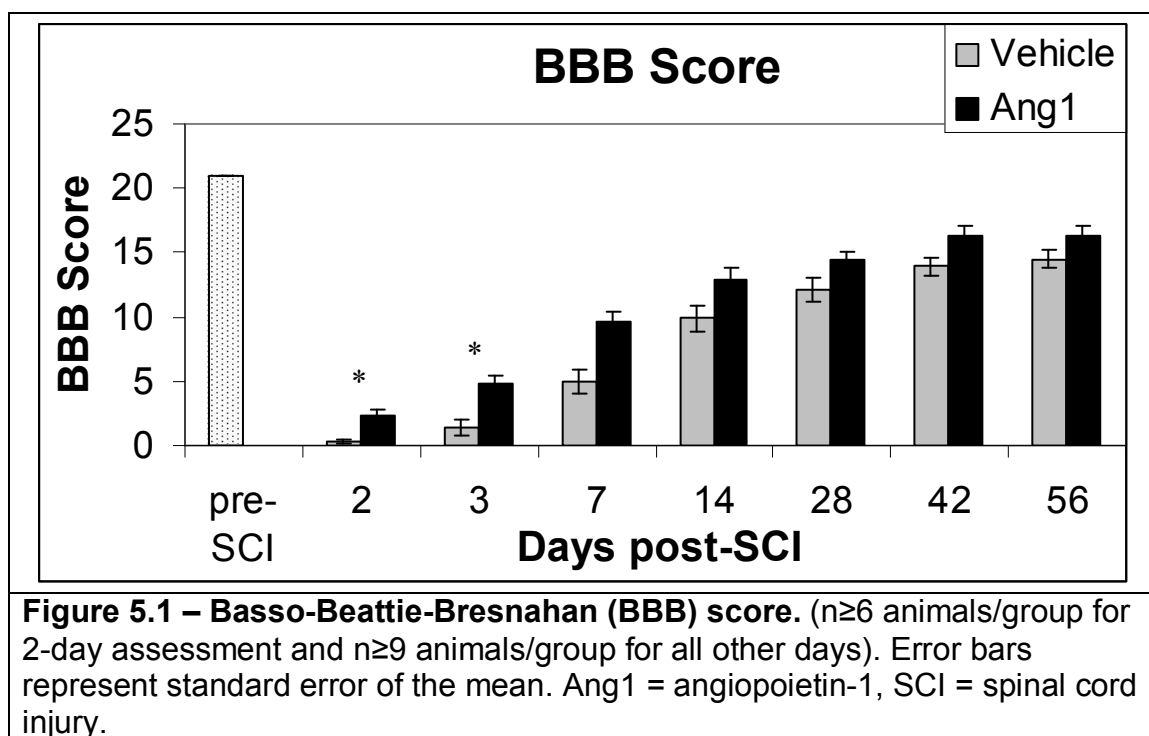


Figure 5.2 displays the inclined plane assessment results over time. There was no significant difference between the groups at any time point.

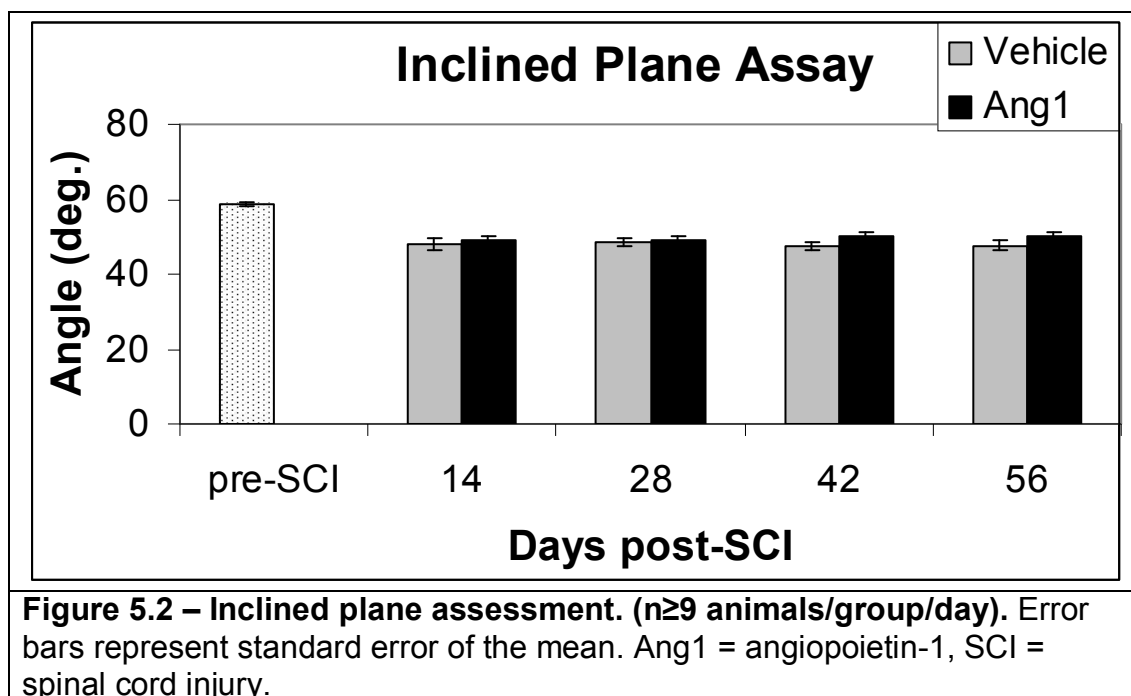


Figure 5.3 displays the grid walk results over time. There was no significant difference between the groups at any time point. It is important to note that for this assay, a smaller value is beneficial (i.e., improved sensory-motor integration between hindlimbs and forelimbs would lead to a reduction in foot falls as the rats traverse the mesh grid).

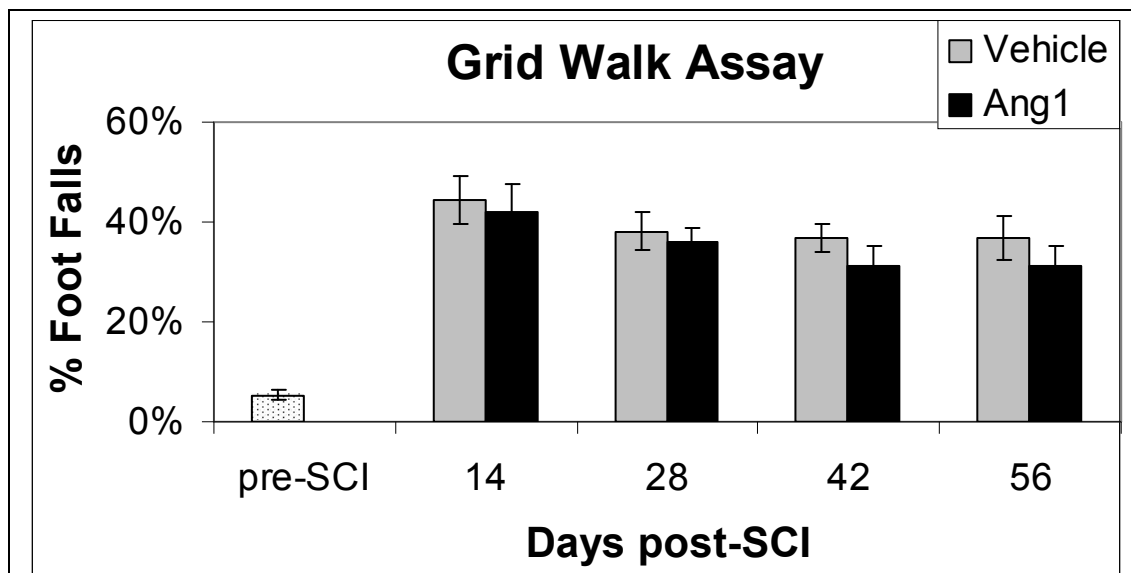
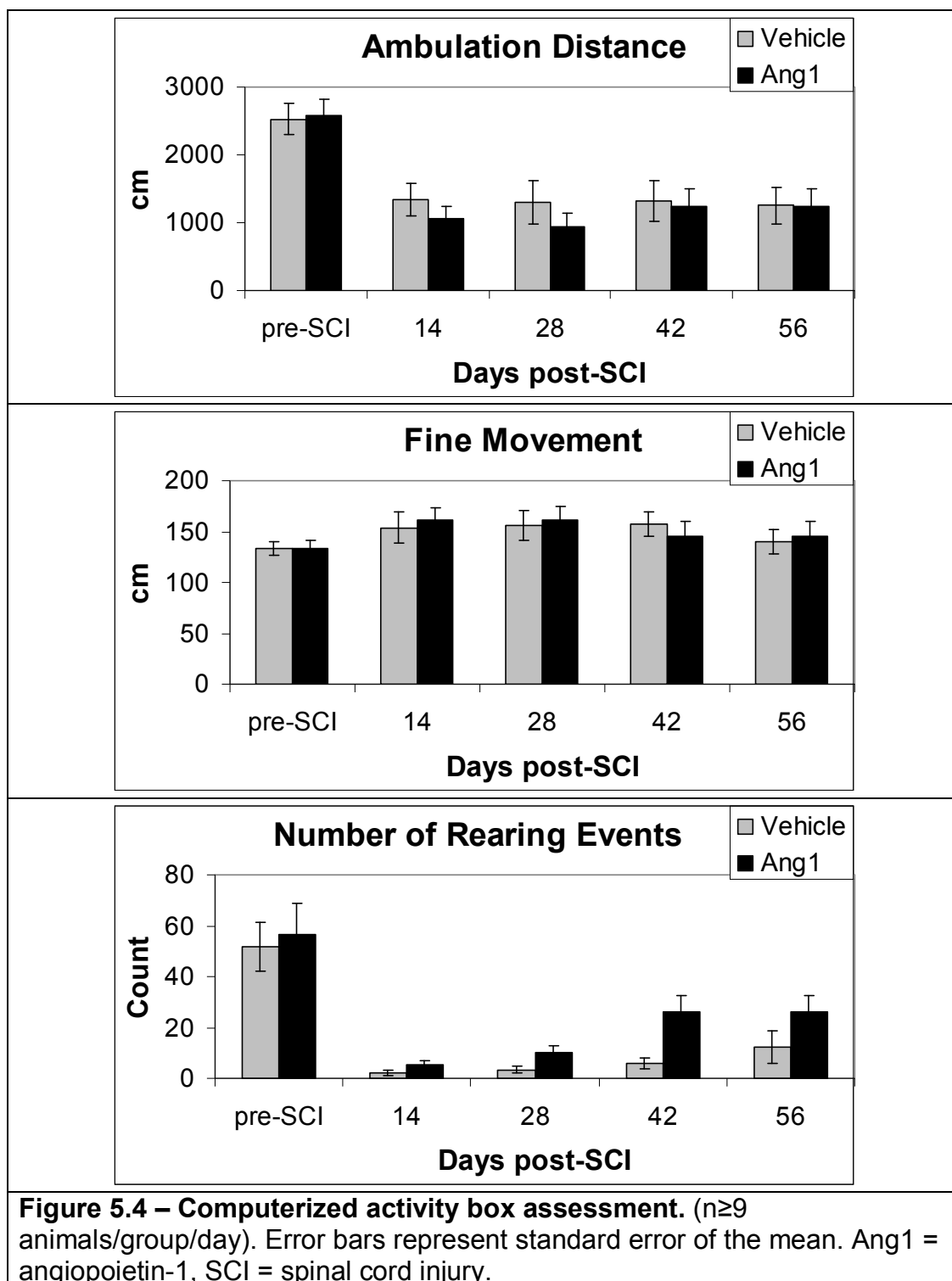
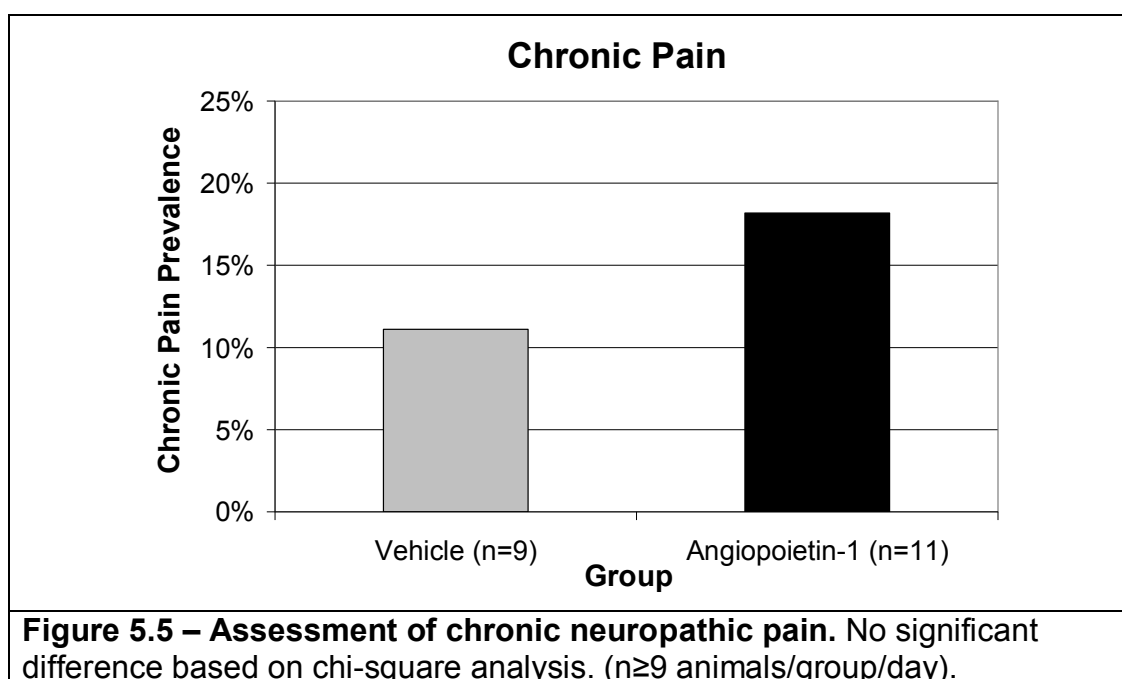


Figure 5.3 – Grid walk assessment. (n≥9 animals/group/day). Error bars represent standard error of the mean. Ang1 = angiotensin-1, SCI = spinal cord injury.

Figure 5.4 displays the computerized activity box results over time. There was no significant difference between the groups at any time point for any of the measures (ambulation distance, fine movement, and number of rearing events).



Previous studies have implicated a role for neurotrophin-3 and vascular endothelial growth factor (VEGF) in the induction of neuropathic pain in models of peripheral nerve injury and spinal cord injury, respectively (Deng et al., 2000; Sundberg, 2009). In the latter study, VEGF's role in causing chronic neuropathic pain (defined in the Materials and Methods chapter) was attributed to preservation of nociceptive neurons in tissue spared by VEGF treatment (Sundberg, 2009). Figure 5.5 displays the results of the von Frey hair test for chronic neuropathic pain. There was no significant difference in prevalence of chronic pain between the two groups. This is an interesting finding in the context of the results of the previous chapter, in which Ang1 was shown to reduce lesion volume in the chronic phase of injury.



Longitudinal correlations

Generalized estimating equation (GEE) method was employed to assess for significant correlations between lesion size, MD, FA, λ_L , λ_T , and BBB scores. The significant longitudinal correlations between the BBB score and DTI and RARE MRI measures are presented in Table 5.5. Significant positive correlations between BBB score and the DTI measures of MD, λ_L , and λ_T were observed in the epicenter region of vehicle-treated animals. In the epicenter and caudal regions of Ang1-treated animals, hyperintense, hypointense, and total lesion size as a percent of spinal cord cross-sectional area negatively correlated with BBB score. This was also the case for vehicle-treated animals but only in for hyperintense lesion in the rostral region.

Correlation Between BBB score and:	Group	Spatial Region	Sign of Correlation	p-value
Hyperintense lesion	Ang1	Caudal	Negative	p<0.012
	Vehicle	Rostral	Negative	p<0.004
Hypointense lesion	Ang1	Caudal	Negative	p<0.007
	Ang1	Epicenter	Negative	p<0.0001
Total lesion	Ang1	Caudal	Negative	p<0.003
	Ang1	Epicenter	Negative	p<0.0001
MD in CST ROI	Vehicle	Epicenter	Positive	p<0.0001
λ_L in CST ROI	Vehicle	Epicenter	Positive	p<0.0001
λ_T in CST ROI	Vehicle	Epicenter	Positive	p<0.0001
Table 5.5 – Significant longitudinal correlations between Basso-Beattie-Bresnahan (BBB) score and measures from high-resolution anatomical and diffusion tensor imaging scans. Ang1 = angiopoietin-1, CST = corticospinal tract, MD = mean diffusivity, λ_L = longitudinal diffusivity, λ_T = transverse diffusivity. (n≥6 animals/group/day).				

Table 5.6 summarizes the significant longitudinal correlations between lesion sizes and DTI measures in the CST. In both groups, hyperintense lesion size positively correlated with hypointense lesion size in each of the three spatial regions. In regards to anatomical-DTI MRI correlations, these were significant only for hyperintense lesions, which positively correlated with MD, λ_L , and λ_T , and negatively correlated with FA.

Measure 1	Measure 2	Group	Spatial Region	Correlation	p-value
Hyperintense lesion	Hypointense lesion	Ang1	Caudal	Positive	p<0.012
		Ang1	Epicenter	Positive	p<0.0001
		Vehicle	Caudal	Positive	p<0.003
		Vehicle	Epicenter	Positive	p<0.0001
		Vehicle	Rostral	Positive	p<0.0001
	Total lesion	Ang1	Caudal	Positive	p<0.0001
		Ang1	Epicenter	Positive	p<0.0001
		Ang1	Rostral	Positive	p<0.0001
		Vehicle	Caudal	Positive	p<0.0001
		Vehicle	Epicenter	Positive	p<0.0001
		Vehicle	Rostral	Positive	p<0.0001
	FA in CST	Ang1	Epicenter	Negative	p<0.0001
	MD in CST	Vehicle	Epicenter	Positive	p<0.002
	λ_L in CST ROI	Ang1	Caudal	Positive	p<0.011
		Vehicle	Epicenter	Positive	P<0.003
	λ_T in CST ROI	Vehicle	Epicenter	Positive	p<0.002
Hypointense lesion	Total lesion	Ang1	Caudal	Positive	p<0.0001
		Ang1	Epicenter	Positive	p<0.0001
		Ang1	Rostral	Positive	p<0.0001
		Vehicle	Caudal	Positive	p<0.0001
		Vehicle	Epicenter	Positive	p<0.0001
		Vehicle	Rostral	Positive	p<0.0001

Table 5.6 – Significant longitudinal correlations between lesion measures and diffusion tensor imaging measures. Ang1 = angiopoietin-1, CST = corticospinal tract, FA = fractional anisotropy, MD = mean diffusivity, λ_L = longitudinal diffusivity, λ_T = transverse diffusivity. (n≥6 animals/group/day).

Summary of results

The DTI, neurobehavioral, and correlational analysis studies described in this chapter indicate that Ang1 administration improves neurobehavioral recovery

in the acute phase of injury, transiently results in reduced axonal integrity during the subacute phase of injury, and improve axonal integrity during the chronic phase. The hyperintense lesion, which was shown in the previous chapter to be significantly reduced during the chronic phase in the Ang1 group, was negatively correlated with FA, a measure of axonal integrity. Finally, despite Ang1-mediated tissue sparing in the chronic phase, chronic neuropathic pain was not observed in this study.

DISCUSSION

Overall, these findings indicate a pattern of reduced axonal integrity in the Ang1 group in the subacute phase (decreased FA and increased MD compared to control) and a pattern of improved axonal integrity in the chronic phase (increased FA and decreased MD compared to control). However, when the MD is subdivided into its constituent components of λ_L and λ_T , the pattern is not as clear. This may be due to the role of multiple modulators of λ_L and λ_T beyond axonal integrity and myelination status, respectively. For example, although much focus of the role of Ang1 is placed on its effects on vascular endothelium, neuronal cells that express Tie-2 have been shown to be directly affected by Ang1. In cultured dorsal root ganglion cells exposed to Ang1, Kosacka et al. observed neurite outgrowth (so-called “sprouting”) (Kosacka et al., 2005; Kosacka et al., 2006) in cells expressing Tie-2. There is also evidence from studies in cultured PC12 cells (modified postganglionic neurons in the medulla of rat adrenal glands) that Ang1 induces sprouting in a Tie-2-independent but $\beta 1$ -integrin-dependent manner (Chen et al., 2009). At the microscopic level, such outgrowth of unmyelinated neurites at different angles relative to the primary axon could contribute to the decreased FA observed in the Ang1 group in the subacute phase. During this phase of injury, the concomitant increase in λ_L and λ_T in the Ang1 group indicates increased diffusion both parallel and perpendicular to the axon. Angiopoietin-1 has also been shown to be neuroprotective via different mechanisms, including prevention of neuronal apoptosis (Valable et al., 2003), promotion of neurogenesis (Rosa et al., 2010), and triggering neuroblast migration to damaged CNS tissue (Ohab et al., 2006).

Although changes in λ_L and λ_T are traditionally thought to be complementary in moderate contusion SCI, i.e. reduced λ_L and increased λ_T (Ellingson et al., 2008), the neuroprotective and sprouting effects of Ang1 may result in simultaneously increased λ_L and λ_T , as was observed in this study.

In two separate cohorts of animals (those used for the acute study and those for the longitudinal study), Ang1 was found to result in improved locomotor recovery during the acute phase. After administering daily injections of Ang1 in a mouse model of SCI, Han et al. reported improved locomotor recovery at days 7-42 post-SCI (Han et al., 2010). These findings suggest that prolonged Ang1 administration beyond a single acute time point may facilitate improved locomotor recovery in our experimental model during the subacute and chronic phases of injury. Another notable finding of the neurobehavioral analysis in this study was the lack of difference in chronic pain between both groups, despite a significant preservation of tissue in the Ang1 group as shown in the previous chapter. Sundberg reported an exacerbation of chronic pain in SCI rats treated with vascular endothelial growth factor (VEGF), which also reduced lesion size compared to her control group (Sundberg, 2009). She postulated that the increased chronic pain in VEGF-treated animals was attributable to the preservation of nociceptive neurons in the tissue salvaged by VEGF therapy (Sundberg, 2009). These results suggest that Ang1 exposure post-SCI may result in the neuromotor benefit of tissue preservation without the unwanted consequence of chronic neuropathic pain, which is part of a spectrum of pain

conditions experienced by up to 80% of patients suffering from spinal cord injury (Hulsebosch et al., 2009).

Gullapalli et al. have previously evaluated white matter tracts in uninjured rat spinal cord (Gullapalli et al., 2006). In the present study, the corticospinal tract was segmented in addition to those previously reported (Deo et al., 2006; Sundberg, 2009) in order to determine any potential correlations between DTI measures in this critical tract and the BBB open-field locomotor score. Longitudinal correlational analysis with GEE method revealed a significant positive correlation between BBB score and MD, λ_L , and λ_T . While the correlation with λ_L may be intuitive, that with MD and λ_T may not be, because increased λ_T has previously been reported to be correlated with demyelination (Herrera et al., 2007). This again points to the possible contributions of other processes (e.g. neurite sprouting) to alterations in DTI measures after spinal cord injury.

In the Ang1 group, the hyperintense lesion was positively correlated with λ_L and negatively correlated with FA. The reduced extent of edema (acute phase) or demyelination (subacute and chronic phases) as evidenced by decreased lesion size in the Ang1 group (previous chapter) may account for the positive correlation. The BBB score was also found to be negatively correlated with total lesion size in the epicenter region of the Ang1 group, which is consistent with Han et al.'s finding of a positive correlation between locomotor score and white matter preservation (Han et al., 2010).

Limitations

The novel DTI-based findings in the corticospinal tract, longitudinal correlations between behavioral and MRI-based measures, and lack of chronic neuropathic pain despite tissue sparing are the main contributions of these studies. The results should also be considered in the context of the study's limitations. Longitudinally scanning the animals in order to ensure reporting of *in vivo* measures is a double-edged sword in that histological analysis can not be performed and correlated with MRI measures at serial time points to provide a biological context to the findings on MRI. Given that an interesting transient reduction in axonal integrity during the subacute phase was observed in the Ang1 group, histological assessment of possible determinants of altered λ_L and λ_T during this phase of injury would be helpful in broadening our understanding of the meaning of the changes in these DTI measures.

CHAPTER 6:

CONCLUSIONS AND FUTURE STUDIES

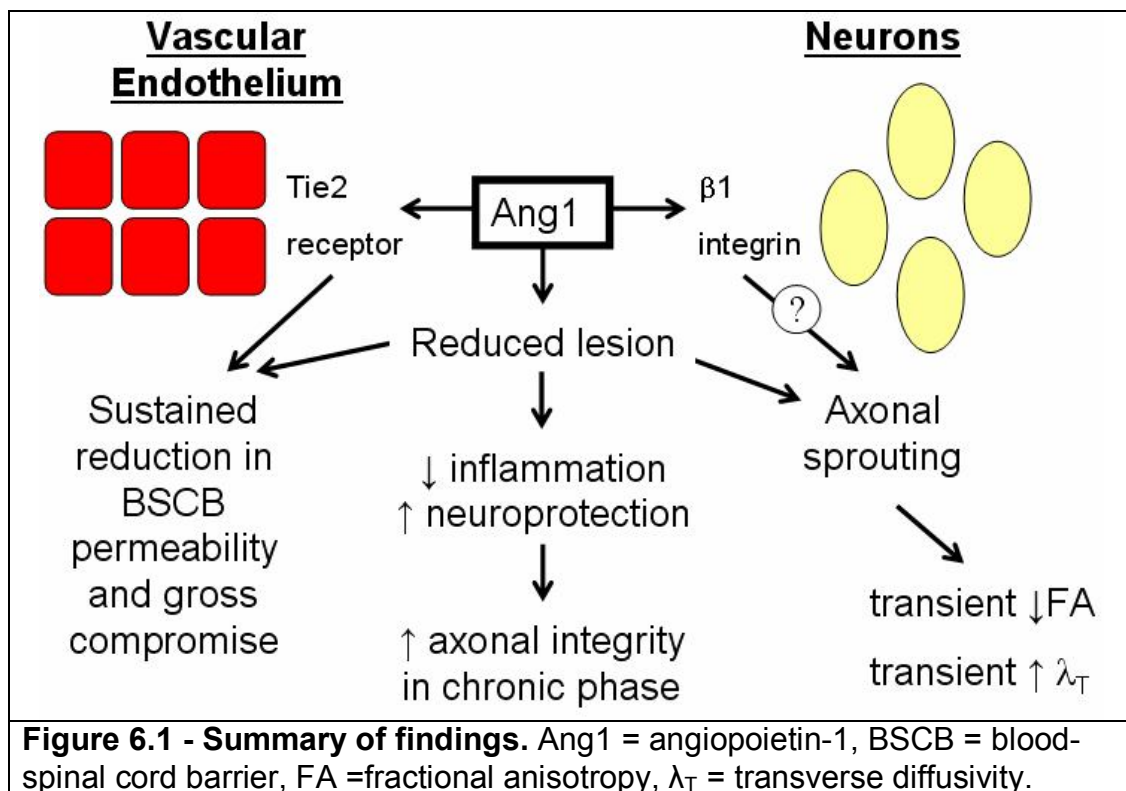
The purpose of these studies was to determine the effects of a single dose of Ang1 administered immediately after spinal cord injury in a rat model of contusion SCI. The summary of results is presented in Table 6.1

SCI Phase	BSCB	Axonal integrity	Lesion	Neurobehavioral Assessment
Acute (2-3 days post-SCI)	↓ Frank enhancement ↓ Permeability	Not studied		↑ BBB score
Subacute (7-14 days post-SCI)	↓ Frank enhancement ↓ Permeability	↓ FA, ↑ MD ↑ λ_L , ↑ λ_T		
Chronic (28-56 day post-SCI)	↓ Frank enhancement ↓ Permeability	↑ FA, ↓ MD ↓ λ_L , ↓ λ_T	↓ Lesion	
Table 6.1 - Summary of study findings. BBB = Basso-Beattie-Bresnahan score, BSCB = blood-spinal cord barrier, FA = fractional anisotropy, MD = mean diffusivity, SCI = spinal cord injury, λ_L = longitudinal diffusivity, λ_T = transverse diffusivity.				

In the acute phase of injury, Ang1 resulted in a reduction in BSCB permeability and the fraction of spinal cord tissue with visually apparent BSCB compromise, and an improvement in the BBB score. In the subacute phase, Ang1's effects on the BSCB were maintained but Ang1 resulted in reduced axonal integrity and the improvement in BBB score was not maintained. In the chronic phase, the effects of Ang1 on the BSCB were maintained and Ang1 resulted in improved axonal integrity with no difference in behavioral outcomes.

Ang1 has been shown to target various components of the BSCB (e.g., occludin (Iizasa et al., 2002; Hori et al., 2004; Wang et al., 2007), vascular endothelial cadherin (Gavard et al., 2008; Mochizuki, 2009), vascular endothelial cells (Thurston et al., 1999; Thurston et al., 2000), and the glycocalyx (Salmon et al., 2009)), resulting in reduced permeability. In addition, Ang1 has been shown to mediate neuroprotective effects on neuronal cells directly (Ohab et al., 2006; Chen

et al., 2009). Because the BSCB is a part of the neurovascular unit (Choi and Kim, 2008), its compromise leads to a number of pathological events, including hemorrhage (via mechanical trauma to the vessels), edema (via extravasation of plasma proteins), inflammation / free-radical production (via neutrophil transendothelial migration), and neuronal apoptosis (via vasospasm and ischemia). The differential effects of Ang1 on the vascular endothelium and neuronal tissue may be mediated through different signaling pathways, each of which involves Ang1 as a ligand. Figure 6.1 summarizes the findings in pictorial form.



A major limitation of these studies is the lack of histological validation of the findings of the various MRI modalities. We have previously shown with qualitative histology that the DCE-MRI K_{ps} parameter is reflective of the extent of albumin

extravasation into the spinal cord (Patel et al., 2009). Correlations between lesions identified on high-resolution anatomical MRI scans have also been identified with histological markers of inflammation (Bilgen et al., 2000; Bilgen et al., 2007). In regards to DTI measures, although controversy remains regarding the specificity of λ_L and λ_T for axonal integrity and myelination status (Budde et al., 2007; Herrera et al., 2007), the seemingly counter-intuitive nature of findings in these metrics observed here may be elucidated with histological analysis. In addition, DTI acquisition during the acute phase of injury may be considered, as DTI measures in the hyperacute phases have been reported to be predictive of locomotor recovery in the chronic phase (Kim et al., 2010).

In regards to neurobehavioral assessment, a lack of chronic pain in the Ang1 group despite tissue sparing, as reflected by the reduced lesion size, is important in the context of previous findings of VEGF-induced chronic neuropathic pain (Sundberg, 2009) with concomitant tissue sparing. Unlike VEGF, Ang1 reduces vascular permeability and is not a potent promoter of angiogenesis. However, when used in concert with VEGF, Ang1 has been shown to normalize vasculature, providing an environment for non-hyperpermeable, “therapeutic” angiogenesis (Zacharek et al., 2007; Hansen et al., 2008; Toyama et al., 2009; Zhao et al., 2009).

Future studies

A consideration for future studies is the role of integrins in SCI. Co-administration of Ang1 and C16 peptide, a ligand for $\alpha v \beta 3$ integrin, was shown to be synergistic in regards to locomotor recovery in the subacute phase but not in the chronic phase of SCI (Han et al., 2010). Although synergy was not observed in regards to white matter sparing or reduced markers of inflammation on histology in the acute and chronic phases in their study, delivering Ang1 in combination with other agents that stimulate pro-survival pathways (e.g., PI3K) in different tissues (e.g., vascular endothelium and neurons) may be another therapeutic avenue to consider in the context of spinal cord injury.

Investigations into the temporal expression of endogenous Ang1 after SCI will be necessary in order to identify the time windows when supplementation with exogenous Ang1 may be warranted. The single dose of Ang1 in this study appears to have resulted in effects during all phases of injury, most prominently during the acute and subacute phases. Thus, it would be desirable in future studies to focus on these periods of injury and perform MRI-histological correlations at serial time points, in order to understand the effects of Ang1 during these phases of injury. In light of the study by Han et al. (Han et al., 2010), the dose and timing of Ang1 administration in this study are two variables that could be optimized. Future studies will use viral vectors encoding Ang1 that are injected into the injury lesion in order to investigate the effects of sustained Ang1 administration in SCI.

BIBLIOGRAPHY

- Abdellatif AA, Pelt JL, Benton RL, Howard RM, Tsoulfas P, Ping P, Xu XM, Whittemore SR (2006) Gene delivery to the spinal cord: comparison between lentiviral, adenoviral, and retroviral vector delivery systems. *J Neurosci Res* 84:553-567.
- Acker T, Beck H, Plate KH (2001) Cell type specific expression of vascular endothelial growth factor and angiopoietin-1 and -2 suggests an important role of astrocytes in cerebellar vascularization. *Mech Dev* 108:45-57.
- Alper J (2009) Geron gets green light for human trial of ES cell-derived product. *Nat Biotechnol* 27:213-214.
- Amar AP, Levy ML (1999) Pathogenesis and pharmacological strategies for mitigating secondary damage in acute spinal cord injury. *Neurosurgery* 44:1027-1039; discussion 1039-1040.
- Anderson DK, Hall ED (1993) Pathophysiology of spinal cord trauma. *Ann Emerg Med* 22:987-992.
- Baffert F, Le T, Thurston G, McDonald DM (2006) Angiopoietin-1 decreases plasma leakage by reducing number and size of endothelial gaps in venules. *Am J Physiol Heart Circ Physiol* 290:H107-118.
- Bai Y, Meng Z, Cui M, Zhang X, Chen F, Xiao J, Shen L, Zhang Y (2009) An Ang1-Tie2-PI3K axis in neural progenitor cells initiates survival responses against oxygen and glucose deprivation. *Neuroscience* 160:371-381.
- Baldwin SA, Broderick R, Osbourne D, Waeg G, Blades DA, Scheff SW (1998) The presence of 4-hydroxynonenal/protein complex as an indicator of

- oxidative stress after experimental spinal cord contusion in a rat model. J Neurosurg 88:874-883.
- Baptiste DC, Fehlings MG (2007) Update on the treatment of spinal cord injury. Prog Brain Res 161:217-233.
- Basso DM (2000) Neuroanatomical substrates of functional recovery after experimental spinal cord injury: implications of basic science research for human spinal cord injury. Phys Ther 80:808-817.
- Basso DM, Beattie MS, Bresnahan JC (1995) A sensitive and reliable locomotor rating scale for open field testing in rats. J Neurotrauma 12:1-21.
- Behrmann DL, Bresnahan JC, Beattie MS, Shah BR (1992) Spinal cord injury produced by consistent mechanical displacement of the cord in rats: behavioral and histologic analysis. J Neurotrauma 9:197-217.
- Bilgen M, Narayana PA (2001) A pharmacokinetic model for quantitative evaluation of spinal cord injury with dynamic contrast-enhanced magnetic resonance imaging. Magn Reson Med 46:1099-1106.
- Bilgen M, Abbe R, Narayana PA (2001) Dynamic contrast-enhanced MRI of experimental spinal cord injury: in vivo serial studies. Magn Reson Med 45:614-622.
- Bilgen M, Dogan B, Narayana PA (2002) In vivo assessment of blood-spinal cord barrier permeability: serial dynamic contrast enhanced MRI of spinal cord injury. Magn Reson Imaging 20:337-341.

- Bilgen M, Abbe R, Liu SJ, Narayana PA (2000) Spatial and temporal evolution of hemorrhage in the hyperacute phase of experimental spinal cord injury: in vivo magnetic resonance imaging. *Magn Reson Med* 43:594-600.
- Bilgen M, Al-Hafez B, Alrefae T, He YY, Smirnova IV, Aldur MM, Festoff BW (2007) Longitudinal magnetic resonance imaging of spinal cord injury in mouse: changes in signal patterns associated with the inflammatory response. *Magn Reson Imaging* 25:657-664.
- Blight AR (1985) Delayed demyelination and macrophage invasion: a candidate for secondary cell damage in spinal cord injury. *Cent Nerv Syst Trauma* 2:299-315.
- Boulis NM, Bhatia V, Brindle TI, Holman HT, Krauss DJ, Blaivas M, Hoff JT (1999) Adenoviral nerve growth factor and beta-galactosidase transfer to spinal cord: a behavioral and histological analysis. *J Neurosurg* 90:99-108.
- Bracken MB (2002) Steroids for acute spinal cord injury. *Cochrane Database Syst Rev*:CD001046.
- Brambilla R, Bracchi-Ricard V, Hu WH, Frydel B, Bramwell A, Karmally S, Green EJ, Bethea JR (2005) Inhibition of astroglial nuclear factor kappaB reduces inflammation and improves functional recovery after spinal cord injury. *J Exp Med* 202:145-156.
- Bresnahan JC, Beattie MS, Todd FD, 3rd, Noyes DH (1987) A behavioral and anatomical analysis of spinal cord injury produced by a feedback-controlled impaction device. *Exp Neurol* 95:548-570.

- Budde MD, Kim JH, Liang HF, Schmidt RE, Russell JH, Cross AH, Song SK (2007) Toward accurate diagnosis of white matter pathology using diffusion tensor imaging. *Magn Reson Med* 57:688-695.
- Cain LD, Nie L, Hughes MG, Johnson K, Echeteu C, Xu GY, Hulsebosch CE, McAdoo DJ (2007) Serum albumin improves recovery from spinal cord injury. *J Neurosci Res* 85:1558-1567.
- Carlos TM, Harlan JM (1994) Leukocyte-endothelial adhesion molecules. *Blood* 84:2068-2101.
- Carlson SL, Parrish ME, Springer JE, Doty K, Dossett L (1998) Acute inflammatory response in spinal cord following impact injury. *Exp Neurol* 151:77-88.
- Chen J, Cui X, Zacharek A, Chopp M (2008) Increasing Ang1/Tie2 expression by simvastatin treatment induces vascular stabilization and neuroblast migration after stroke. *J Cell Mol Med*.
- Chen X, Fu W, Tung CE, Ward NL (2009) Angiopoietin-1 induces neurite outgrowth of PC12 cells in a Tie2-independent, beta1-integrin-dependent manner. *Neurosci Res* 64:348-354.
- Childs EW, Tharakan B, Byrge N, Tinsley JH, Hunter FA, Smythe WR (2008) Angiopoietin-1 inhibits intrinsic apoptotic signaling and vascular hyperpermeability following hemorrhagic shock. *Am J Physiol Heart Circ Physiol* 294:H2285-2295.
- Choi YK, Kim KW (2008) Blood-neural barrier: its diversity and coordinated cell-to-cell communication. *BMB Rep* 41:345-352.

- Cohen DM, Patel CB, Ahobila P, Sundberg LM, Chacko T, Liu SJ, Narayana PA (2009) Blood-Spinal Cord Barrier Permeability in Experimental Spinal Cord Injury: Dynamic Contrast-Enhanced MRI. *NMR Biomed*.
- Coleman MP, Perry VH (2002) Axon pathology in neurological disease: a neglected therapeutic target. *Trends Neurosci* 25:532-537.
- Couzin J (2009) Biotechnology. Celebration and concern over U.S. trial of embryonic stem cells. *Science* 323:568.
- Cui X, Chen J, Zacharek A, Roberts C, Savant-Bhonsale S, Chopp M (2008a) Treatment of stroke with (Z)-1-[N-(2-aminoethyl)-N-(2-ammonioethyl) amino] diazen-1-ium-1, 2-diolate and bone marrow stromal cells upregulates angiopoietin-1/Tie2 and enhances neovascularization. *Neuroscience* 156:155-164.
- Cui X, Chen J, Zacharek A, Roberts C, Yang Y, Chopp M (2008b) Nitric oxide donor up-regulation of SDF1/CXCR4 and Ang1/Tie2 promotes neuroblast cell migration after stroke. *J Neurosci Res*.
- Davis S, Aldrich TH, Jones PF, Acheson A, Compton DL, Jain V, Ryan TE, Bruno J, Radziejewski C, Maisonpierre PC, Yancopoulos GD (1996) Isolation of angiopoietin-1, a ligand for the TIE2 receptor, by secretion-trap expression cloning. *Cell* 87:1161-1169.
- Deng X, Ramu J, Narayana PA (2007) Spinal cord atrophy in injured rodents: high-resolution MRI. *Magn Reson Med* 57:620-624.

- Deng YS, Zhong JH, Zhou XF (2000) Effects of endogenous neurotrophins on sympathetic sprouting in the dorsal root ganglia and allodynia following spinal nerve injury. *Exp Neurol* 164:344-350.
- Deo AA, Grill RJ, Hasan KM, Narayana PA (2006) In vivo serial diffusion tensor imaging of experimental spinal cord injury. *J Neurosci Res* 83:801-810.
- Ditor DS, John S, Cakiroglu J, Kittmer C, Foster PJ, Weaver LC (2008) Magnetic resonance imaging versus histological assessment for estimation of lesion volume after experimental spinal cord injury. Laboratory investigation. *J Neurosurg Spine* 9:301-306.
- Ellingson BM, Kurpad SN, Schmit BD (2008) Ex vivo diffusion tensor imaging and quantitative tractography of the rat spinal cord during long-term recovery from moderate spinal contusion. *J Magn Reson Imaging* 28:1068-1079.
- Estores IM (2003) The consumer's perspective and the professional literature: what do persons with spinal cord injury want? *J Rehabil Res Dev* 40:93-98.
- Faden AI, Stoica B (2007) Neuroprotection: challenges and opportunities. *Arch Neurol* 64:794-800.
- Farooque M, Isaksson J, Olsson Y (1999) Improved recovery after spinal cord trauma in ICAM-1 and P-selectin knockout mice. *Neuroreport* 10:131-134.
- Farooque M, Isaksson J, Olsson Y (2001) White matter preservation after spinal cord injury in ICAM-1/P-selectin-deficient mice. *Acta Neuropathol* 102:132-140.
- Fenyes DA, Narayana PA (1998) In vivo echo-planar imaging of rat spinal cord. *Magn Reson Imaging* 16:1249-1255.

- Fenyves DA, Narayana PA (1999) In vivo diffusion tensor imaging of rat spinal cord with echo planar imaging. *Magn Reson Med* 42:300-306.
- Fleming JC, Bao F, Chen Y, Hamilton EF, Gonzalez-Lara LE, Foster PJ, Weaver LC (2009) Timing and duration of anti- $\alpha 4 \beta 1$ integrin treatment after spinal cord injury: effect on therapeutic efficacy. *J Neurosurg Spine* 11:575-587.
- Fleming JC, Norenberg MD, Ramsay DA, Dekaban GA, Marcillo AE, Saenz AD, Pasquale-Styles M, Dietrich WD, Weaver LC (2006) The cellular inflammatory response in human spinal cords after injury. *Brain* 129:3249-3269.
- Galbraith SM, Lodge MA, Taylor NJ, Rustin GJ, Bentzen S, Stirling JJ, Padhani AR (2002) Reproducibility of dynamic contrast-enhanced MRI in human muscle and tumours: comparison of quantitative and semi-quantitative analysis. *NMR Biomed* 15:132-142.
- Gavard J, Patel V, Gutkind JS (2008) Angiopoietin-1 prevents VEGF-induced endothelial permeability by sequestering Src through mDia. *Dev Cell* 14:25-36.
- Gimenez y Ribotta M, Gaviria M, Menet V, Privat A (2002) Strategies for regeneration and repair in spinal cord traumatic injury. *Prog Brain Res* 137:191-212.
- Gullapalli J, Krejza J, Schwartz ED (2006) In vivo DTI evaluation of white matter tracts in rat spinal cord. *J Magn Reson Imaging* 24:231-234.

- Hagg T, Oudega M (2006) Degenerative and spontaneous regenerative processes after spinal cord injury. *J Neurotrauma* 23:264-280.
- Haggstrom Rudolfsson S, Johansson A, Franck Lissbrant I, Wikstrom P, Bergh A (2003) Localized expression of angiopoietin 1 and 2 may explain unique characteristics of the rat testicular microvasculature. *Biol Reprod* 69:1231-1237.
- Hall ED, Springer JE (2004) Neuroprotection and acute spinal cord injury: a reappraisal. *NeuroRx* 1:80-100.
- Hamada Y, Ikata T, Katoh S, Nakauchi K, Niwa M, Kawai Y, Fukuzawa K (1996) Involvement of an intercellular adhesion molecule 1-dependent pathway in the pathogenesis of secondary changes after spinal cord injury in rats. *J Neurochem* 66:1525-1531.
- Han S, Arnold SA, Sithu SD, Mahoney ET, Geraldts JT, Tran P, Benton RL, Maddie MA, D'Souza SE, Whittemore SR, Hagg T Rescuing vasculature with intravenous angiopoietin-1 and alphavbeta3 integrin peptide is protective after spinal cord injury. *Brain* 133:1026-1042.
- Han S, Arnold SA, Sithu SD, Mahoney ET, Geraldts JT, Tran P, Benton RL, Maddie MA, D'Souza SE, Whittemore SR, Hagg T (2010) Rescuing vasculature with intravenous angiopoietin-1 and alphavbeta3 integrin peptide is protective after spinal cord injury. *Brain* 133:1026-1042.
- Hansen TM, Moss AJ, Brindle NP (2008) Vascular endothelial growth factor and angiopoietins in neurovascular regeneration and protection following stroke. *Curr Neurovasc Res* 5:236-245.

- Harfouche R, Hassessian HM, Guo Y, Faivre V, Srikant CB, Yancopoulos GD, Hussain SN (2002) Mechanisms which mediate the antiapoptotic effects of angiopoietin-1 on endothelial cells. *Microvasc Res* 64:135-147.
- Hasan KM, Narayana PA (2003) Computation of the fractional anisotropy and mean diffusivity maps without tensor decoding and diagonalization: Theoretical analysis and validation. *Magn Reson Med* 50:589-598.
- Hasan KM, Narayana PA (2006) Retrospective measurement of the diffusion tensor eigenvalues from diffusion anisotropy and mean diffusivity in DTI. *Magn Reson Med* 56:130-137.
- Hasan KM, Alexander AL, Narayana PA (2004) Does fractional anisotropy have better noise immunity characteristics than relative anisotropy in diffusion tensor MRI? An analytical approach. *Magn Reson Med* 51:413-417.
- Hayes AJ, Huang WQ, Mallah J, Yang D, Lippman ME, Li LY (1999) Angiopoietin-1 and its receptor Tie-2 participate in the regulation of capillary-like tubule formation and survival of endothelial cells. *Microvasc Res* 58:224-237.
- Hejcl A, Urdzikova L, Sedy J, Lesny P, Pradny M, Michalek J, Burian M, Hajek M, Zamecnik J, Jendelova P, Sykova E (2008) Acute and delayed implantation of positively charged 2-hydroxyethyl methacrylate scaffolds in spinal cord injury in the rat. *J Neurosurg Spine* 8:67-73.
- Herrera JJ, Chacko T, Narayana PA (2007) Histological correlation of diffusion tensor imaging metrics in experimental spinal cord injury. *J Neurosci Res*.
- Herrera JJ, Nesic-Taylor DO, Narayana PA (2009) Reduced Vascular Endothelial Growth Factor Expression In Contusive Spinal Cord Injury. *J Neurotrauma*.

- Hori S, Ohtsuki S, Hosoya K, Nakashima E, Terasaki T (2004) A pericyte-derived angiopoietin-1 multimeric complex induces occludin gene expression in brain capillary endothelial cells through Tie-2 activation in vitro. *J Neurochem* 89:503-513.
- Huang WL, King VR, Curran OE, Dyll SC, Ward RE, Lal N, Priestley JV, Michael-Titus AT (2007) A combination of intravenous and dietary docosahexaenoic acid significantly improves outcome after spinal cord injury. *Brain* 130:3004-3019.
- Hughenoltz H (2003) Methylprednisolone for acute spinal cord injury: not a standard of care. *Cmaj* 168:1145-1146.
- Hughes DP, Marron MB, Brindle NP (2003) The antiinflammatory endothelial tyrosine kinase Tie2 interacts with a novel nuclear factor-kappaB inhibitor ABIN-2. *Circ Res* 92:630-636.
- Hui C, Zhou YX, Narayana PA (submitted) A Fast Algorithm for Calculation of Inhomogeneity Gradient in MRI Data. *JMRI*.
- Hulsebosch CE, Hains BC, Crown ED, Carlton SM (2009) Mechanisms of chronic central neuropathic pain after spinal cord injury. *Brain Res Rev* 60:202-213.
- Iizasa H, Bae SH, Asashima T, Kitano T, Matsunaga N, Terasaki T, Kang YS, Nakashima E (2002) Augmented expression of the tight junction protein occludin in brain endothelial cell line TR-BBB by rat angiopoietin-1 expressed in baculovirus-infected Sf plus insect cells. *Pharm Res* 19:1757-1760.

- Imhof BA, Aurrand-Lions M (2006) Angiogenesis and inflammation face off. *Nat Med* 12:171-172.
- Isaksson J, Farooque M, Holtz A, Hillered L, Olsson Y (1999) Expression of ICAM-1 and CD11b after experimental spinal cord injury in rats. *J Neurotrauma* 16:165-173.
- Jones LL, Tuszynski MH (2001) Chronic intrathecal infusions after spinal cord injury cause scarring and compression. *Microsc Res Tech* 54:317-324.
- Jones TB, McDaniel EE, Popovich PG (2005) Inflammatory-mediated injury and repair in the traumatically injured spinal cord. *Curr Pharm Des* 11:1223-1236.
- Joussen AM, Poulaki V, Tsujikawa A, Qin W, Qaum T, Xu Q, Moromizato Y, Bursell SE, Wiegand SJ, Rudge J, Ioffe E, Yancopoulos GD, Adamis AP (2002) Suppression of diabetic retinopathy with angiopoietin-1. *Am J Pathol* 160:1683-1693.
- Juurlink BH, Paterson PG (1998) Review of oxidative stress in brain and spinal cord injury: suggestions for pharmacological and nutritional management strategies. *J Spinal Cord Med* 21:309-334.
- Kaptanoglu E, Beskonakli E, Solaroglu I, Kilinc A, Taskin Y (2003) Magnesium sulfate treatment in experimental spinal cord injury: emphasis on vascular changes and early clinical results. *Neurosurg Rev* 26:283-287.
- Kim I, Moon SO, Park SK, Chae SW, Koh GY (2001) Angiopoietin-1 reduces VEGF-stimulated leukocyte adhesion to endothelial cells by reducing ICAM-1, VCAM-1, and E-selectin expression. *Circ Res* 89:477-479.

- Kim JH, Loy DN, Wang Q, Budde MD, Schmidt RE, Trinkaus K, Song SK (2010) Diffusion tensor imaging at 3 hours after traumatic spinal cord injury predicts long-term locomotor recovery. *J Neurotrauma* 27:587-598.
- Klussmann S, Martin-Villalba A (2005) Molecular targets in spinal cord injury. *J Mol Med* 83:657-671.
- Kobiler D, Lustig S, Shapira S (2001) Blood-brain barrier : drug delivery and brain pathology. New York: Kluwer Academic/Plenum.
- Koh GY, Kim I, Kwak HJ, Yun MJ, Leem JC (2002) Biomedical significance of endothelial cell specific growth factor, angiopoietin. *Exp Mol Med* 34:1-11.
- Kosacka J, Figiel M, Engele J, Hilbig H, Majewski M, Spänel-Borowski K (2005) Angiopoietin-1 promotes neurite outgrowth from dorsal root ganglion cells positive for Tie-2 receptor. *Cell Tissue Res* 320:11-19.
- Kosacka J, Nowicki M, Kacza J, Borlak J, Engele J, Spänel-Borowski K (2006) Adipocyte-derived angiopoietin-1 supports neurite outgrowth and synaptogenesis of sensory neurons. *J Neurosci Res* 83:1160-1169.
- Lee TT, Green BA, Dietrich WD, Yeziarski RP (1999) Neuroprotective effects of basic fibroblast growth factor following spinal cord contusion injury in the rat. *J Neurotrauma* 16:347-356.
- Liu W, Ahmad SA, Reinmuth N, Shaheen RM, Jung YD, Fan F, Ellis LM (2000) Endothelial cell survival and apoptosis in the tumor vasculature. *Apoptosis* 5:323-328.
- Lynskey JV, Sandhu FA, Dai HN, McAtee M, Slotkin JR, MacArthur L, Bregman BS (2006) Delayed intervention with transplants and neurotrophic factors

- supports recovery of forelimb function after cervical spinal cord injury in adult rats. *J Neurotrauma* 23:617-634.
- Madi S, Hasan KM, Narayana PA (2005) Diffusion tensor imaging of in vivo and excised rat spinal cord at 7 T with an icosahedral encoding scheme. *Magn Reson Med* 53:118-125.
- Maikos JT, Shreiber DI (2007) Immediate damage to the blood-spinal cord barrier due to mechanical trauma. *J Neurotrauma* 24:492-507.
- Mann C, Lee JH, Liu J, Stammers AM, Sohn HM, Tetzlaff W, Kwon BK (2008) Delayed treatment of spinal cord injury with erythropoietin or darbepoetin--a lack of neuroprotective efficacy in a contusion model of cord injury. *Exp Neurol* 211:34-40.
- Mautes AE, Weinzierl MR, Donovan F, Noble LJ (2000) Vascular events after spinal cord injury: contribution to secondary pathogenesis. *Phys Ther* 80:673-687.
- McDonald JW, Belegu V (2006) Demyelination and remyelination after spinal cord injury. *J Neurotrauma* 23:345-359.
- McTigue DM, Tripathi RB (2008) The life, death, and replacement of oligodendrocytes in the adult CNS. *J Neurochem* 107:1-19.
- Mills CD, Grady JJ, Hulsebosch CE (2001) Changes in exploratory behavior as a measure of chronic central pain following spinal cord injury. *J Neurotrauma* 18:1091-1105.

- Mochizuki N (2009) Vascular integrity mediated by vascular endothelial cadherin and regulated by sphingosine 1-phosphate and angiopoietin-1. *Circ J* 73:2183-2191.
- Nakayama T, Yao L, Tosato G (2004) Mast cell-derived angiopoietin-1 plays a critical role in the growth of plasma cell tumors. *J Clin Invest* 114:1317-1325.
- Nelson E, Gertz SD, Rennels ML, Ducker TB, Blaumanis OR (1977) Spinal cord injury. The role of vascular damage in the pathogenesis of central hemorrhagic necrosis. *Arch Neurol* 34:332-333.
- Nishi RA, Liu H, Chu Y, Hamamura M, Su MY, Nalcioğlu O, Anderson AJ (2007) Behavioral, histological, and ex vivo magnetic resonance imaging assessment of graded contusion spinal cord injury in mice. *J Neurotrauma* 24:674-689.
- Noble LJ, Maxwell DS (1983) Blood-spinal cord barrier response to transection. *Exp Neurol* 79:188-199.
- Noble LJ, Wrathall JR (1985) Spinal cord contusion in the rat: morphometric analyses of alterations in the spinal cord. *Exp Neurol* 88:135-149.
- Noble LJ, Wrathall JR (1987) The blood-spinal cord barrier after injury: pattern of vascular events proximal and distal to a transection in the rat. *Brain Res* 424:177-188.
- Noble LJ, Wrathall JR (1988) Blood-spinal cord barrier disruption proximal to a spinal cord transection in the rat: time course and pathways associated with protein leakage. *Exp Neurol* 99:567-578.

- Noble LJ, Wrathall JR (1989) Distribution and time course of protein extravasation in the rat spinal cord after contusive injury. *Brain Res* 482:57-66.
- Noble LJ, Donovan F, Igarashi T, Goussev S, Werb Z (2002) Matrix metalloproteinases limit functional recovery after spinal cord injury by modulation of early vascular events. *J Neurosci* 22:7526-7535.
- Nourhaghighi N, Teichert-Kuliszewska K, Davis J, Stewart DJ, Nag S (2003) Altered expression of angiopoietins during blood-brain barrier breakdown and angiogenesis. *Lab Invest* 83:1211-1222.
- Nout YS, Mihai G, Tovar CA, Schmalbrock P, Bresnahan JC, Beattie MS (2009) Hypertonic saline attenuates cord swelling and edema in experimental spinal cord injury: a study utilizing magnetic resonance imaging. *Crit Care Med* 37:2160-2166.
- Novikova LN, Novikov LN, Kellerth JO (2000) Survival effects of BDNF and NT-3 on axotomized rubrospinal neurons depend on the temporal pattern of neurotrophin administration. *Eur J Neurosci* 12:776-780.
- Nyberg F, Sharma HS (2002) Repeated topical application of growth hormone attenuates blood-spinal cord barrier permeability and edema formation following spinal cord injury: an experimental study in the rat using Evans blue, ([125]I)-sodium and lanthanum tracers. *Amino Acids* 23:231-239.
- Ohab JJ, Fleming S, Blesch A, Carmichael ST (2006) A neurovascular niche for neurogenesis after stroke. *J Neurosci* 26:13007-13016.
- Olby NJ, Blakemore WF (1996) A new method of quantifying the extent of tissue loss following spinal cord injury in the rat. *Exp Neurol* 138:82-92.

- Onda T, Honmou O, Harada K, Houkin K, Hamada H, Kocsis JD (2008) Therapeutic benefits by human mesenchymal stem cells (hMSCs) and Ang-1 gene-modified hMSCs after cerebral ischemia. *J Cereb Blood Flow Metab* 28:329-340.
- Pan W, Kastin AJ (2001) Increase in TNFalpha transport after SCI is specific for time, region, and type of lesion. *Exp Neurol* 170:357-363.
- Pan W, Kastin AJ (2008) Cytokine transport across the injured blood-spinal cord barrier. *Curr Pharm Des* 14:1620-1624.
- Pan W, Kastin AJ, Gera L, Stewart JM (2001) Bradykinin antagonist decreases early disruption of the blood-spinal cord barrier after spinal cord injury in mice. *Neurosci Lett* 307:25-28.
- Pan W, Zhang L, Liao J, Csernus B, Kastin AJ (2003) Selective increase in TNF alpha permeation across the blood-spinal cord barrier after SCI. *J Neuroimmunol* 134:111-117.
- Papapetropoulos A, Garcia-Cardena G, Dengler TJ, Maisonpierre PC, Yancopoulos GD, Sessa WC (1999) Direct actions of angiopoietin-1 on human endothelium: evidence for network stabilization, cell survival, and interaction with other angiogenic growth factors. *Lab Invest* 79:213-223.
- Papapetropoulos A, Fulton D, Mahboubi K, Kalb RG, O'Connor DS, Li F, Altieri DC, Sessa WC (2000) Angiopoietin-1 inhibits endothelial cell apoptosis via the Akt/survivin pathway. *J Biol Chem* 275:9102-9105.
- Patel CB, Cohen DM, Ahobila-Vajjula P, Sundberg LM, Chacko T, Narayana PA (2009) Effect of VEGF treatment on the blood-spinal cord barrier

- permeability in experimental spinal cord injury: dynamic contrast-enhanced magnetic resonance imaging. *J Neurotrauma* 26:1005-1016.
- Peng XM, Zhou ZG, Glorioso JC, Fink DJ, Mata M (2006) Tumor necrosis factor- α contributes to below-level neuropathic pain after spinal cord injury. *Ann Neurol* 59:843-851.
- Peters KG, Kontos CD, Lin PC, Wong AL, Rao P, Huang L, Dewhirst MW, Sankar S (2004) Functional significance of Tie2 signaling in the adult vasculature. *Recent Prog Horm Res* 59:51-71.
- Popovich PG, Horner PJ, Mullin BB, Stokes BT (1996) A quantitative spatial analysis of the blood-spinal cord barrier. I. Permeability changes after experimental spinal contusion injury. *Exp Neurol* 142:258-275.
- Priebe MM, Chiodo AE, Scelza WM, Kirshblum SC, Wuermser LA, Ho CH (2007) Spinal cord injury medicine. 6. Economic and societal issues in spinal cord injury. *Arch Phys Med Rehabil* 88:S84-88.
- Qian J, Herrera JJ, Narayana PA (2010) Neuronal and axonal degeneration in experimental spinal cord injury: in vivo proton magnetic resonance spectroscopy and histology. *J Neurotrauma* 27:599-610.
- Rafati DS, Geissler K, Johnson K, Unabia G, Hulsebosch C, Nesic-Taylor O, Perez-Polo JR (2007) Nuclear factor-kappaB decoy amelioration of spinal cord injury-induced inflammation and behavior outcomes. *J Neurosci Res*.
- Rivlin AS, Tator CH (1977) Objective clinical assessment of motor function after experimental spinal cord injury in the rat. *J Neurosurg* 47:577-581.

- Rosa AI, Goncalves J, Cortes L, Bernardino L, Malva JO, Agasse F (2010) The angiogenic factor angiopoietin-1 is a proneurogenic peptide on subventricular zone stem/progenitor cells. *J Neurosci* 30:4573-4584.
- Runge VM, Wells JW, Baldwin SA, Scheff SW, Blades DA (1997) Evaluation of the temporal evolution of acute spinal cord injury. *Invest Radiol* 32:105-110.
- Salmon AH, Neal CR, Sage LM, Glass CA, Harper SJ, Bates DO (2009) Angiopoietin-1 alters microvascular permeability coefficients in vivo via modification of endothelial glycocalyx. *Cardiovasc Res* 83:24-33.
- Sasaki M, Li B, Lankford KL, Radtke C, Kocsis JD (2007) Remyelination of the injured spinal cord. *Prog Brain Res* 161:419-433.
- Scholtes F, Phan-Ba R, Theunissen E, Adriaenssens P, Brook G, Franzen R, Bouhy D, Gelan J, Martin D, Schoenen J (2008) Rapid, postmortem 9.4 T MRI of spinal cord injury: correlation with histology and survival times. *J Neurosci Methods* 174:157-167.
- Sharma HS (2000) A bradykinin BK2 receptor antagonist HOE-140 attenuates blood-spinal cord barrier permeability following a focal trauma to the rat spinal cord. An experimental study using Evans blue, [¹³¹I]-sodium and lanthanum tracers. *Acta Neurochir Suppl* 76:159-163.
- Sharma HS (2003) Neurotrophic factors attenuate microvascular permeability disturbances and axonal injury following trauma to the rat spinal cord. *Acta Neurochir Suppl* 86:383-388.
- Sharma HS (2005) Pathophysiology of blood-spinal cord barrier in traumatic injury and repair. *Curr Pharm Des* 11:1353-1389.

- Sharma HS (2006) Post-traumatic application of brain-derived neurotrophic factor and glia-derived neurotrophic factor on the rat spinal cord enhances neuroprotection and improves motor function. *Acta Neurochir Suppl* 96:329-334.
- Sharma HS, Sjoquist PO, Mohanty S, Wiklund L (2006a) Post-injury treatment with a new antioxidant compound H-290/51 attenuates spinal cord trauma-induced c-fos expression, motor dysfunction, edema formation, and cell injury in the rat. *Acta Neurochir Suppl* 96:322-328.
- Sharma HS, Skottner A, Lundstedt T, Flardh M, Wiklund L (2006b) Neuroprotective effects of melanocortins in experimental spinal cord injury. An experimental study in the rat using topical application of compounds with varying affinity to melanocortin receptors. *J Neural Transm* 113:463-476.
- Sharma HS, Nyberg F, Westman J, Alm P, Gordh T, Lindholm D (1998) Brain derived neurotrophic factor and insulin like growth factor-1 attenuate upregulation of nitric oxide synthase and cell injury following trauma to the spinal cord. An immunohistochemical study in the rat. *Amino Acids* 14:121-129.
- Sharma HS, Ali SF, Dong W, Tian ZR, Patnaik R, Patnaik S, Sharma A, Boman A, Lek P, Seifert E, Lundstedt T (2007) Drug delivery to the spinal cord tagged with nanowire enhances neuroprotective efficacy and functional recovery following trauma to the rat spinal cord. *Ann N Y Acad Sci* 1122:197-218.
- Stoeltzing O, Ahmad SA, Liu W, McCarty MF, Wey JS, Parikh AA, Fan F, Reinmuth N, Kawaguchi M, Bucana CD, Ellis LM (2003) Angiopoietin-1

inhibits vascular permeability, angiogenesis, and growth of hepatic colon cancer tumors. *Cancer Res* 63:3370-3377.

Sundberg C, Kowanetz M, Brown LF, Detmar M, Dvorak HF (2002) Stable expression of angiopoietin-1 and other markers by cultured pericytes: phenotypic similarities to a subpopulation of cells in maturing vessels during later stages of angiogenesis in vivo. *Lab Invest* 82:387-401.

Sundberg LM (2009) In vivo Longitudinal Studies of Spinal Cord Injury and Vascular Endothelial Growth Factor Treatment. In: Department of Diagnostic and Interventional Imaging, p 180. Houston, TX: University of Texas Health Science Center at Houston Graduate School of Biomedical Sciences.

Suri C, Jones PF, Patan S, Bartunkova S, Maisonpierre PC, Davis S, Sato TN, Yancopoulos GD (1996) Requisite role of angiopoietin-1, a ligand for the TIE2 receptor, during embryonic angiogenesis. *Cell* 87:1171-1180.

Sykova E, Jendelova P, Urdzikova L, Lesny P, Hejcl A (2006) Bone marrow stem cells and polymer hydrogels--two strategies for spinal cord injury repair. *Cell Mol Neurobiol* 26:1113-1129.

Tadros A, Hughes DP, Dunmore BJ, Brindle NP (2003) ABIN-2 protects endothelial cells from death and has a role in the antiapoptotic effect of angiopoietin-1. *Blood* 102:4407-4409.

Tator CH, Koyanagi I (1997) Vascular mechanisms in the pathophysiology of human spinal cord injury. *J Neurosurg* 86:483-492.

- Thurston G, Suri C, Smith K, McClain J, Sato TN, Yancopoulos GD, McDonald DM (1999) Leakage-resistant blood vessels in mice transgenically overexpressing angiopoietin-1. *Science* 286:2511-2514.
- Thurston G, Rudge JS, Ioffe E, Zhou H, Ross L, Croll SD, Glazer N, Holash J, McDonald DM, Yancopoulos GD (2000) Angiopoietin-1 protects the adult vasculature against plasma leakage. *Nat Med* 6:460-463.
- Tian DS, Dong Q, Pan DJ, He Y, Yu ZY, Xie MJ, Wang W (2007) Attenuation of astrogliosis by suppressing of microglial proliferation with the cell cycle inhibitor olomoucine in rat spinal cord injury model. *Brain Res* 1154:206-214.
- Tofts PS, Brix G, Buckley DL, Evelhoch JL, Henderson E, Knopp MV, Larsson HB, Lee TY, Mayr NA, Parker GJ, Port RE, Taylor J, Weisskoff RM (1999) Estimating kinetic parameters from dynamic contrast-enhanced T(1)-weighted MRI of a diffusable tracer: standardized quantities and symbols. *J Magn Reson Imaging* 10:223-232.
- Toyama K, Honmou O, Harada K, Suzuki J, Houkin K, Hamada H, Kocsis JD (2009) Therapeutic benefits of angiogenetic gene-modified human mesenchymal stem cells after cerebral ischemia. *Exp Neurol* 216:47-55.
- Uemura A, Ogawa M, Hirashima M, Fujiwara T, Koyama S, Takagi H, Honda Y, Wiegand SJ, Yancopoulos GD, Nishikawa S (2002) Recombinant angiopoietin-1 restores higher-order architecture of growing blood vessels in mice in the absence of mural cells. *J Clin Invest* 110:1619-1628.

- Valable S, Bellail A, Lesne S, Liot G, Mackenzie ET, Vivien D, Bernaudin M, Petit E (2003) Angiopoietin-1-induced PI3-kinase activation prevents neuronal apoptosis. *Faseb J* 17:443-445.
- Valable S, Montaner J, Bellail A, Berezowski V, Brillault J, Cecchelli R, Divoux D, Mackenzie ET, Bernaudin M, Roussel S, Petit E (2005) VEGF-induced BBB permeability is associated with an MMP-9 activity increase in cerebral ischemia: both effects decreased by Ang-1. *J Cereb Blood Flow Metab* 25:1491-1504.
- Wang YL, Hui YN, Guo B, Ma JX (2007) Strengthening tight junctions of retinal microvascular endothelial cells by pericytes under normoxia and hypoxia involving angiopoietin-1 signal way. *Eye* 21:1501-1510.
- Warfield SK, Zou KH, Wells WM (2004) Simultaneous truth and performance level estimation (STAPLE): an algorithm for the validation of image segmentation. *IEEE Trans Med Imaging* 23:903-921.
- Waxman SG (1992) Demyelination in spinal cord injury and multiple sclerosis: what can we do to enhance functional recovery? *J Neurotrauma* 9 Suppl 1:S105-117.
- Weirich SD, Cotler HB, Narayana PA, Hazle JD, Jackson EF, Coupe KJ, McDonald CL, Langford LA, Harris JH, Jr. (1990) Histopathologic correlation of magnetic resonance imaging signal patterns in a spinal cord injury model. *Spine* 15:630-638.

- Whetstone WD, Hsu JY, Eisenberg M, Werb Z, Noble-Haeusslein LJ (2003) Blood-spinal cord barrier after spinal cord injury: relation to revascularization and wound healing. *J Neurosci Res* 74:227-239.
- Wrathall JR, Teng YD, Marriott R (1997) Delayed antagonism of AMPA/kainate receptors reduces long-term functional deficits resulting from spinal cord trauma. *Exp Neurol* 145:565-573.
- Wu B, Ren X (2009) Promoting axonal myelination for improving neurological recovery in spinal cord injury. *J Neurotrauma* 26:1847-1856.
- Zacharek A, Chen J, Cui X, Li A, Li Y, Roberts C, Feng Y, Gao Q, Chopp M (2007) Angiopoietin1/Tie2 and VEGF/Fik1 induced by MSC treatment amplifies angiogenesis and vascular stabilization after stroke. *J Cereb Blood Flow Metab* 27:1684-1691.
- Zhang ZG, Zhang L, Croll SD, Chopp M (2002) Angiopoietin-1 reduces cerebral blood vessel leakage and ischemic lesion volume after focal cerebral embolic ischemia in mice. *Neuroscience* 113:683-687.
- Zhao Y, Li Z, Wang R, Wei J, Li G, Zhao H (2009) Angiopoietin 1 counteracts vascular endothelial growth factor-induced blood-brain barrier permeability and alleviates ischemic injury in the early stages of transient focal cerebral ischemia in rats. *Neurol Res.*
- Zhu Y, Shwe Y, Du R, Chen Y, Shen FX, Young WL, Yang GY (2006) Effects of angiopoietin-1 on vascular endothelial growth factor-induced angiogenesis in the mouse brain. *Acta Neurochir Suppl* 96:438-443.

VITA

Chirag Biresh Patel was born in Birmingham, England on May 22, 1979, the son of Biresh Ishwarbhai Patel and Daksha Biresh Patel. After completing high school at Klein High School (Spring, TX) in 1997, he entered Johns Hopkins University in Baltimore, Maryland. He received the degree of Bachelor of Science with a major in Biomedical Engineering (concentration in Electrical and Computer Engineering) and minors in Mathematics and Spanish in May 2001 and the degree of Master of Science in Engineering with a major in Biomedical Engineering in May 2004. In June 2003 he entered the University of Texas Health Science Center at Houston Graduate School of Biomedical Sciences and Medical School.

Permanent address:

2121 Hepburn Street

Houston, TX 77054